The multifaceted role of hyaluronan and proteoglycan link protein 1 (HAPLN1) in multiple myeloma

By

Hae Yeun Chang

A dissertation submitted in partial fulfillment of the requirements for the degree of

Doctor of Philosophy
(Cancer Biology)

at the
UNIVERSITY OF WISCONSIN - MADISON
2023

Date of final oral examination: June 30th, 2023

The dissertation is approved by the following members of the Final Oral Committee:
Shigeki Miyamoto: Professor, Department of Oncology
Avtar Roopra: Professor, Department of Neuroscience
Lixin Rui: Associate Professor, Department of Medicine, Hematology-Oncology
Bill Sugden: Professor, Department of Oncology
Beth Weaver: Professor, Department of Cell and Regenerative Biology

TABLE OF CONTENTS

LIST OF FIGURES AND TABLES

Chapter 1

Chapter 2

Chapter 3

Appendix

ACKNOWLEDGEMENTS

I am deeply grateful for the guidance, encouragement, and emotional support that I received throughout the process. The tremendous help and support of so many people along the way made it possible for me to complete this thesis. Without their invaluable help, I could not have accomplished it.

Dr. Shigeki Miyamoto, my exceptional and brilliant mentor, thank you for bringing me into such an amazing lab with such amazing people. From the moment I joined your lab, you have provided me with invaluable insights and endless encouragement. I feel privileged to be mentored by someone as remarkable as you. Your enthusiasm for science and your positivity, even in the face of my discouraging data, have inspired me to envision the kind of scientist I aspire to become.

The Miyamoto lab family, I want to thank you for being my family in Madison. Every member (past and present) has played an instrumental role in my life. I appreciate all the life and scientific advice. Thank you for being the greatest friends, supporters, colleagues throughout my journey.

My committee members, Bill Sugden, Avtar Roopra, Lixin Rui and Beth Weaver, thank you for your encouragement, scientific perspective, and guidance throughout my graduate student career.

My collaborators, Dr. Natalie Callander, Dr. Peiman Hematti, Dr. Avtar Roopra, Dr. Irene Ong, and so many more, without you, the progress would not have been possible.

The Cancer Biology Graduate Program, the best program at the University of Wisconsin-Madison. This program has allowed me to make invaluable friendships and build a strong support network. I would like specifically thank Julie Hoang, John Tucker, Rebecca DeStefanis, for our friendship.

My friends in Seoul and Madison. Thank you for checking in on me and being there for me in both the good and hard times.

My family. Thank you for your unconditional love and support throughout this entire process and throughout my entire life. There are no words to describe how much I love you.

ABSTRACT

The multifaceted role of hyaluronan and proteoglycan link protein 1 (HAPLN1) in multiple myeloma

Hae Yeun Chang

Under the direction of Dr. Shigeki Miyamoto

at the University of Wisconsin – Madison

Multiple myeloma (MM) is the second most frequent hematologic malignancy, currently considered an incurable cancer. Malignant plasma cells reside in multiple bone marrow (BM) sites that promote MM cell survival, proliferation, and drug resistance. The BM microenvironment is critical for survival and dissemination of MM cells, however mechanisms responsible for MM dissemination and homing to the BM niche are incompletely understood. Here my thesis investigated a new role for a fragment of the extracellular matrix protein, known as matrikine, derived from hyaluronan and proteoglycan link protein 1 (HAPLN1), in MM cell BM homing. I found that HAPLN1 matrikine increases MM cell adhesion to endothelial cells, BM-enriched extracellular matrix protein fibronectin, and BM stromal cells, as well as upregulates their chemotactic and chemokinetic migration *in vitro*. Moreover, MM cells preferentially home to HAPLN1-conditioned BM *in vivo*. Bioinformatic analyses of mRNAs induced by HAPLN1 matrikine and functional studies identified the transcription factor STAT1 as a mediator of MM BM homing. Finally, I also provide evidence for a positive association between high HAPLN1 levels in the BM and poor progression-free survival in newly diagnosed MM patients. These findings reveal that HAPLN1 matrikine present in the BM microenvironment plays

an important role in BM homing of MM cells via STAT1 signaling and may help predict patients with poor clinical outcomes. Combined with its ability to induce drug resistance in MM cells, these findings collectively identify HAPLN1 matrikine as a critical mediator of MM disease progression. My study also provides a mechanistic rationale for targeting HAPLN1 matrikine in MM therapy.

ABBREVIATIONS

AA	Amino acid
AlphaLISA	Amplified luminescent proximity homogenous assay-linked immunosorbent assay
Ang-1	Angiopoietin-1
ATM	Ataxia telangiectasia mutated
ATR	Ataxia telangiectasia and Rad3 related
BAFF	B-cell activating factor
BCL2	B-cell lymphoma 2
BCL2A	BCL2-related protein A
BCL2L1	BCL2-like 1
BIRC2	Baculoviral IAP repeat-containing protein 2
BIRC3	Baculoviral IAP repeat-containing protein 3
BM	Bone marrow
BMSC	Bone marrow stromal cell
BRAF	B-Raf Proto-oncogene
CA	Chromosomal abnormalities
CAM-DR	Cell adhesion-mediated drug resistance
CBP	CREB binding protein
CCR	C-C chemokine receptor
CD	Cluster of differentiation
CFLAR	CASP8 and FADD-like apoptosis regulator (c-FLIP)
CH60	Chaperonin 60
ChIP-seq	Chromatin immunoprecipitation sequencing
CNV	Copy number variation
CRAB	Hypercalcaemia, renal dysfunction, anaemia and bone lesions
CRTL1	Cartilage link protein 1
CSC	Cancer stem cell
CSF	Colony-stimulating factor
CXCL12	C-X-C chemokine ligand 12
CXCR4	C-X-C chemokine receptor type 4
DAMP	Damage-associated molecular pattern
ECM	Extracellular matrix
ECs	Endothelial cells
EGFR	Epidermal growth factor receptor
ELISA	Enzyme-linked immunosorbent assay

EMT	Epithelial-mesenchymal transition
ERK	Extracellular signal regulated kinase
EV	Empty vector
FBS	Fetal bovine serum
FGF	Fibroblast growth factor
FISH	Fluorescence *in situ* hybridization
FMI	Forward migration index
GFs	Growth factors
GPCR	G protein-coupled receptor
Gy	Gray
H1	HAPLN1
HA	Hyaluronic acid
HAPLN1	Hyaluronan and proteoglycan link protein 1
HAT	Histone acetyltransferase
HGF	Hepatocyte growth factor
HIF1α	Hypoxia inducible factor 1α
HLA-I	Human leukocyte antigen class I
HSC	Hematopoietic stem cell
ICAM-1	Intercellular adhesion molecule 1
IER3	Immediate early response 3 (IEX-1L)
IFN	Interferon
Ig	Immunoglobulin-like
IGF-1	Insulin-like growth factor 1
IgG	Immunoglobulin G
IgH	Immunoglobulin heavy chain
IHC	Immunohistochemistry
IKK	IκB kinase
IL	Interleukin
IP	Immunoprecipitation
IP-10/CXCL10	Interferon gamma-induced protein 10
JAK	Janus kinase
KEGG	Kyoto Encyclopedia of Genes and Genomes
KO	Knockout
KRAS	Kirsten rat sarcoma viral oncogene homolog
LDH	Lactate dehydrogenase
LFA	Lymphocyte function-associated antigen
LP	Link protein

LPS	Lipopolysaccharide
LTβ	Lymphotoxin β
MAGIC	Mining algorithm for genetic controllers
MAPK	Mitogen-activated protein kinase
MBP	Maltose-binding protein
MCP-1/CCL2	Monocyte chemoattractant protein-1
MDE	Myeloma-defining events
MDR	Multi-drug resistance
MEK	Mitogen-activated protein kinase kinase
MGUS	Monoclonal gammopathy of undetermined significance
MHC	Major histocompatibility complex
MIP-1α/CCL3	Macrophage inflammatory protein-1α
MM	Multiple myeloma
MMPs	Matrix metalloproteinases
MRD	Minimal residual disease
MRI	Magnetic resonance imaging
MT1-MMP	Membrane type 1 matrix metalloproteinase
MVD	Microvessel density
NCAM	Neural cell adhesion molecule
NDMM	Newly diagnosed multiple myeloma
NEMO	NF-κB essential modulator
NF-κB	Nuclear factor-κB
NGF	Next-generation flow cytometry
NGS	Next generation sequencing
NIK	NF-κB-inducing kinase
NLS	Nuclear localization sequence
NRAS	Neuroblastoma RAS viral oncogene homolog
OS	Overall survival
PDGF	Platelet-derived growth factor
PDGFR	Platelet-derived growth factor receptor
PFS	Progression-free survival
PI3K/AKT	Phosphatidylinositol 3-kinase/Protein kinase B
PIAS	Protein inhibitors of activated STATs
PKH26	Red fluorescent cell dye
Pol II	RNA polymerase II
PSGL-1	P-selectin Glycoprotein Ligand-1
PSME1	Proteasome activator complex subunit 1

PTP	Protein tyrosine phosphatases
PTR	Proteoglycan tandem repeat
qPCR	Quantitative polymerase chain reaction
qRT-PCR	Quantitative reverse transcription polymerase chain reaction
R-ISS	Revised-International Staging System
RANKL	Receptor activator of NF-κB ligand
RhoA	Ras homolog family member A
RNA-seq	RNA sequencing
RPKM	Reads per kilobase million
RRMM	Relapsed/Refractory multiple myeloma
RTK	Receptor tyrosine kinase
RUNX2	Runt-related transcription actor 2
SDC1	Syndecan 1
SDF-1	Stromal cell-derived factor 1
SH2	Src homology 2
shControl	Control knockdown
shSTAT1	STAT1 knockdown
SMA	Smooth muscle actin
SMM	Smoldering multiple myeloma
SOCS	Suppressors of cytokine signaling
SP	Signal peptide
STAT	Signal transducer and activator of transcription
TGFβ	Transforming growth factor β
TLR4	Toll-like Receptor 4
TME	Tumor microenvironment
TNFR	Tumor necrosis factor receptor
TNFα	Tumor necrosis factor α
TRAF	TNF receptor-associated factor
TYK2	Tyrosine kinase 2
VEGF	Vascular endothelial growth factor
VLA-4	Very late antigen 4
VLA-5	Very late antigen 5
WT	Wild type
β2M	β2-microglobulin

Chapter I

Introduction

Multiple Myeloma (MM)

Multiple myeloma (MM) is a malignancy of plasma cells accumulating in the bone marrow (BM), currently considered an incurable disease[1]. In the United States, MM is the second most prevalent hematologic malignancy, with 35,730 new cases and estimated 12,590 deaths in 2023[2]. The current 5-year relative survival rate for MM is 58%[3]. MM cells secrete clonal antibodies resulting in high levels of serum monoclonal immunoglobulin, also known as the M protein. The overgrowth of MM cells in the BM and elevated M proteins can cause end-organ damage[4]. The symptoms of active MM may include hyper*c*alcemia, *r*enal dysfunction, *a*nemia and *b*one lesions, referred to as the CRAB features. The diagnostic criteria for active MM require 10% or more plasma cells in the BM or plasmacytoma from biopsy, along with one or more of myeloma-defining events (MDEs). MDEs include 1) a CRAB symptom, 2) 60% or greater clonal plasma cells, 3) an involved-to-uninvolved serum free light chain ratio of 100 or greater, and 4) one or more focal lesions on MRI that are at least 5 mm or greater in size[5].

MM arises from asymptomatic precursor diseases, known as monoclonal gammopathy of undetermined significance (MGUS) and smoldering multiple myeloma (SMM)[6]. Recently, efforts have been made to detect the premalignant stage of MM for early therapeutic interventions and prevention of the progression from MGUS to SMM and finally to MM. The diagnostic criteria for these preceding conditions are serum M protein level <3 g/dL and BM plasma cells <10% for MGUS, and serum M protein level ≥3 g/dL or BM plasma cells ≥ 10% for SMM, both in the absence of CRAB symptoms. The progression rate of MGUS to MM is 1% per year and the progression rate of SMM to MM is 10% per year[7,8].

Bone Marrow Microenvironment in Multiple Myeloma

The English surgeon, Stephen Paget proposed the “seed and soil” hypothesis in 1889[9]. Cancer cells (the “seed”) are supported by the malignant microenvironment (the “soil”), consisting of cellular and non-cellular compartments. The BM microenvironment is essential for the survival, proliferation and drug resistance of MM cells[10]. MM cells are heavily dependent on the BM microenvironment which activates multiple cellular pathways, protecting these cells from apoptosis[11,12]. The BM niche is an intricate microenvironment composed of extracellular matrix (ECM) components and various cells, such as bone marrow stromal cells (BMSCs), hematopoietic stem and progenitor cells, endothelial cells (ECs), and immune cells, among others, nurturing and protecting MM cells[10].

The interactions of MM cells with the ECM explain the retention of plasma cells within the BM niche. The abundant ECM proteins in the BM microenvironment include fibronectin, collagen and laminin[13]. Adhesion of MM cells to the ECM is well-known to elicit cell adhesion-mediated drug resistance (CAM-DR) through adhesion molecules including very late antigen 4 (VLA-4, integrin α4β1), VLA-5 (integrin α5β1), integrin β7, CD44, and syndecan 1 (SDC1, CD138)[14,15]. The activation of integrins on MM cell surface is necessary for VLA-4 and integrin β7 to bind to fibronectin, one of the most abundant ECM proteins in the BM microenvironment[16,17]. MM cell binding to fibronectin via VLA-4 induces nuclear factor-κB (NF-κB) activation and pro-survival genes. Integrin β7-fibronectin interaction also activates NF-κB and induces drug resistance. Hyaluronan, a major glycosaminoglycan in the BM microenvironment, is recognized by CD44, a hyaluronan receptor[18]. Blocking the CD44-hyaluronan interaction in MM cells induces

anti-proliferative effects[19]. Syndecan-1, a heparan sulfate proteoglycan and a marker of plasma cells, has numerous ECM binding partners[20,21]. The ectodomain of syndecan-1 is capable of binding to ECM proteins, such as fibronectin and type I collagen, as well as cytokines and growth factors in the BM microenvironment. The interaction of ECM proteins via MM cell surface receptors is implicated in pro-survival signaling and adhesive and migratory properties.

Importantly, the interaction between MM cells and BMSCs is critical for MM cell survival, angiogenesis and drug resistance[22]. The crosstalk can occur directly through cell adhesion or indirectly through secreted soluble factors. MM cell surface expression of adhesion molecules, e.g., integrin β7, VLA-4, VLA-5, leukocyte function-associated antigen 1 (LFA-1, integrin αLβ2) and intercellular adhesion molecule 1 (ICAM-1), can directly bind to BMSCs, activating protective pro-survival and anti-apoptotic signaling in MM cells and leading to CAM-DR[16,23]. BMSCs secrete cytokines, chemokines and growth factors that create a protective BM niche for normal and abnormal cells in the BM microenvironment. These soluble factors include interleukin-6 (IL-6), stromal cell-derived factor 1 (SDF-1/CXCL12), vascular endothelial growth factor (VEGF), fibroblast growth factor (FGF), insulin-like growth factor 1 (IGF-1), tumor necrosis factor α (TNFα) and transforming growth factor β (TGFβ), triggering pro-survival signaling such as NF-κB, MEK/MAPK, JAK/STAT, and PI3K/AKT pathways[24]. In particular, IL-6, secreted by both MM cells and BMSCs, is a key pathogenic factor in MM[25]. After MM-BMSC adhesion, BMSCs secrete IL-6. MM cells also produce autocrine IL-6, which can potently activate the JAK/STAT pathway. The reciprocal loop of MM-BMSC interaction generates the

protective BM microenvironment for MM. MM cell survival and drug resistance heavily rely on BMSCs through soluble factors and cell adhesion.

Adhesion of MM cells to endothelial cells increases invasiveness and angiogenesis[26]. BM endothelial cells upregulate the secretion of matrix metalloproteinase (MMP)-9 in MM cells, further enhancing their invasiveness. The BM microenvironment contains abundant angiogenic cytokines produced by multiple cellular compartments. MM cells, BMSCs and endothelial cells all secrete such cytokines. When MM cells colonize and crowd the BM, a hypoxic microenvironment is generated. In MM cells, stabilization of hypoxia induced factor 1α (HIF1α) upregulates the transcription of pro-angiogenic cytokines, such as VEGF, platelet derived growth factor (PDGF) and angiopoietin-1 (Ang-1)[27]. The increased level of angiogenesis, as indicated by microvessel density (MVD), correlates with the malignant progression of the disease[28].

MM patients suffer from osteolytic lesions which are due to imbalanced bone resorption and bone formation. Osteoclast activation occurs in the vicinity of MM cells by cytokines including IL-1, IL-6 and hepatocyte growth factor (HGF)[29]. Macrophage inflammatory protein-1α (MIP-1α), secreted by MM cells, acts as an osteoclastogenic factor recognized by C-chemokine receptor 1 (CCR1) and CCR5 in osteoclasts[30,31]. Binding of MM cells to BMSCs via VLA-4 and VCAM-1 interaction leads to the production of receptor activator of NF-κB ligand (RANKL)[32]. RANKL stimulates osteoclasts and enhances osteoclastogenesis and bone resorption. Unlike osteoclast activation, osteoblast activity is suppressed in MM[33]. The formation of osteoblastic cells is inhibited by the direct binding of MM cells via VLA-4 and VCAM-1, blocking the activity of Runt-related transcription factor 2 (RUNX2)[34]. Additionally, cytokines such as IL-3 and IL-7 can

also inhibit Runx2 activity as well. When osteoblasts are co-cultured with MM cells, they secrete IL-6, supporting MM cell growth[35]. Overall, the crosstalk between the BM microenvironment and MM cells alters the microenvironment in favor of fostering cancerous cell growth.

Biomarkers in MM

The current prognostic staging system for MM utilizes the Revised-International Staging System (R-ISS), which can stratify the risk for patients[36]. The criteria for R-ISS were established based on clinical and laboratory data from 3,060 newly diagnosed MM (NDMM) patients in 11 clinical trials. These criteria include values of β_2-microglobulin (β_2M), albumin and lactate dehydrogenase (LDH) in serum, as well as chromosomal abnormalities (CA) assayed by fluorescence *in situ* hybridization (FISH). β_2M, a component of major histocompatibility complex (MHC) class I molecules, emerged as a tumor marker of lymphoproliferative disease in the 1970s[37]. Low serum albumin is caused by inflammatory cytokines secreted by the tumor microenvironment (TME). High LDH is a marker of aggressive, highly proliferative tumors[38]. Cytogenetic risk is a key factor in the prognosis of MM[39]. Common cytogenetic abnormalities include copy number variations (CNVs), loss or gain of chromosome arms (e.g., deletion of *TP53* gene locus on chromosome 17p), and translocations of the *immunoglobulin heavy chain (IgH)* gene locus on chromosome 14. The most common translocations include t(11;14) (CCND1), t(4;14) (FGFR3 and MMSET), t(6;14) (CCND3), t(14;16) (c-MAF and CCND2), and t(14;20) (MAFB), which lead to overexpression of translocation partner oncogenes[40]. The definition of R-ISS stages is as follows: stage I includes serum β_2-microglobulin level <3.5

mg/L, serum albumin level ≥3.5 g/dL, no high-risk chromosomal abnormalities [del(17p) and/or t(4;14) and/or t(14;16)], and normal LDH level; R-ISS III includes serum β_2-microglobulin level >5.5 mg/L and high-risk chromosomal abnormalities or high LDH level; and R-ISS II includes neither stage I nor III. Studies have shown that R-ISS stage III correlates with poor overall survival (OS)[36].

As mentioned above, current risk stratification partly focuses on cytogenetic aberrations. Although it is well-established that chromosomal aberrations significantly contribute to MM pathogenesis and are associated with inferior survival, several other genomic and proteomic markers have been reported to be useful in prognosis. Next generation sequencing (NGS) has identified mutations in genes involved in critical pathways that have prognostic significance, such as the NF-κB pathway (*TRAF, CYLD, LTB*), mitogen-activated protein kinase (MAPK) pathway (*KRAS, NRAS, BRAF*) and DNA repair pathways (*TP53, ATM, ATR*)[41,42]. Proteomic profiling of relapsed/refractory MM (RRMM) patients who received proteasome inhibitor (bortezomib)-based therapy identified upregulation of proteasome activator complex subunit 1 (PSME1)[43]. Interestingly, Glavey *et al*. conducted ECM profiling in premalignant status (MGUS), MM and healthy donors to identify a biomarker of ECM remodeling[44]. The ECM signature revealed upregulation of two ECM-affiliated proteins, Annexin A2 (ANXA2) and Galectin-1 (LGALS1) which were associated with inferior OS. Although the ECM is a major component of the TME, the role of ECM proteins per se as biomarkers remains incompletely understood. Collectively, genomic and proteomic markers have the potential for use in prognosis, but further validation is needed in clinical settings.

Bone Marrow Homing and Dissemination

As the name 'multiple' indicates, MM cells typically reside in multiple sites of the BM at diagnosis[45]. As the disease progresses, MM cells further disseminate to multiple different BM sites by exiting the bone marrow niche, re-entering the circulation, and migrating to a distant BM site[10]. Thus, adhesion, migration, and BM homing of MM cells are crucial steps in the pathogenesis of the disease.

The migration of MM cell towards the BM niche involves several steps. Initially, circulating MM cells adhere to the vascular endothelium, undergo transendothelial migration, penetrate the basement membrane and ECM, and, finally, localize into a niche[46]. During the extravasation step, MM cells transiently adhere to endothelial cells via tethering and rolling processes. Tethering and rolling are mediated by CD44 and P-selectin glycoprotein ligand-1 (PSGL-1) on the MM cell surface[47,48]. The chemokine SDF-1, produced by endothelial cells, further induces rolling and firm adhesion of MM cells. SDF-1-activated VLA-4 on MM cells allows the arrest of MM cells to endothelial cells and subsequent extravasation[49]. MM cells then traverse the basement membrane and ECM through the action of matrix metalloproteinases (MMPs). MM cells constitutively secrete MMP-9[50]. Moreover, exposure to SDF-1 on MM cells increases the expression of MMP-9 and membrane type 1-MMP (MT1-MMP)[51].

After transendothelial migration, MM cells localize into a BM niche, which relies on their responsiveness to chemoattractants. There are several such chemoattractants secreted by the BM cellular compartment, but only one has been particularly well-defined in the context of MM, namely, SDF-1[52]. SDF-1 is mainly secreted by BMSCs and enriched in the BM, and its cognate receptor, CXCR4 is highly expressed in circulating MM cells.

SDF-1 induces strong adhesion of circulating MM cells to the ECs, transendothelial migration, and homing into the BM (Figure 1.1). Other potential chemoattractants and promigratory factors in the BM microenvironment include chemokines and cytokines, such as monocyte chemoattractant protein-1 (MCP-1/CCL2)[53], macrophage inflammatory protein-1-α (MIP-1α/CCL3)[54], interferon gamma-induced protein 10 (IP-10/CXCL10)[55], insulin-like growth factor-1 (IGF-1)[56] and HGF[57]. Once localized within the niche, MM cell retention is mediated by adhesion to the ECM and BMSCs in the BM microenvironment via adhesion molecules[15].

Dissemination of MM cells involves their release from the BM niche and entry into the circulation[58]. As MM cells proliferate, the BM microenvironment becomes hypoxic, which reduces MM cell adhesion to BMSCs. HIF1α also induces an epithelial-mesenchymal transition (EMT)-like phenotype in MM cells[59]. Circulating MM cells exhibit lower levels of adhesion molecules, including integrin αL, αM, α4, α5, β1 (components of VLA-4, VLA-5, LFA-1), and syndecan-1, compared to their BM counterparts[60]. The process of egress is initiated by the loss of MM cell adhesion to the BM microenvironment, followed by migration to the vasculature and entry into the circulation. Dissemination and homing of MM cells occur continuously as the disease progresses.

The SDF-1/CXCR4 axis

SDF-1, also known as CXCL12 (C-X-C motif chemokine ligand 12), is a chemokine that plays a crucial role in various biological processes, including hematopoiesis, angiogenesis, cell migration and tumor metastasis[61]. SDF-1, mainly secreted by BMSCs, induces migration of hematopoietic stem cells, endothelial cells and leukocytes. It exerts

its effects by binding to G protein-coupled receptors, CXCR4[62] and CXCR7[63]. SDF-1 was first identified by cloning cytokines secreted from a bone marrow stromal cell line[64] and is a well-established chemokine in MM pathogenesis. It acts as a retention factor for MM cells in the BM microenvironment.

The effects of SDF-1 on MM cell migration are dose-dependent. At low concentrations (i.e., $\leq$50 nM), SDF-1 promotes MM cell chemotaxis, facilitating their migration. However, at higher concentrations (i.e., >50 nM), SDF-1 inhibits MM cell migration contributing to the retention of MM cells in the BM, where SDF-1 is enriched. This displays a bell-shaped curve in a dose-response migration assay, thus promoting MM cell migration in a dose-dependent manner at lower concentrations (e.g., in circulation) but slows their migration and retains MM cells in the BM where SDF-1 concentrations can be high[52]. Also, as a true chemoattractant, SDF-1 prevents migration in the negative gradient or in the absence of a gradient[65], which can also be responsible for the retention of the MM cells in the BM.

The receptor CXCR4, one of the receptors for SDF-1, plays a critical role in MM cell trafficking. Binding of SDF-1 to CXCR4 triggers the MM cell adhesion to fibronectin and BMSCs, and initiates migration through G protein signaling and dimerization of CXCR4[66–68]. Upon SDF-1 binding, the G protein complex dissociates and activates multiple downstream pathways. The SDF-1/CXCR4-induced migration has been shown to activate the phosphatidylinositol 3 kinase (PI3K) and extracellular signal-regulated kinase/mitogen-activated protein kinase (ERK/MAPK) pathways[52]. RhoA, a small GTPase, is also implicated in both MM cell adhesion and chemotaxis[68].

Previous studies have focused on the SDF-1/CXCR4 axis in MM homing. Roccaro *et al.* showed that neutralizing SDF-1 using selective anti-SDF-1 oligonucleotide (olaptesed) delays MM cell BM engraftment and tumor growth[69]. Also, ablating the SDF-1/CXCR4 axis by a CXCR4 small molecule inhibitor, AMD3100 (plerixafor), slows BM homing of human MM cells to ~40% of control mice by *in vivo* imaging[52]. These findings highlight the critical role of SDF-1 as a BM homing factor in MM.

Matrikine

Matrikine is an ECM-derived peptide formed by partial proteolysis of ECM macromolecules, which can regulate cellular activities[70]. The matrikine concept has been proposed to define protein fragments from ECM components that can cue the extracellular signal to surrounding cells. Importantly, the bioactivity of matrikine differs from that of its native, full-length ECM macromolecules due to the exposure of cryptic functional sites that are not exposed in the native, full-length parental ECM molecules. These enzymatic fragments of ECM macromolecules act as signaling molecules by binding to specific cell surface receptors of cytokines, chemokines and growth factors. Subsequently, numerous signaling pathways are activated, modulating cellular adhesion, migration, wound-healing, angiogenesis and/or proliferation depending on the different cell types being investiaged[71].

Multiple matrikines have been described in the literature as pro-migratory factors under various disease conditions. For instance, a collagen-derived matrikine, N-acetyl Pro-Gly-Pro (PGP), which signals via CXCR2, has been shown to act as a neutrophil chemoattractant during airway inflammation[72]. Moreover, in the context of pulmonary

emphysema, elastin fragments are upregulated in the diseased sites of lung. These elastin-derived matrikines attract monocytes contributing to the disease progression[73].

In the field of cancer, it is well-established that cancer cells remodel the TME, and extensive tissue remodeling contributes to cancer progression[74]. During ECM degradation, proteases including MMPs cleave ECM proteins releasing biologically active ECM fragments[75]. It has been shown that elastin fragments can stimulate cancer cell migration and invasion, as well as increase NF-κB activation in melanoma cells[76,77]. Similarly, laminin-derived matrikines signal through integrin[78] and epidermal growth factor receptor (EGFR)[79] promoting a pro-migratory phenotype in solid cancers.

In the context of MM, to date, one matrikine called versikine, derived from versican, has been studied for its effects on tumor-infiltrating immune cells and immunosurveillance. Versikine acts as a damage-associated molecular pattern (DAMP), promoting anti-tumor immunogenicity and antagonizing the tolerogenic actions of intact versican[80]. These findings indicate that ECM-derived peptides have distinct functions in the cellular milieu as signaling molecules under various disease conditions.

Hyaluronan and proteoglycan link protein 1 (HAPLN1)

HAPLN1, also known as cartilage link protein 1 (CRTL1) or link protein (LP), is an ECM protein, that functions in cartilage formation and tissue architecture[81]. HAPLN1 stabilizes the interaction between hyaluronic acid (HA) backbone and proteoglycans such as versican or aggrecan. It is a 354-amino acid glycoprotein with 3 domains after cleavage of the N-terminal signal peptide (SP): an immunoglobulin-like (Ig) domain, and two proteoglycan tandem repeat (PTR) domains (PTR1 and PTR2) (Figure 1.2). The Ig

domain binds to proteoglycans, while the PTR domains bind to HA, supporting ECM function[82]. HAPLN1 is thought to bind to a proteoglycan monomer in a 1:1 ratio, forming proteoglycan aggregates of HAPLN1-proteoglycan-HA in the cartilage ECM[83].

While HAPLN1 is well-known as a major component of cartilage, it is also expressed ubiquitously in various tissues including the intestine, placenta, heart, brain and others[82,84,85]. To understand the role of HAPLN1 in embryonic development and normal physiology, researchers have generated knockout and transgenic overexpression mouse models. While HAPLN1 overexpression in mouse cartilage has no overt phenotype, HAPLN1-null mice are post-natally lethal[86]. Most of the homozygous HAPLN1 null mice die shortly after birth due to respiratory failure, with only 7% surviving[81]. The surviving mice develop severe dwarfism and skeletal deformities. During cardiac development, HAPLN1 knockout mice exhibit atrioventricular septal defects and thin myocardium syndrome[84]. Additionally, in knockout mice, HAPLN1-deficiency attenuates perineuronal nets that control neuronal plasticity[85].

In contrast to its normal function in tissue architecture and development, mounting evidence suggests that HAPLN1 overexpression is associated with various types of solid cancer, either secreted by cancer cells themselves or by stromal cells. In malignant pleural mesothelioma, HAPLN1 mRNA expression was found to be 23-fold higher compared to matched normal healthy peritoneum as assessed by microarray analysis[87]. Higher expression of HAPLN1 mRNA in malignant pleural mesothelioma patients is associated with a poor prognosis making it as a potential prognostic marker. Similarly, HAPLN1 is overexpressed in highly metastatic melanoma when comparing the protein composition of the ECM in a human melanoma mouse xenograft model[88]. Proteomic

analysis identified that HAPLN1 is exclusively secreted by melanoma cells, as only human HAPLN1, not murine HAPLN1, was detected in a mouse xenograft model. Moreover, it has been reported that the tumorigenic role of HAPLN1 is mediated by ECM remodeling. HAPLN1 secreted from cancer-associated fibroblasts (CAFs) in gastric cancer promotes tumor migration and invasion[89]. In this scenario, malignant cells manipulate fibroblasts to upregulate HAPLN1 expression. HAPLN1 is the most upregulated gene in CAFs compared to their respective normal fibroblasts in gastric cancer patients, and higher HAPLN1 levels positively correlate with tumor staging and lymph node metastasis. Although the link between HAPLN1 and cancer is evident, the mechanistic understanding of how HAPLN1 plays a role in malignancies remains unclear.

NF-κB signaling

The nuclear factor-kappaB (NF-κB) protein was first discovered by the Baltimore group in the 1980s while characterizing the proteins that bind to the immunoglobulin κ light chain gene enhancers in activated B lymphocytes[90]. It was named based on how the authors identified the protein, *N*uclear *F*actor binding near the *κ* light chain gene in *B* cells, or NF-κB[91]. The NF-κB signaling pathway plays a central role in regulating various normal biological functions, including immune response, inflammation, cell survival, differentiation and proliferation, among others[92]. Importantly, dysregulation of NF-κB is implicated in various diseases, including cancer, where aberrant or constitutive NF-κB activation has been detected.

The NF-κB family consists of five members: NF-κB1 (p50/p105), NF-κB2 (p52/p100), RelA (p65), c-Rel and RelB[91]. The family members share a common Rel

Homology Domain (RHD), which mediates DNA binding, dimerization and inhibitor of κB (IκB) binding, followed by a nuclear localization sequence (NLS). The precursor proteins NF-κB1 (p105) and NF-κB2 (p100) have C-terminal ankyrin repeats that are proteolytically processed to generate p50 and p52, respectively. RelA (p65), c-Rel and RelB have a transactivation domain (TAD), In resting states, the inactive NF-κB dimers are bound to IκBα (NFKBIA), IκBβ (NFKBIB), IκBε (NFKBIE), or precursor proteins (p105, p100) in the cytoplasm. Upon stimulation, the NF-κB dimer is rapidly released from IκB, translocates into the nucleus, and finally binds to κB sites to regulate expression of target genes.

There are 2 general types of NF-κB pathways: the canonical and non-canonical pathways[93]. The canonical pathway involves the proteasomal degradation of IκBs, while the non-canonical pathway involves proteasomal processing of p100 rather than complete degradation. Due to distinct binding partners of IκB and p100, the canonical and noncanonical NF-κB pathways may regulate different target genes. The canonical pathway is rapid and transient, involving a kinase complex called the IκB kinase (IKK) complex. It can be activated by various stimuli, such as inflammatory cytokines and growth factors, which in turn activate the IKK complex (IKKα, IKKβ, and IKKγ/NEMO (NF-κB essential modulator)) with the IKKβ subunit mainly phosphorylating serine residues of IκB. Phosphorylated IκB then undergoes ubiquitination and subsequent degradation by the 26S proteasome. The released NF-κB dimer translocates to the nucleus and regulates its target genes. The canonical pathway NF-κB dimer contains either RelA or c-Rel, along with p50. In contrast to the canonical pathway, the non-canonical pathway displays slow and sustained kinetics and involves the activation of IKKα. The activators of the non-

canonical pathway are a subset of TNFR superfamily members, including lymphotoxin β (LTβ), B-cell activating factor (BAFF), CD40 and RANKL. Upon stimulation, the non-canonical pathway stabilizes the NF-κB-inducing kinase (NIK) and primarily activates IKKα. p100 is phosphorylated by IKKα and subsequently processed into a mature p52. The NF-κB signaling can be controlled by IκBα and IκBε, which translocate to the nucleus and capture DNA-bound NF-κB. Moreover, negative feedback is established via the induction of IκBα by NF-κB. Overall, different NF-κB dimers have distinct biological functions and their activities are tightly controlled.

STAT signaling

The signal transducer and activator of transcription (STAT) signaling pathway plays a central role in regulating various biological functions, including immune response, tissue repair, apoptosis and hematopoiesis[94]. It serves as a major pathway for transmitting external signals, i.e., ligand interactions with cell surface receptors, to the nucleus. Ligands involved in STAT signaling include growth factors (GFs), interferons (IFN), interleukins (ILs), hormones and colony-stimulating factors (CSFs) (Figure 1.3)[95].

The STAT family consists of 7 family members: STAT1, STAT2, STAT3, STAT4, STAT5A, STAT5B, and STAT6. These STAT proteins share high homology and contains 6 domains: an N-terminal domain, a DNA-binding domain, a Src homology 2 (SH2) domain, a coiled-coil domain, a linker domain, and a transcriptional activation domain[95]. Extracellular signals, via ligand binding to cell surface receptors, can activate latent cytoplasmic STAT proteins[96]. Receptors that can phosphorylate STAT include those carrying intrinsic kinase activity, i.e., receptor tyrosine kinases (RTKs), such as epidermal

growth factor receptor (EGFR), platelet-derived growth factor receptor (PDGFR), as well as receptors associated with Janus kinases (JAKs), such as interferon (IFN) receptors[97]. Upon ligand binding to its receptor, JAKs associated with the receptor are activated and mediate receptor phosphorylation and recruitment of STAT proteins for phosphorylation. The JAK family members include JAK1, JAK2, JAK3 and tyrosine kinase 2 (TYK2). JAKs have high homology with 4 domains, an N-terminal FERM (Four-point-one/4.1, Ezrin, Radixin and Moesin) domain, a SH2 domain, a pseudokinase domain and a C-terminal tyrosine kinase domain[98]. When a ligand binds to a receptor, the receptor dimerizes and brings associated JAKs together, allowing them to phosphorylate each other. Once activated, JAKs phosphorylate the receptor and the recruited STATs on tyrosine residues. Phosphorylation of a single tyrosine residue, typically around amino acid residue 700 in the transcriptional activation domain is required for STAT activation. Activated STATs then dimerize via phosphotyrosine-SH2 domain interactions and translocate to the nucleus, where they recognize specific DNA sequences ($TTCN_{3-4}GAAA$) to regulate target genes.

Several negative regulators of STAT signaling have been identified, including protein tyrosine phosphatases (PTPs), suppressors of cytokine signaling (SOCS) and protein inhibitors of activated STATs (PIAS). PTPs simply dephosphorylate or reverse the phosphorylation of STATs or JAKs. One well-known PTP is SHP-1[99], which can also bind to the IFNα receptor and reverse IFNα-induced STAT signaling[100]. SHP-1-null mouse macrophages show enhanced IFNα/β activation of the JAK/STAT pathway. The SOCS family comprises 8 members, including SOCS1, SOCS2, SOCS3, SOCS4, SOCS5, SOCS6, SOCS7 and cytokine-inducible SH2 domain protein (CIS)[98]. SOCS proteins are

transcription targets of STATs and participate in negative feedback loops. They directly bind to phospho-tyrosine regions of receptors and phosphorylated JAKs, inhibiting STAT recruitment and JAK activity. For instance, SOCS3 can simultaneously bind to JAK2 and gp130, a receptor component of IL-6 family cytokines. SOCS3 obstructs the substrate-binding site on JAK2, thereby blocking JAK/STAT signaling[101]. Additionally, SOCS proteins interact with elonginBC-cullin5 ubiquitin ligase, facilitating the ubiquitination and subsequent proteasomal degradation of JAKs and STATs[102]. Lastly, PIAS family members (PIAS1, PIAS3, PIASx and PIASy) are transcriptional co-regulators that interact with activated STAT dimers. PIAS1 and PIAS3 sequester STAT1 and STAT3, respectively, from binding to DNA sequences[103,104]. Moreover, PIAS acts as an E3 small ubiquitin-like modifier (SUMO) ligase. The lysine residue 703 (K703) in STAT1 can be sumoylated by PIAS1, PIAS3, and PIASx[105,106]. This SUMO-modified lysine residue is in close proximity to the regulatory tyrosine 701 residue (Y701) phosphorylated by JAKs. Mutation of lysine 703 in STAT1 increases the response to IFNγ. Overall, different STATs have distinct biological functions, and their activities are tightly controlled.

STAT signaling in MM

The STAT pathway is involved in the regulation of cell proliferation, differentiation and apoptosis. Under normal physiological conditions, STAT activity is transient and tightly controlled. However, constitutive activation has been observed in several types of cancer[95]. Among the STAT family members, STAT1 and STAT3 are the most studied for their role in cancer. STAT1 was first discovered in 1988 as a component of interferon-stimulated gene factor 3 (ISGF3), required for IFN signaling and an anti-viral response[107–

[110]. Upon stimulation, STAT1 is phosphorylated by JAK1/2 and TYK2 at tyrosine 701 residue and subsequently dimerizes and localizes to the nucleus as homo- or heterodimers[111–114]. Similar to STAT1, STAT3 is activated by tyrosine phosphorylation followed by dimerization and localization to the nucleus.

STAT1 has a complicated role in cancer[115]. STAT1 is well-established for its tumor suppressor function in various types of cancers[116]. It has been reported that the STAT1 expression is associated with a better prognosis in cancer indicating the tumor suppressive role. However, the role of STAT1 in tumor promotion is very context-dependent. Emerging evidence supports its tumor promoter role as well[117]. STAT1 has been implicated in chemoresistance[118], metastasis[119], epithelial-to-mesenchymal transition (EMT)[120,121], and adhesion and migration[122]. In terms of cancer metastasis and migration, STAT1 activation by cancer upregulated gene 2 (CUG2) in colon cancer cells enhanced the migratory ability[121]. In serous papillary endometrial cancer cells, STAT1 augments cell adhesion, migration, and tumor progression[123]. In the context of MM, STAT1 is not well understood and only a few papers have been published on this topic. IL-6 derived from BMSCs activates STAT1 and STAT3 in MM cells which in turn oppositely regulate the expression of CD38, the target of anti-CD38 monoclonal antibody (daratumumab) therapy[124]. While STAT3 downregulates CD38 expression which is not favorable to daratumumab therapy, STAT1 upregulates CD38 expression. Additionally, IFNγ-mediated STAT1 activation in MM cells upregulates B-cell CLL/lymphoma 6 (BCL6) expression[125]. BCL6 is a transcription factor known for its role in MM cell survival and proliferation, suggesting the pro-tumorigenic role of STAT1 in MM. Thus far, the role of STAT1 as a tumor suppressor or oncogene in MM pathogenesis is not definitive.

On the other hand, most of the earlier studies on STAT family members in MM have been carried out on STAT3. Constitutive activation of STAT3 is an unfavorable prognostic marker of MM[126]. Patients with activated STAT3, measured by immunohistochemistry analysis on BM tissue sections, have poorer progression-free survival (PFS) and overall survival (OS) than the phosphotyrosine-STAT3 negative patients. The aberrant activation may be due to hyperactivation of upstream kinase, JAK2, or disruption of the negative feedback loop[127]. Hotspot mutation of JAK2 (V617F) is identified in myeloproliferative disorder (MPD), which leads to constitutive phosphorylation and cytokine hypersensitivity[128]. Yet, the presence of this mutation in MM remains unclear[129]. The negative regulators, SHP-1, SHP-2 and SOCS-1 are abnormally repressed in MM patients[130]. Cytokines are abundant in the BM microenvironment. Among those, IL-6 is a key survival factor for MM cells and is a potent activator of the STAT3 pathway. IL-6 secreted by BMSCs activates STAT3 in MM cells through JAK1, JAK2 and TYK2. In addition to paracrine production of IL-6, autocrine IL-6 is involved in high proliferative capacity and drug resistance[131]. STAT3 mediates many biological functions responsible for MM cell survival and proliferation. STAT3 induces anti-apoptotic Bcl2 family proteins, including Bcl-xL, Mcl-1 and survivin, and resistance to Fas-mediated apoptosis[132,133]. Given the importance of STAT signaling in MM, these findings suggest a great potential for the JAK/STAT pathway as a therapeutic target.

Aims of the Thesis

MM cells continuously disseminate to multiple different BM sites as the disease progresses. MM cell adhesion, migration, and BM homing are key steps in MM

pathogenicity. Homing of MM cells to a protective BM niche is crucial in MM dissemination, but the involved mechanisms are incompletely understood. Previous studies have mainly focused on SDF-1 as a BM homing factor in MM. Nonetheless, blocking the SDF-1/CXCR4 axis is not sufficient to abrogate MM homing[134] indicating that SDF-1 is critical but not the sole BM homing factor so there are other BM homing factors yet to be determined.

The BM microenvironment is critical for the dissemination, growth and survival of MM cells. Interestingly, our group identified HAPLN1 matrikine as a novel pathogenic factor and drug resistance inducer in MM[135]. It was found that HAPLN1 is detectable in MM patient BM plasma, secreted by BMSCs, and processed by MMP2 to act as a matrikine[135,136]. In MM patient BM plasma samples, variable levels of HAPLN1 and its small fragments containing PTR domains are detected. Moreover, the detection of these fragments correlated with patients having progressive disease, an unfavorable category of treatment response criteria[137]. However, the role of this HAPLN1-derived matrikine is not well understood. The study revealed that the recombinant PTR domains, but not full-length HAPLN1, can activate NF-κB inducing drug resistance in MM cells. However, little is known of any other potential functions of HAPLN1 and its matrikine.

In this thesis, I hypothesized that the HAPLN1-derived matrikine is a novel pro-migratory and BM homing factor in MM. This thesis aims to investigate the potential role of the HAPLN1 matrikine in MM cell adhesion, migration, and *in vivo* BM homing using a human MM mouse xenograft model. I utilized a recombinant protein of a specific HAPLN1 PTR domain(s) as a representative HAPLN1-derived matrikine. In addition, I identified the downstream malignant signaling pathway of the matrikine to be STAT1. This study

demonstrates that the matrikine is an important player in MM BM homing and the unexplored function of STAT1 in MM. Overall, my thesis reveals for the first time the role of any matrikine in MM cell migration, adhesion, or homing in this incurable disease.

Additionally, I developed an immunoassay to measure HAPLN1 levels in patient BM plasma fraction to assess their clinical relevance. Finally, I also completed a study which was initiated by a previous graduate student, demonstrating HAPLN1 matrikine as an inducer of MM cell resistance to multiple therapeutic drugs (Appendix). Together, my thesis study demonstrates HAPLN1 as a pathogenic factor in MM, acting as a BM homing factor and an inducer of drug resistance. Also, I demonstrated that high HAPLN1 levels in BM samples are associated with poor clinical outcomes in NDMM patients, thus suggesting its potential use as a prognostic marker and therapeutic target.

REFERENCES

1. Bianchi, G. & Anderson, K. C. Understanding biology to tackle the disease: Multiple myeloma from bench to bedside, and back. *Ca Cancer J Clin* 64, 422–444 (2014).

2. *Cancer Facts & Figures 2023, American Cancer Society*. (American Cancer Society, 2023).

3. The Surveillance, Epidemiology, and End Results (SEER) Program, National Cancer Institute. https://seer.cancer.gov/statfacts.

4. Ho, M. *et al.* Changing paradigms in diagnosis and treatment of monoclonal gammopathy of undetermined significance (MGUS) and smoldering multiple myeloma (SMM). *Leukemia* 34, 3111–3125 (2020).

5. Rajkumar, S. V. *et al.* International Myeloma Working Group updated criteria for the diagnosis of multiple myeloma. *Lancet Oncol* 15, e538–e548 (2014).

6. Rajkumar, S. V. MGUS and Smoldering Multiple Myeloma: Update on Pathogenesis, Natural History, and Management. *Hematology* 2005, 340–345 (2005).

7. Kyle, R. A. *et al.* Clinical Course and Prognosis of Smoldering (Asymptomatic) Multiple Myeloma. *New Engl J Medicine* 356, 2582–2590 (2007).

8. Kyle, R. A. *et al.* Long-Term Follow-up of Monoclonal Gammopathy of Undetermined Significance. *New Engl J Med* 378, 241–249 (2018).

9. Paget, S. The distribution of secondary growths in cancer of the breast. 1889. *Cancer Metastasis Rev* 8, 98–101 (1989).

10. Manier, S., Sacco, A., Leleu, X., Ghobrial, I. M. & Roccaro, A. M. Bone Marrow Microenvironment in Multiple Myeloma Progression. *J Biomed Biotechnol* 2012, 157496 (2012).

11. Hallek, M., Bergsagel, P. L. & Anderson, K. C. Multiple myeloma: increasing evidence for a multistep transformation process. *Blood* 91, 3–21 (1998).

12. Noonan, K. & Borrello, I. The immune microenvironment of myeloma. *Cancer Microenviron* 4, 313–323 (2011).

13. Kibler, C. *et al.* Adhesive Interactions of Human Multiple Myeloma Cell Lines with Different Extracellular Matrix Molecules. *Cell Commun Adhesion* 5, 307–323 (2009).

14. Balakumaran, A., Robey, P. G., Fedarko, N. & Landgren, O. Bone marrow microenvironment in myelomagenesis: its potential role in early diagnosis. *Expert Rev Mol Diagn* 10, 465–480 (2010).

15. Moser-Katz, T., Joseph, N. S., Dhodapkar, M. V., Lee, K. P. & Boise, L. H. Game of Bones: How Myeloma Manipulates Its Microenvironment. *Frontiers Oncol* 10, 625199 (2021).

16. Neri, P. *et al.* Integrin β7-mediated regulation of multiple myeloma cell adhesion, migration, and invasion. *Blood* 117, 6202–6213 (2011).

17. Landowski, T. H., Olashaw, N. E., Agrawal, D. & Dalton, W. S. Cell adhesion-mediated drug resistance (CAM-DR) is associated with activation of NF-kappa B (RelB/p50) in myeloma cells. *Oncogene* 22, 2417–21 (2003).

18. Chen, C., Zhao, S., Karnad, A. & Freeman, J. W. The biology and role of CD44 in cancer progression: therapeutic implications. *J. Hematol. Oncol.* 11, 64 (2018).

19. Bjorklund, C. C. *et al.* Evidence of a role for CD44 and cell adhesion in mediating resistance to lenalidomide in multiple myeloma: therapeutic implications. *Leukemia* 28, 373–383 (2014).

20. Elenius, K., Salmivirta, M., Inki, P., Mali, M. & Jalkanen, M. Binding of human syndecan to extracellular matrix proteins. *J Biol Chem* 265, 17837–17843 (1990).

21. Stepp, M. A., Pal-Ghosh, S., Tadvalkar, G. & Pajoohesh-Ganji, A. Syndecan-1 and Its Expanding List of Contacts. *Adv Wound Care* 4, 235–249 (2015).

22. Hideshima, T. & Anderson, K. C. Molecular mechanisms of novel therapeutic approaches for multiple myeloma. *Nat. Rev. Cancer* 2, 927–937 (2002).

23. Uchiyama, H., Barut, B. A., Chauhan, D., Cannistra, S. A. & Anderson, K. C. Characterization of adhesion molecules on human myeloma cell lines. *Blood* 80, 2306–2314 (1992).

24. Hideshima, T. & Anderson, K. C. Signaling Pathway Mediating Myeloma Cell Growth and Survival. *Cancers* 13, 216 (2021).

25. Hideshima, T., Nakamura, N., Chauhan, D. & Anderson, K. C. Biologic sequelae of interleukin-6 induced PI3-K/Akt signaling in multiple myeloma. *Oncogene* 20, 5991–6000 (2001).

26. Broek, I. V. *et al.* Bone marrow endothelial cells increase the invasiveness of human multiple myeloma cells through upregulation of MMP-9: evidence for a role of hepatocyte growth factor. *Leukemia* 18, 976–982 (2004).

27. Bhaskar, A. & Tiwary, B. N. Hypoxia inducible factor-1 alpha and multiple myeloma. *Int J Adv Res* 4, 706–715 (2016).

28. Rajkumar, S. V. *et al.* Bone marrow angiogenesis in 400 patients with monoclonal gammopathy of undetermined significance, multiple myeloma, and primary amyloidosis. *Clin Cancer Res Official J Am Assoc Cancer Res* 8, 2210–6 (2002).

29. Papadopoulou, E. C., Batzios, S. P., Dimitriadou, M., Perifanis, V. & Garipidou, V. Multiple myeloma and bone disease: pathogenesis and current therapeutic approaches. *Hippokratia* 14, 76–81 (2010).

30. Choi, S. J. *et al.* Antisense inhibition of macrophage inflammatory protein 1-alpha blocks bone destruction in a model of myeloma bone disease. *J Clin Investigation* 108, 1833–41 (2001).

31. Oba, Y. *et al.* MIP-1α utilizes both CCR1 and CCR5 to induce osteoclast formation and increase adhesion of myeloma cells to marrow stromal cells. *Exp Hematol* 33, 272–278 (2005).

32. Michigami, T. *et al.* Cell–cell contact between marrow stromal cells and myeloma cells via VCAM-1 and α4β1-integrin enhances production of osteoclast-stimulating activity. *Blood* 96, 1953–1960 (2000).

33. Giuliani, N., Rizzoli, V. & Roodman, G. D. Multiple myeloma bone disease: pathophysiology of osteoblast inhibition. *Blood* 108, 3992–3996 (2006).

34. Giuliani, N. *et al.* Myeloma cells block RUNX2/CBFA1 activity in human bone marrow osteoblast progenitors and inhibit osteoblast formation and differentiation. *Blood* 106, 2472–2483 (2005).

35. Barille, S., Collette, M., Bataille, R. & Amiot, M. Myeloma cells upregulate interleukin-6 secretion in osteoblastic cells through cell-to-cell contact but downregulate osteocalcin. *Blood* 86, 3151–3159 (1995).

36. Palumbo, A. *et al.* Revised International Staging System for Multiple Myeloma: A Report From International Myeloma Working Group. *J. Clin. Oncol.* 33, 2863–2869 (2015).

37. Cassuto, J. P., Krebs, B. P., Viot, G., Dujardin, P. & Masseyeff, R. Beta 2 microglobulin, a tumour marker of lymphoproliferative disorder. *Lancet Lond. Engl.* 2, 950 (1978).

38. Dimopoulos, M. A., Barlogie, B., Smith, T. L. & Alexanian, R. High serum lactate dehydrogenase level as a marker for drug resistance and short survival in multiple myeloma. *Ann. Intern. Medicine* 115, 931–5 (1991).

39. Ross, F. M. *et al.* Report from the European Myeloma Network on interphase FISH in multiple myeloma and related disorders. *Haematologica* 97, 1272–1277 (2012).

40. Soliman, A. M., Das, S. & Teoh, S. L. Next-Generation Biomarkers in Multiple Myeloma: Understanding the Molecular Basis for Potential Use in Diagnosis and Prognosis. *Int. J. Mol. Sci.* 22, 7470 (2021).

41. Chapman, M. A. *et al.* Initial genome sequencing and analysis of multiple myeloma. *Nature* 471, 467–472 (2011).

42. Wallington-Beddoe, C. T. & Mynott, R. L. Prognostic and predictive biomarker developments in multiple myeloma. *J. Hematol. Oncol.* 14, 151 (2021).

43. Dytfeld, D. *et al.* Comparative proteomic profiling of refractory/relapsed multiple myeloma reveals biomarkers involved in resistance to bortezomib-based therapy. *Oncotarget* 7, 56726–56736 (2016).

44. Glavey, S. V. *et al.* Proteomic characterization of human multiple myeloma bone marrow extracellular matrix. *Leukemia* 31, 2426–2434 (2017).

45. Shain, K. Metastatic myeloma? *Blood* 119, 5612–5613 (2012).

46. Hideshima, T., Mitsiades, C., Tonon, G., Richardson, P. G. & Anderson, K. C. Understanding multiple myeloma pathogenesis in the bone marrow to identify new therapeutic targets. *Nat Rev Cancer* 7, 585–598 (2007).

47. Asosingh, K. *et al.* A unique pathway in the homing of murine multiple myeloma cells: CD44v10 mediates binding to bone marrow endothelium. *Cancer Res* 61, 2862–5 (2001).

48. Azab, A. K. *et al.* P-selectin glycoprotein ligand regulates the interaction of multiple myeloma cells with the bone marrow microenvironment. *Blood* 119, 1468–1478 (2012).

49. Parmo-Cabañas, M. *et al.* Integrin α4β1 involvement in stromal cell-derived factor-1α-promoted myeloma cell transendothelial migration and adhesion: role of cAMP and the actin cytoskeleton in adhesion. *Exp Cell Res* 294, 571–580 (2004).

50. Barillé, S. *et al.* Metalloproteinases in Multiple Myeloma: Production of Matrix Metalloproteinase-9 (MMP-9), Activation of proMMP-2, and Induction of MMP-1 by Myeloma Cells. *Blood* 90, 1649–1655 (1997).

51. Parmo-Cabañas, M. *et al.* Role of metalloproteinases MMP-9 and MT1-MMP in CXCL12-promoted myeloma cell invasion across basement membranes. *J. Pathol.* 208, 108–118 (2006).

52. Alsayed, Y. *et al.* Mechanisms of regulation of CXCR4/SDF-1 (CXCL12)-dependent migration and homing in multiple myeloma. *Blood* 109, 2708–2717 (2007).

53. Vanderkerken, K. *et al.* Monocyte chemoattractant protein-1 (MCP-1), secreted by bone marrow endothelial cells, induces chemoattraction of 5T multiple myeloma cells. *Clin Exp Metastas* 19, 87–90 (2002).

54. Lentzsch, S. *et al.* Macrophage inflammatory protein 1-alpha (MIP-1α) triggers migration and signaling cascades mediating survival and proliferation in multiple myeloma (MM) cells. *Blood* 101, 3568–3573 (2003).

55. Lee, J.-H. *et al.* CXCL10 Promotes Osteolytic Bone Metastasis by Enhancing Cancer Outgrowth and Osteoclastogenesis. *Cancer Res* 72, 3175–3186 (2012).

56. Qiang, Y.-W., Yao, L., Tosato, G. & Rudikoff, S. Insulin-like growth factor I induces migration and invasion of human multiple myeloma cells. *Blood* 103, 301–308 (2004).

57. Holt, R. U. *et al.* Hepatocyte growth factor promotes migration of human myeloma cells. *Haematologica* 93, 619–622 (2008).

58. Zeissig, M. N., Zannettino, A. C. W. & Vandyke, K. Tumour Dissemination in Multiple Myeloma Disease Progression and Relapse: A Potential Therapeutic Target in High-Risk Myeloma. *Cancers* 12, 3643 (2020).

59. Azab, A. K. *et al.* Hypoxia promotes dissemination of multiple myeloma through acquisition of epithelial to mesenchymal transition-like features. *Blood* 119, 5782–5794 (2012).

60. Paiva, B. *et al.* Detailed characterization of multiple myeloma circulating tumor cells shows unique phenotypic, cytogenetic, functional, and circadian distribution profile. *Blood* 122, 3591–3598 (2013).

61. Teicher, B. A. & Fricker, S. P. CXCL12 (SDF-1)/CXCR4 Pathway in Cancer. *Clin Cancer Res* 16, 2927–2931 (2010).

62. Bleul, C. C. *et al.* The lymphocyte chemoattractant SDF-1 is a ligand for LESTR/fusin and blocks HIV-1 entry. *Nature* 382, 829–833 (1996).

63. Balabanian, K. *et al.* The Chemokine SDF-1/CXCL12 Binds to and Signals through the Orphan Receptor RDC1 in T Lymphocytes*. *J Biol Chem* 280, 35760–35766 (2005).

64. Tashiro, K. *et al.* Signal Sequence Trap: a Cloning Strategy for Secreted Proteins and Type I Membrane Proteins. *Science* 261, 600–603 (1993).

65. Gorter, D. J. J. de *et al.* The small GTPase Ral mediates SDF-1-induced migration of B cells and multiple myeloma cells. *Blood* 111, 3364–3372 (2008).

66. Vila-Coro, A. J. *et al.* The chemokine SDF-1alpha triggers CXCR4 receptor dimerization and activates the JAK/STAT pathway. *FASEB journal : official publication of the Federation of American Societies for Experimental Biology* 13, 1699–1710 (1999).

67. Sanz-Rodríguez, F., Hidalgo, A. & Teixidó, J. Chemokine stromal cell-derived factor-1alpha modulates VLA-4 integrin-mediated multiple myeloma cell adhesion to CS-1/fibronectin and VCAM-1. *Blood* 97, 346–351 (2001).

68. Azab, A. K. *et al.* RhoA and Rac1 GTPases play major and differential roles in stromal cell-derived factor-1-induced cell adhesion and chemotaxis in multiple myeloma. *Blood* 114, 619–629 (2009).

69. Roccaro, A. M. *et al.* SDF-1 inhibition targets the bone marrow niche for cancer therapy. *Cell Reports* 9, 118–128 (2014).

70. Maquart, F.-X., Pasco, S., Ramont, L., Hornebeck, W. & Monboisse, J.-C. An introduction to matrikines: extracellular matrix-derived peptides which regulate cell activity. Implication in tumor invasion. *Crit Rev Oncol Hemat* 49, 199–202 (2004).

71. Ricard-Blum, S. & Salza, R. Matricryptins and matrikines: biologically active fragments of the extracellular matrix. *Exp Dermatol* 23, 457–463 (2014).

72. Weathington, N. M. *et al.* A novel peptide CXCR ligand derived from extracellular matrix degradation during airway inflammation. *Nat Med* 12, 317–323 (2006).

73. Hunninghake, G. W. *et al.* Elastin fragments attract macrophage precursors to diseased sites in pulmonary emphysema. *Science* 212, 925–927 (1981).

74. Slany, A. *et al.* Extracellular matrix remodeling by bone marrow fibroblast-like cells correlates with disease progression in multiple myeloma. *J Proteome Res* 13, 844–854 (2014).

75. Winkler, J., Abisoye-Ogunniyan, A., Metcalf, K. J. & Werb, Z. Concepts of extracellular matrix remodelling in tumour progression and metastasis. *Nat Commun* 11, 5120–19 (2020).

76. Pocza, P., Süli-Vargha, H., Darvas, Z. & Falus, A. Locally generated VGVAPG and VAPG elastin-derived peptides amplify melanoma invasion via the galectin-3 receptor. *Int. J. Cancer* 122, 1972–1980 (2008).

77. Debret, R. *et al.* Elastin fragments induce IL-1beta upregulation via NF-kappaB pathway in melanoma cells. *J Invest Dermatol* 126, 1860–1868 (2006).

78. Tsuruta, D. *et al.* Laminin-332-integrin interaction: a target for cancer therapy? *Curr Med Chem* 15, 1968–1975 (2008).

79. Grahovac, J. & Wells, A. Matrikine and matricellular regulators of EGF receptor signaling on cancer cell migration and invasion. *Lab Invest* 94, 31–40 (2014).

80. Hope, C. *et al.* Immunoregulatory roles of versican proteolysis in the myeloma microenvironment. *Blood* 128, 680–685 (2016).

81. Watanabe, H. & Yamada, Y. Mice lacking link protein develop dwarfism and craniofacial abnormalities. *Nat Genet* 21, 225–229 (1999).

82. Spicer, A. P., Joo, A. & Bowling, R. A. A hyaluronan binding link protein gene family whose members are physically linked adjacent to chondroitin sulfate proteoglycan core protein genes: the missing links. *J Biological Chem* 278, 21083–91 (2003).

83. Neame, P. J. & Barry, F. P. The link proteins. *Experientia* 49, 393–402 (1993).

84. Wirrig, E. E. *et al.* Cartilage link protein 1 (Crtl1), an extracellular matrix component playing an important role in heart development. *Dev Biol* 310, 291–303 (2007).

85. Carulli, D. *et al.* Animals lacking link protein have attenuated perineuronal nets and persistent plasticity. *Brain* 133, 2331–2347 (2010).

86. Czipri, M. *et al.* Genetic Rescue of Chondrodysplasia and the Perinatal Lethal Effect of Cartilage Link Protein Deficiency*. *J Biol Chem* 278, 39214–39223 (2003).

87. Ivanova, A. V. *et al.* Protumorigenic Role of HAPLN1 and Its IgV Domain in Malignant Pleural Mesothelioma. *Clin Cancer Res* 15, 2602–2611 (2009).

88. Naba, A. *et al.* The Matrisome: In Silico Definition and In Vivo Characterization by Proteomics of Normal and Tumor Extracellular Matrices*. *Mol Cell Proteom Mcp* 11, M111.014647 (2012).

89. Zhang, T. *et al.* Cancer-associated fibroblasts-derived HAPLN1 promotes tumour invasion through extracellular matrix remodeling in gastric cancer. *Gastric Cancer* 25, 346–359 (2022).

90. Sen, R. & Baltimore, D. Multiple nuclear factors interact with the immunoglobulin enhancer sequences. *Cell* 46, 705–716 (1986).

91. Zhang, Q., Lenardo, M. J. & Baltimore, D. 30 Years of NF-κB: A Blossoming of Relevance to Human Pathobiology. *Cell* 168, 37–57 (2017).

92. Dolcet, X., Llobet, D., Pallares, J. & Matias-Guiu, X. NF-kB in development and progression of human cancer. *Virchows Arch.* 446, 475–482 (2005).

93. Hayden, M. S. & Ghosh, S. Shared Principles in NF-κB Signaling. *Cell* 132, 344–362 (2008).

94. Owen, K. L., Brockwell, N. K. & Parker, B. S. JAK-STAT Signaling: A Double-Edged Sword of Immune Regulation and Cancer Progression. *Cancers* 11, 2002 (2019).

95. Hu, X., li, J., Fu, M., Zhao, X. & Wang, W. The JAK/STAT signaling pathway: from bench to clinic. *Signal Transduct Target Ther* 6, 402 (2021).

96. Jr., J. E. D., Kerr, Ian M. & Stark, G. R. Jak-STAT Pathways and Transcriptional Activation in Response to IFNs and Other Extracellular Signaling Proteins. *Science* 264, 1415–1421 (1994).

97. Jr., J. E. D. STATs and Gene Regulation. *Science* 277, 1630–1635 (1997).

98. Seif, F. *et al.* The role of JAK-STAT signaling pathway and its regulators in the fate of T helper cells. *Cell Commun Signal Ccs* 15, 23 (2017).

99. Ram, P. A. & Waxman, D. J. Interaction of Growth Hormone-activated STATs with SH2-containing Phosphotyrosine Phosphatase SHP-1 and Nuclear JAK2 Tyrosine Kinase*. *J Biol Chem* 272, 17694–17702 (1997).

100. David, M., Chen, H. E., Goelz, S., Larner, A. C. & Neel, B. G. Differential regulation of the alpha/beta interferon-stimulated Jak/Stat pathway by the SH2 domain-containing tyrosine phosphatase SHPTP1. *Mol Cell Biol* 15, 7050–7058 (1995).

101. Kershaw, N. J. *et al.* SOCS3 binds specific receptor–JAK complexes to control cytokine signaling by direct kinase inhibition. *Nat Struct Mol Biol* 20, 469–476 (2013).

102. Babon, J. J. *et al.* The SOCS Box Domain of SOCS3: Structure and Interaction with the ElonginBC-Cullin5 Ubiquitin Ligase. *J Mol Biol* 381, 928–940 (2008).

103. Liu, B. *et al.* Inhibition of Stat1-mediated gene activation by PIAS1. *Proc National Acad Sci* 95, 10626–10631 (1998).

104. Chung, C. D. *et al.* Specific Inhibition of Stat3 Signal Transduction by PIAS3. *Science* 278, 1803–1805 (1997).

105. Ungureanu, D. *et al.* PIAS proteins promote SUMO-1 conjugation to STAT1. *Blood* 102, 3311–3 (2003).

106. Rogers, R. S., Horvath, C. M. & Matunis, M. J. SUMO Modification of STAT1 and Its Role in PIAS-mediated Inhibition of Gene Activation*. *J Biol Chem* 278, 30091–30097 (2003).

107. Levy, D. E., Kessler, D. S., Pine, R., Reich, N. & Darnell, J. E. Interferon-induced nuclear factors that bind a shared promoter element correlate with positive and negative transcriptional control. *Gene Dev* 2, 383–393 (1988).

108. Fu, X. Y., Kessler, D. S., Veals, S. A., Levy, D. E. & Darnell, J. E. ISGF3, the transcriptional activator induced by interferon alpha, consists of multiple interacting polypeptide chains. *Proc National Acad Sci* 87, 8555–9 (1990).

109. Fu, X. Y. A transcription factor with SH2 and SH3 domains is directly activated by an interferon alpha-induced cytoplasmic protein tyrosine kinase(s). *Cell* 70, 323–35 (1992).

110. Shuai, K., Stark, G. R., Kerr, I. M. & Darnell, J. E. A single phosphotyrosine residue of Stat91 required for gene activation by interferon-gamma. *Science* 261, 1744–6 (1993).

111. Velazquez, L., Fellous, M., Stark, G. R. & Pellegrini, S. A protein tyrosine kinase in the interferon alpha/beta signaling pathway. *Cell* 70, 313–22 (1992).

112. Müller, M. *et al.* The protein tyrosine kinase JAK1 complements defects in interferon-alpha/beta and -gamma signal transduction. *Nature* 366, 129–35 (1993).

113. Shuai, K. *et al.* Interferon activation of the transcription factor Stat91 involves dimerization through SH2-phosphotyrosyl peptide interactions. *Cell* 76, 821–8 (1994).

114. Chen, X. *et al.* Crystal structure of a tyrosine phosphorylated STAT-1 dimer bound to DNA. *Cell* 93, 827–39 (1998).

115. Meissl, K., Macho-Maschler, S., Müller, M. & Strobl, B. The good and the bad faces of STAT1 in solid tumours. *Cytokine* 89, 12–20 (2017).

116. Zhang, Y. & Liu, Z. STAT1 in cancer: friend or foe? *Discovery medicine* 24, 19–29 (2017).

117. Adámková, L., Soucková, K. & Kovarík, J. Transcription protein STAT1: biology and relation to cancer. *Folia biologica* 53, 1–6 (2007).

118. Khodarev, N. N. *et al.* STAT1 is overexpressed in tumors selected for radioresistance and confers protection from radiation in transduced sensitive cells. *Proc National Acad Sci* 101, 1714–1719 (2004).

119. STAT1 pathway mediates amplification of metastatic potential and resistance to therapy. *Plos One* 4, e5821 (2009).

120. Kaowinn, S., Kaewpiboon, C., Koh, S. S., Krämer, O. H. & Chung, Y.-H. STAT1-HDAC4 signaling induces epithelial-mesenchymal transition and sphere formation of cancer cells overexpressing the oncogene, CUG2. *Oncol Rep* 40, 2619–2627 (2018).

121. Malilas, W. *et al.* Cancer upregulated gene 2, a novel oncogene, enhances migration and drug resistance of colon cancer cells via STAT1 activation. *Int J Oncol* 43, 1111–1116 (2013).

122. Xie, B. *et al.* Focal adhesion kinase activates Stat1 in integrin-mediated cell migration and adhesion. *J Biol Chem* 276, 19512–19523 (2001).

123. Kharma, B. *et al.* STAT1 drives tumor progression in serous papillary endometrial cancer. *Cancer Res* 74, 6519–6530 (2014).

124. Ogiya, D. *et al.* The JAK-STAT pathway regulates CD38 on myeloma cells in the bone marrow microenvironment: therapeutic implications. *Blood* 136, 2334–2345 (2020).

125. Ujvari, D. *et al.* Interferon γ is a strong, STAT1-dependent direct inducer of BCL6 expression in multiple myeloma cells. *Biochem Bioph Res Co* 498, 502–508 (2018).

126. Jung, S.-H. *et al.* STAT3 expression is associated with poor survival in non-elderly adult patients with newly diagnosed multiple myeloma. *Blood Res* 52, 293–299 (2017).

127. Chong, P. S. Y., Chng, W.-J. & Mel, S. de. STAT3: A Promising Therapeutic Target in Multiple Myeloma. *Cancers* 11, 731 (2019).

128. Levine, R. L. *et al.* The JAK2V617F activating mutation occurs in chronic myelomonocytic leukemia and acute myeloid leukemia, but not in acute lymphoblastic leukemia or chronic lymphocytic leukemia. *Blood* 106, 3377–9 (2005).

129. Fiorini, A. *et al.* Screening of JAK2 V617F mutation in multiple myeloma. *Leukemia* 20, 1912–1913 (2006).

130. Beldi-Ferchiou, A. *et al.* Abnormal repression of SHP-1, SHP-2 and SOCS-1 transcription sustains the activation of the JAK/STAT3 pathway and the progression of the disease in multiple myeloma. *Plos One* 12, e0174835 (2017).

131. Frassanito, M. A., Cusmai, A., Iodice, G. & Dammacco, F. Autocrine interleukin-6 production and highly malignant multiple myeloma: relation with resistance to drug-induced apoptosis. *Blood* 97, 483–489 (2001).

132. Catlett-Falcone, R. *et al.* Constitutive Activation of Stat3 Signaling Confers Resistance to Apoptosis in Human U266 Myeloma Cells. *Immunity* 10, 105–115 (1999).

133. Epling-Burnette, P. K. *et al.* Inhibition of STAT3 signaling leads to apoptosis of leukemic large granular lymphocytes and decreased Mcl-1 expression. *J Clin Invest* 107, 351–362 (2001).

134. Alsayed, Y. *et al.* Mechanisms of regulation of CXCR4/SDF-1 (CXCL12)-dependent migration and homing in multiple myeloma. *Blood* 109, 2708–2717 (2007).

135. Huynh, M. *et al.* Hyaluronan and proteoglycan link protein 1 (HAPLN1) activates bortezomib-resistant NF-κB activity and increases drug resistance in multiple myeloma. *J Biol Chem* 293, 2452–2465 (2018).

136. Mark, C., Warrick, J., Callander, N. S., Hematti, P. & Miyamoto, S. A Hyaluronan and Proteoglycan Link Protein 1 Matrikine: Role of Matrix Metalloproteinase 2 in Multiple Myeloma NF-κB Activation and Drug Resistance. *Mol Cancer Res* 20, 1456–1466 (2022).

137. Rajkumar, S. V. *et al.* Consensus recommendations for the uniform reporting of clinical trials: report of the International Myeloma Workshop Consensus Panel 1. *Blood* 117, 4691–4695 (2011).

Figure 1.1

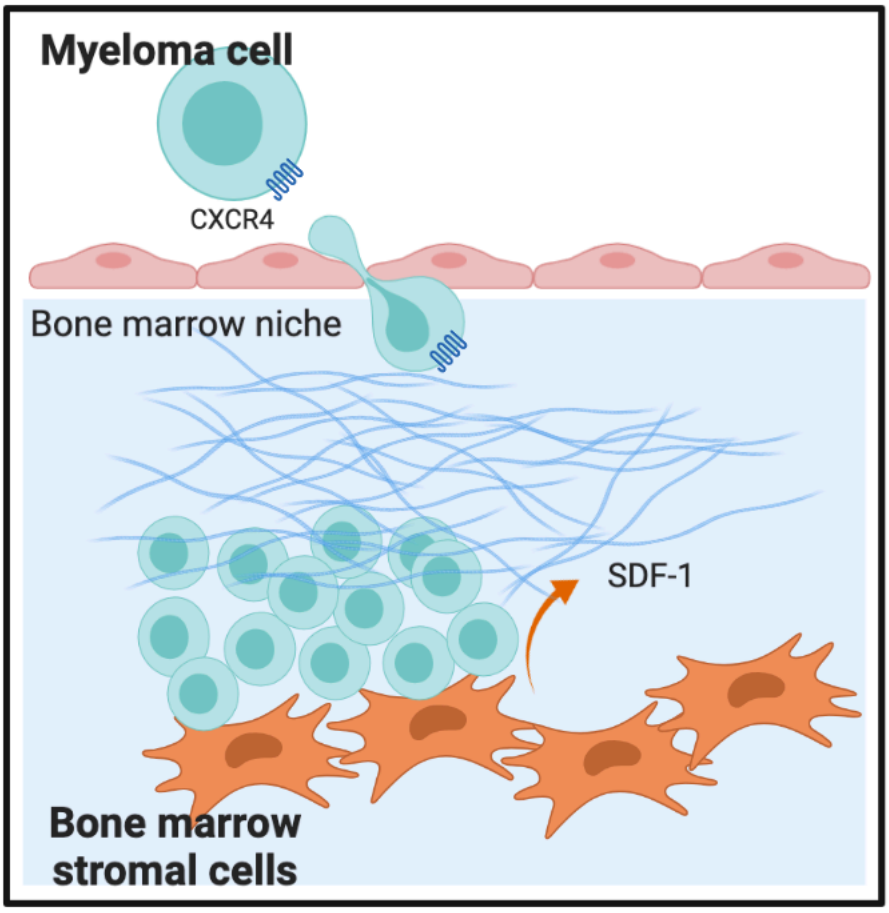

Figure 1.1. Diagram depicting bone marrow homing of myeloma cells. Multiple myeloma (MM) cells localize into a BM niche following transendothelial migration. The homing process of MM cells relies on their responsiveness to chemoattractants. SDF-1, a well-established chemoattractant for MM cells, is mainly secreted by bone marrow stromal cells (BMSCs). The cognate receptor, CXCR4 is highly expressed in circulating MM cells. Upon binding of SDF-1, circulating MM cells undergo strong adhesion to ECs. SDF-1 induces transendothelial migration, and homing into the BM.

Figure 1.2

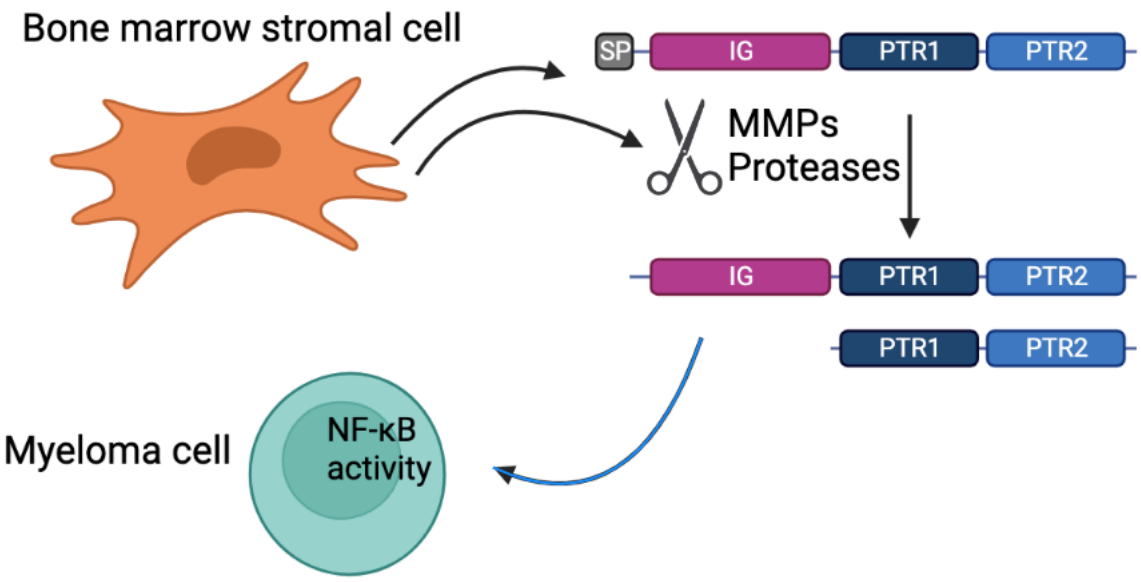

Figure 1.2. Diagram depicting the generation of HAPLN1 matrikine. The full-length HAPLN1 can be cleaved by matrix metalloproteinases (MMPs) and proteases, resulting in the generation of a fragment containing all three domains and the C-terminal fragments containing only PTR1/2 domains.

Figure 1.3

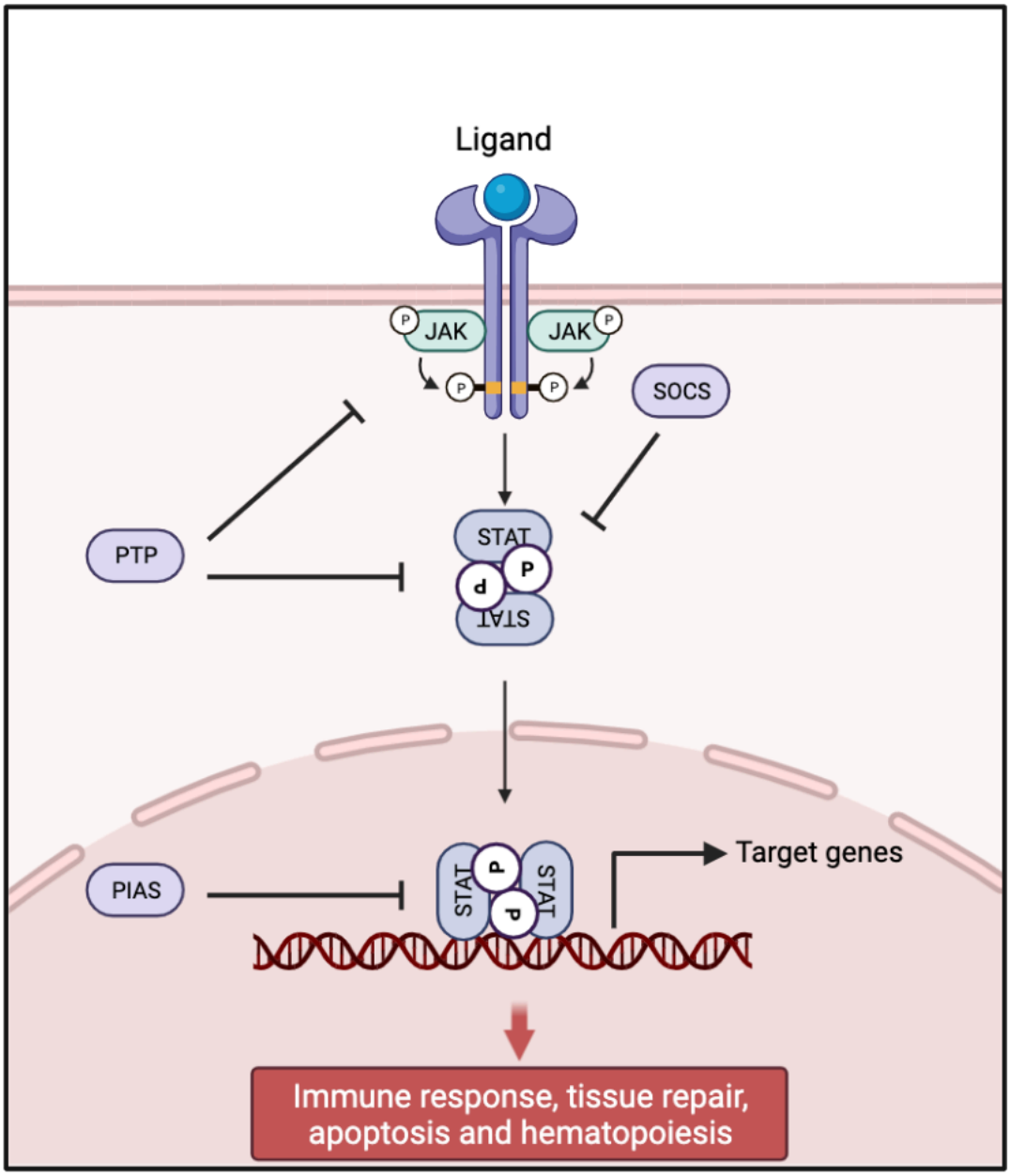

Figure 1.3. Diagram depicting the signal transducer and activator of transcription (STAT) signaling pathway. Upon ligand binding to its receptor, the receptor dimerizes and brings associated Janus kinases (JAKs) together. Activated JAKs then phosphorylate both the receptor and the recruited STATs. Once activated, the phosphorylated STATs

form dimers and translocate to the nucleus, where they regulate the transcription of target genes. Negative regulators of the STAT signaling pathway include protein tyrosine phosphatases (PTPs), suppressors of cytokine signaling (SOCS), and protein inhibitors of activated STATs (PIAS).

Chapter II

HAPLN1 matrikine:

A bone marrow homing factor linked to poor MM patient outcomes

---

This Chapter has been accepted for publication:
Hae Yeun Chang, Mailee Huynh, Avtar Roopra, Natalie S. Callander and Shigeki Miyamoto. Blood Advances (2023)

Contributions: Figures 2.2C & 2.10 were performed in collaboration with N.S.C. Figure 2.3A was performed in collaboration with M.H. Figure 2.6A-B were performed by M.H. and A.R. Figure 2.8A-C were performed in collaboration with A.R. The remaining experiments were performed by H.Y.C.

Abstract

The bone marrow (BM) microenvironment is critical for dissemination, growth and survival of multiple myeloma (MM) cells. Homing of myeloma cells to the BM niche is a crucial step in MM dissemination, but the mechanisms involved are incompletely understood. In particular, any role for matrikines, neofunctional peptides derived from extracellular matrix proteins, remains unknown. Here, we report that a matrikine derived from hyaluronan and proteoglycan link protein 1 (HAPLN1) induces MM cell adhesion to the BM stromal components, such as fibronectin, endothelial cells and stromal cells, and further induces their chemotactic and chemokinetic migration. In a mouse xenograft model, we show that MM cells preferentially home to HAPLN1 matrikine-conditioned BM. The transcription factor STAT1 is activated by HAPLN1 matrikine and is necessary to induce MM cell adhesion, migration, migration-related genes and BM homing. STAT1 activation is mediated by interferon β (IFNβ), which is induced by NF-κB following stimulation by HAPLN1 matrikine. Finally, we also provide evidence that higher levels of HAPLN1 in BM samples correlate with poorer progression-free survival of newly diagnosed MM patients. These data reveal that a matrikine present in the BM microenvironment acts as a chemoattractant, plays an important role in BM homing of MM cells via NF-κB-IFNβ-STAT1 signaling, and may help identify patients with poor outcomes. This study also provides a mechanistic rationale for targeting HAPLN1 matrikine in MM therapy.

Introduction

Multiple myeloma (MM) is a plasma cell malignancy frequently detected in multiple bone marrow (BM) sites where cancer cells are dependent on the BM microenvironment for their survival and proliferation[1]. As the disease progresses, MM cells further disseminate to distant BM sites via a BM homing process involving adhesion of circulating MM cells to vascular endothelium, transendothelial migration and localization into the BM niche[2,3]. BM homing of MM cells is dependent on chemoattractant gradients and the best studied is stromal cell-derived factor-1 (SDF-1)/CXCL12[4]. SDF-1 is mainly secreted by bone marrow stromal cells (BMSCs) and enriched in the BM, and its cognate receptor CXCR4 is highly expressed on MM cells. Nonetheless, blocking the SDF-1/CXCR4 axis is not sufficient to abrogate MM BM homing, indicating that SDF-1 is critical but not the sole BM homing factor[4,5].

Cancer cell behaviors may be modulated by soluble factors not only secreted by other cell types but also produced by partial proteolysis of extracellular matrix (ECM) proteins, known as matrikine[6]. Matrikine can control migration of different normal or malignant cell types, including neutrophils via collagen matrikine[7], monocytes and melanoma cells via elastin matrikine[8,9] and various other solid cancer cell types via laminin matrikine[10]. In addition, in the context of MM, to date, one matrikine, versikine derived from versican, has been studied on the effect of tumor-infiltrating immune cells and immunosurveillance. Versikine acts as a damage-associated molecular pattern (DAMP), promotes anti-tumor immunogenicity and antagonizes the tolerogenic actions of intact versican[11]. Finally, proteolytic processing of hyaluronan and proteoglycan link protein 1 (HAPLN1) by matrix metalloproteinase 2 (MMP2), both secreted by BMSCs,

produces HAPLN1 matrikine which can cause NF-κB signaling and resistance of MM cells to several classes of anti-MM therapeutic agents[12-14]. In MM patient BM samples, variable levels of HAPLN1 matrikine forms could be detected[12]. Despite known roles in regulation of both normal and cancer cell behaviors, however, a role for any matrikine in MM cell BM homing and whether such a matrikine could predict poor patient outcomes remain unknown.

In this study, we investigated the potential role of HAPLN1 matrikine in MM cell adhesion, migration and BM homing. HAPLN1 matrikine was found to function as a chemotactic factor that could induce MM cell migration, adhesion and BM homing. In addition, further analyses have identified the transcription factor STAT1 as the critical mediator of HAPLN1 matrikine-induced MM cell migration and BM homing. We also provide evidence that STAT1 activation is mediated by interferon β (IFNβ) which is induced by NF-κB following stimulation of MM cells by HAPLN1 matrikine. Finally, we measured HAPLN1 levels in BM samples of newly diagnosed MM patients and found their high levels to correlate with poor patient outcomes. This study reveals HAPLN1 matrikine to be a novel regulator of BM homing via STAT1 signaling in MM disease progression and its potential role as a marker for poor prognosis for certain MM patients.

Results

HAPLN1 matrikine stimulates MM cell adhesion and migration

HAPLN1 is composed of an N-terminal signal peptide followed by three structural domains, immunoglobulin-like (IG) and proteoglycan tandem repeat 1 and 2 (PTR1 and PTR2)[15]. We previously reported that along with a fragment containing all three domains, smaller fragments of HAPLN1 containing PTR1 and PTR2 domains are detectable in patient BM samples[12] and similar fragments are produced by MMP2 proteolysis of recombinant full-length HAPLN1[13]. While both recombinant PTR1 and PTR2 domains can induce NF-κB signaling separately or together, the PTR1 domain was found to possess the stronger signaling activity[12]. Thus, we employed recombinant PTR1 tagged with maltose-binding protein (MBP-PTR1)[16] and MBP alone as a negative control to assess whether HAPLN1 matrikine could modulate MM cell adhesion and migration. We first assessed MM cell adhesion to fibronectin, prevalent in the BM[17] using fluorescently labeled RPMI8226 and MM.1S human MM cell lines. Pretreatment with MBP-PTR1 induced an increase in adhesion of MM cells after 2 hours of incubation (Figure 2.1A-B). MBP-PTR1 also increased MM cell adhesion to HMEC-1 human endothelial cells (Figure 2.1C). We next assessed whether MBP-PTR1 could function as a chemoattractant for MM cells. Fluorescently labeled MM cells were placed in the upper Transwell chamber in serum-free media and MBP-PTR1, MBP or SDF1, a well-established chemoattractant for MM cells, was added in the bottom chamber and cells that migrated through the pore and adhered to the bottom of the insert were imaged and counted 16 hours later. MBP-PTR1 induced a 3- and 1.5-fold increase in the migration of RPMI8226 and MM.1S cell lines, respectively, whose magnitudes were comparable to those induced by SDF-1 (Figure

2.2A-B). MBP-PTR1 could also induce Transwell migration of primary MM patient cells (Figure 2.2C). Thus, HAPLN1 matrikine is capable of stimulating MM cell adhesion and migration.

The two most common cellular migratory behaviors are chemotaxis (a directional motility towards a chemical gradient) and chemokinesis (an increase in the motility speed without any directionality)[18,19]. Dual increases in chemotactic and chemokinetic motility are associated with metastasis of certain cancer types[20,21]. SDF-1 is known to induce MM cell chemotaxis, but not chemokinesis[22]. To determine if HAPLN1 matrikine could induce chemotactic and/or chemokinetic migrations in MM cells, the Zigmond-Hirsch migration assay[23] was next performed using the linear migration dose range of MBP-PTR1 (0-30 nM, Figure 2.2D). The largest positive gradient (0 nM in upper and 30 nM in lower chambers) caused the greatest MM cell migration (Figure 2.2E, left bottom grid), demonstrating chemotactic migration toward MBP-PTR1. Increasing concentrations on both sides of the chamber without any gradient (diagonal grid) caused correspondingly increased MM cell migration, thus indicative of chemokinetic migration.

To further define the pro-migratory activities of HAPLN1 matrikine on MM cells, a time-lapse μ-Slide migration assay[24,25] was implemented for 16 hours with each recording at 10-minute intervals. This assay tracks each MM cell to enable computation of migration parameters, such as directionality, traveled distance, and speed[25]. We performed this assay using three groups, a positive gradient group (-/+; MBP/MBP-PTR1), a no gradient group (+/+; MBP-PTR1/MBP-PTR1), and a negative control group (-/-; MBP/MBP) and the ImageJ plugin was used to track cells in the time-lapse sequences (Figure 2.2F). The directionality of migration was assessed from the trajectory data using the forward

migration index (FMI), which was calculated by averaging the endpoint of migrated cells divided by the accumulated distance, representing the efficiency of migration in direction parallel (FMI^{II}) or perpendicular ($FMI^{\perp}$) to the chemotactic gradient[24,25]. In the -/+ group, the FMI^{II} is significantly greater, thus more chemotactic, than the other two groups (Figure 2.2G). Moreover, the FMI^{II} of the -/+ group is significantly higher than its $FMI^{\perp}$, indicating the induction of directional migration towards MBP-PTR1. Finally, the positive gradient (-/+) group displayed the highest speed, and the cell speed in no gradient (+/+) group was higher than the negative control (-/-) group (Figure 2.2H), indicative of chemokinetic migration. Taken together, both the Zigmond-Hirsch and time-lapse μ-Slide migration assays demonstrated that HAPLN1 matrikine has dual chemotactic and chemokinetic effects on MM cells, thus distinguishing itself from the well-established chemotactic-only factor SDF-1.

HAPLN1 matrikine promotes BM homing in vivo

We next tested the ability of HAPLN1 matrikine to induce MM cell BM homing *in vivo*. First, we established BMSCs capable of secreting biologically active HAPLN1 matrikine, which could be injected into mouse tibia to locally produce the matrikine. To this end, we initially attempted to generate a HS-5 human BMSC line secreting only the PTR1 domain of HAPLN1 but were unsuccessful. Instead, we were able to generate a HS-5 cell line (HS-5/H1) secreting HAPLN1 fragment (32-354 aa) (Figure 2.3A) which represents a product of MMP cleavage[26] and is capable of activating NF-κB while the full-length HAPLN1 lacked such activity[12]. An ELISA of conditioned media demonstrated that HS-5/H1 cells secreted 69.5 nM HAPLN1 fragment (32-354 aa) at steady state, which

was in the range of MBP-PTR1 concentrations used in the migration assays (Figure 2.2A-D). Moreover, when MM cells were incubated on top of a confluent monolayer of HS-5/H1 or empty vector control (HS-5/EV) cells for 2 hours, significantly increased adhesion was observed for HS-5/H1 cells relative to HS-5/EV cells (Figure 2.3B). Similarly, Transwell migration assays demonstrated that MM cells migrated significantly more towards HS-5/H1 in the bottom chamber than HS-5/EV (Figure 2.3C). To verify whether the overexpressed HAPLN1 fragment is acting as a migratory factor and not the endogenous HAPLN1, we generated HAPLN1 knockdown HS-5 cells. Endogenous HAPLN1 was not detected in the conditioned media (Figure 2.3D). The migratory potential induced by the HAPLN1 fragment was lost when HAPLN1 was knocked down in HS-5/H1 cells (Figure 2.3E). Thus, exogenous HAPLN1 matrikine produced by HS-5/H1 cells was responsible for stimulation of MM cell migration.

We assessed whether HS-5 cells would remain in the injected mouse BM site without forming a tumor. HS-5 cells stably expressing the *luciferase* gene were injected into NSG mouse tibiae and monitored for their presence by bioluminescence imaging. The human HS-5 cells were maintained in the injected sites for at least 2 weeks without any obvious growth or migration to other BM sites (Figure 2.4A). To test the impact of HAPLN1 matrikine secreted by HS-5/H1 *in vivo*, both tibiae in individual NSG mice were injected with either HS-5/H1 or HS-5/EV cells (Figure 2.4B). Two weeks later a sublethal dose of radiation (3 Gy) was given to facilitate MM cell BM engraftment and PKH26-labeled MM.1S cells were then injected via the intracardiac route a day later to induce MM cell homing to the BM within 48-72 hours[27,28]. The BM of two tibiae was collected 72 hours after the MM engraftment and subjected to flow cytometry to quantify percentages

of the PKH26-labeled MM cells among BM mononuclear cells (Figure 2.4C). Because individual mice had different engraftment efficiencies, the MM cells homed to injection-naive femur were used as an internal control to calculate the tibia-to-femur ratio for each mouse. Significantly, the tibia/femur ratio of MM cells was ~2.5-fold greater for HS-5/H1 than HS-5/EV injected mice (Figure 2.4D).

To rule out the potential for any unintended systemic effect induced by the injection of HS-5/H1 cells, MM cell homing within individual mice was assessed by injecting HS-5/H1 cells in one tibia and HS-5/EV cells in the opposite tibia before systemic MM cell introduction (Figure 2.5A). Since initial analysis with the flow cytometry assay became unreliable due to low MM cell yields from a tibia, each tibia was subjected to immunohistochemistry (IHC) analysis to quantify injected MM cells by anti-CD138 staining and HS-5 cells by anti-HLA class I (HLA-I) staining. CD138-positive MM cells were not co-stained with the HLA-I antibody (Figure 2.5B), similar to many cancer cell types that display lower levels of HLA-I to evade immunity[29]. The numbers of MM cells and HS-5 cells were normalized to the areas of BM sections imaged. The normalized CD138+ MM cell number in HS-5/H1-injected tibia was ~2.5-fold greater than that in the HS-5/EV counterpart (Figure 2.5C). By contrast, the normalized HLA-I$^+$ HS-5 staining was similar in both cases (Figure 2.5C), thus the observed difference in MM cell homing was not due to different numbers of HS-5 cells retained in the BM.

To further validate the differences in MM cell homing to HS-5/H1 versus HS-5/EV injected tibia, we quantified the number of MM cells in each tibia by means of MM cell-specific genomic DNA. An MM.1S cell clone with the *luciferase* gene stably integrated into the genome was used in BM homing experiments as in Figure 2.5A, and the

luciferase copy number was quantified to measure the MM cells homed to each BM. The BM of femur and tibia were collected 72 hours after the MM cell injection and subjected to genomic DNA and total RNA extraction. The tibia-to-femur ratio of the *luciferase* copy number was calculated for each leg in each mouse. Comparable to the above two distinct BM homing experiments (Figures 2.4C-D vs 2.5B-E), the number of *luciferase* labeled MM cells was a ~1.9-fold greater in the HS-5/H1-injected tibia compared to the HS-5/EV-injected tibia (Figure 2.5D). When human *HAPLN1* mRNA was quantified by qRT-PCR using human *SMA* stromal gene as a normalization control, significantly higher *HAPLN1* mRNA was detected in the HS-5/H1-injected tibia relative to its counterpart (Figure 2.5E), indicating that the injected HS-5/H1 cells were expressing the *HAPLN1* gene. These three independent assays collectively demonstrated that HAPLN1 matrikine promoted BM homing of MM cells *in vivo*.

HAPLN1 matrikine activates STAT1 in MM cells

We previously performed RNA-seq analysis of RPMI8226 MM cells exposed to recombinant PTR1 (GSE202672) and identified NF-κB and JAK/STAT as potentially enriched signaling pathways[14]. We previously confirmed NF-κB activation[12] but STAT activation has not been demonstrated by stimulation of MM cells with HAPLN1 matrikine. To further assess the potential involvement of STAT factors, we also evaluated the RNA-seq data using a novel bioinformatics tool, *M*ining *A*lgorithm for *G*enet*I*c *C*ontrollers (MAGIC)[30], and again identified NF-κB and STAT transcription factors as among the top potential drivers of transcriptional changes in the HAPLN1 matrikine-induced genes (Figure 2.6A, Table 2.1). The RNA-seq data also showed that transcripts encoding NF-

κB family members (RelA, RelB, c-Rel, NFKB1, and NFKB2) and STAT family members (STAT1, STAT3, STAT4 and STAT5A) were significantly induced in MM cells stimulated with HAPLN1 matrikine relative to control cells (Figure 2.6B). Interestingly, STAT1 had the highest RPKM among these potential master regulators. To test the activation of STAT transcription factors, we next performed a *luciferase* reporter assay using a construct containing the STAT1/3 responsive M67 promoter[31]. Consistent with the bioinformatics predictions, MBP-PTR1 significantly increased the reporter activity in MM cells at a level similar to the positive control IL-6 (Figure 2.6C). Next, electrophoretic mobility shift and anti-STAT1/3 super shift assays were performed using an M67 probe, which demonstrated the presence of STAT1, but STAT3 (Figure 2.6D). Consistently, Western blot analysis demonstrated that STAT1 phosphorylation at tyrosine 701 was induced in a dose-dependent manner within 3 hours following MBP-PTR1 treatment, which lasted 24 hours (Figure 2.6E-F). Total STAT1 level was also increased after MBP-PTR1 treatment (Figure 2.6F), consistent with the induction of *STAT1* gene expression (Figure 2.6B). In contrast, STAT3 tyrosine 705 phosphorylation and its total level were only minimally induced (Figure 2.6E-F). These results revealed that HAPLN1 matrikine primarily activates STAT1, not STAT3, in MM cells.

STAT1 is required for HAPLN1 matrikine-induced MM cell migration and BM homing

To test whether STAT1 activation is critical for HAPLN1 matrikine functions, we generated STAT1 (shSTAT1) or control (shControl) knockdown MM.1S cells (Figure 2.7A) and assayed for *in vitro* migration. While basal migration (MBP only) was not

affected, the increased migration observed in MBP-PTR1-treated shControl cells was absent in shSTAT1cells (Figure 2.7B). Similarly, *in vivo* BM homing of MM cells to control HS-5/EV-injected tibia was similar but was reduced to the control level in HS-5/H1-injected tibia (Figure 2.7C-D). To confirm that STAT3 does not play a role in HAPLN1-induced migration, we generated STAT3 KO cells and conducted a migration assay. The STAT3 KO induced both comparable STAT1 activation and HAPLN1-induced migratory potential to those of the WT cells (Figure 2.7E-F). These results confirmed that STAT3 does not participate in HAPLN1-induced migration. Together, these data indicate that STAT1, not STAT3, is necessary for HAPLN1 matrikine-induced MM cell migration and BM homing.

To identify STAT1-dependent migration-related genes whose expression was induced by HAPLN1 treatment, a similar RNA-seq analysis was performed as previously done on RPMI8226 cells[14], except for using control and STAT1 knockout cells (Figure 2.7G, GSE237216), the latter of which also showed defective MBP-PTR1-induced migration (Figure 2.7H). Cluster analysis identified 11 clusters in the differentially expressed genes (Figure 2.8A-B). We were particularly interested in the one in which the lack of STAT1 did not affect the basal expression but abrogated MBP-PTR1-induced gene expression (red cluster, Figure 2.8B, Table 2.2). Enrichment Analysis using the KEGG pathway database showed that the genes in this cluster were enriched in JAK/STAT pathway and those previously identified to be involved in adhesion, migration and BM homing of MM cells (e.g., *CD44, CXCR5, ICAM-1, VAV1, DOCK10*), among others (Figure 2.8C and Table 2.3). We confirmed the MBP-PTR1-dependent induction of the well-established MM BM homing-related genes, *CD44*, *SDF-1*, and *ICAM-1*, by

qRT-PCR (Figure 2.8D). These homing-related genes were not reduced in STAT3 KO cells, but some (*ICAM-1* and *CD44*) were increased instead (Figure 2.8E). Taken together, these results demonstrated that HAPLN1 matrikine activates STAT1 to induce migration- and BM homing-related genes in MM cells.

HAPLN1 matrikine activates STAT1 via NF-κB-induced IFNβ in MM cells

We previously demonstrated that HAPLN1 matrikine can activate NF-κB signaling and induce NF-κB regulated drug resistance genes in MM cells[12,14]. This study showed peak NF-κB activation occurring within 2 hours after HAPLN1-PTR1 treatment in RPMI8226 cells, while peak STAT1 phosphorylation was delayed and observed 3-6 hours post stimulation. This temporal sequence suggests that STAT1 phosphorylation takes place after NF-κB activation. Thus, we investigated whether NF-κB signaling was involved in HAPLN1-induced STAT1 activation. To test this possibility, we co-treated cells with MBP-PTR1 and IKK16, an IκB kinase (IKK) inhibitor which we previously demonstrated to block MBP-PTR1-induced NF-κB signaling[32]. Importantly, this co-treatment completely inhibited STAT1 phosphorylation (Figure 2.9A). Additionally, to determine whether any secreted factor downstream of NF-κB is activating STAT1, we treated RPMI8226 cells with cycloheximide to block new protein synthesis or brefeldin A to block secretion. Both reagents effectively abrogated HAPLN1-induced STAT1 phosphorylation (Figure 2.9B). Furthermore, conditioned medium from HAPLN1-treated cells was capable of inducing STAT1 activity within 15 minutes of treatment (Figure 2.9C) indicating that newly synthesized and secreted factor(s), downstream of NF-κB signaling, mediate STAT1 activation in an autocrine/paracrine manner. To determine which factor activates STAT1

after HAPLN1-induced NF-κB activation, we identified candidate cytokines, e.g., IL-6 and IFNβ, which are encoded by NF-κB target genes and are well-established activators of STAT1 signaling, in the red cluster genes from the RNA-seq analysis (Figure 2.9D). A previous study demonstrated that LPS stimulation of macrophages induces TLR4- and NF-κB-dependent STAT1 signaling via autocrine/paracrine production of IFNβ[33]. Because HAPLN1 activates NF-κB through the TLR4-CH60 cell surface receptor complex[16], we tested whether IFNβ is involved in the HAPLN1-activated STAT1. The co-treatment of IKK16 significantly reduced the HAPLN1-induced *IFNB1* mRNA level (Figure 2.9E). In addition, the co-treatment of the FDA-approved type I IFN receptor blocking antibody, anifrolumab, completely inhibited HAPLN1-induced STAT1 phosphorylation (Figure 2.9F). In contrast, a neutralizing antibody against IL-6 had no effect (not shown). Taken together, these results support the notion that autocrine/paracrine production of IFNβ by NF-κB signaling is required for HAPLN1-induced STAT1 signaling.

High HAPLN1 levels in BM aspirates correlate with poor patient outcomes

We previously reported that HAPLN1 matrikine is capable of inducing resistance to multiple classes of therapeutic agents in MM cells[14]. We also showed that soluble HAPLN1 fragments are detectable in BM plasma but highly variable from patient to patient, similar to HAPLN1 mRNA levels in patient BMSCs[12,13]. Therefore, given the dual role of HAPLN1 in inducing drug resistance and BM homing, we hypothesized that soluble HAPLN1 in the BM may contribute to poor outcomes of MM patients. To quantify soluble HAPLN1 levels in the plasma of BM aspirates, we developed an AlphaLISA (see Materials and Methods) which detected HAPLN1 with minimal cross-reactivity to highly homologous

HAPLN3 protein (Figure 2.10A). HAPLN1 levels in BM plasma samples from 26 newly diagnosed MM (NDMM) patients were measured by the above AlphaLISA, and the patients were grouped into high and low groups based on the median cut-off value (Table 2.4). Both sex and age of the patients were not different between these groups (Figure 2.10B). Significantly, the high HAPLN1 group exhibited worse progression-free survival (PFS) than the low group (Figure 2.10C). The median PFS for the low and high HAPLN1 groups was 57 months and 28 months, respectively (hazard ratio, 3.027). Furthermore, patients in the high HAPLN1 group underwent a significantly higher number of therapies (Figure 2.10D). We further stratified the patients based on cytogenetic risk assessed by fluorescence *in situ* hybridization (FISH) based on the Revised International Staging System (R-ISS) and the second revision of the ISS (R2-ISS)[34,35]. Interestingly, patients with standard cytogenetic risk showed a stark difference in PFS (hazard ratio, 5.861; Figure 2.10E). Although the sample size is too small to draw conclusive results, patients with high/ultra-high cytogenetic risk did not exhibit a significant difference in PFS (Figure 2.10F). These results suggest the level of HAPLN1, a MM cell-extrinsic factor derived from ECM protein in the tumor microenvironment, can serve as a prognostic marker in MM. Furthermore, patients with higher STAT1 mRNA level (n=47) exhibited significantly worse PFS than the STAT1 low group (n=48) (hazard ratio, 1.7539; Figure 2.10G) in the CoMMpass trial RNA-seq dataset from the Multiple Myeloma Research Foundation Researcher Gateway. Altogether, the results suggest that the HAPLN1 level in the BM and the STAT1 mRNA level in MM cells can be predictive markers of prognosis in MM patients.

Discussion

In the present study, we uncovered for the first time that an ECM-derived matrikine could stimulate migration and BM homing of human MM cells. Specifically, the PTR1 domain of HAPLN1 or a larger fragment containing all three domains of HAPLN1 (IG, PTR1 and PTR2 domains), representing "HAPLN1 matrikine", could promote such activities. Similarly larger and smaller fragments of HAPLN1 containing the PTR1 domain were detected in BM aspirates of some relapsed/refractory MM patients with progressive disease, an unfavorable category of treatment response[12]. We also previously found that HAPLN1 matrikine could promote resistance of MM cells to a variety of therapeutic agents[14]. Thus, HAPLN1 matrikine may be a potentially important MM progression factor via two unique and distinct mechanisms: enhancing migration and homing to multiple BM sites and increasing multi-drug resistance. Accordingly, higher HAPLN1 levels in BM plasma correlated with shorter progression-free survival of newly diagnosed MM patients relative to that of the low HAPLN1 group.

Although we previously found NF-κB to be a drug resistance factor[14], the discovery of STAT1 as the main MM cell migration and BM homing mechanism induced by HAPLN1 matrikine was unanticipated. Previous studies have demonstrated co-activation of NF-κB and STAT3 in a variety of human malignancies[36,37] and the role for STAT3, not STAT1, as an oncogenic driver in MM[38,39]. However, biochemical and genetic studies clearly revealed the activation of STAT1, not STAT3, and its requirement for HAPLN1 matrikine-induced MM cell migration and BM homing. Moreover, our study demonstrated that NF-κB is upstream of STAT1 activation and likely involves the NF-κB dependent synthesis and secretion of IFNβ to induce subsequent STAT1 activation. Thus, HAPLN1 matrikine

as a sequential activator of NF-κB and STAT1 adds to the emerging evidence supporting a tumor promoter role for STAT1 observed in other cancer types. For example, STAT1 has been implicated in migration of colon cancer cells[40], and cell adhesion, migration, and progression of serous papillary endometrial cancer cells[41]. STAT1 has also been implicated in chemoresistance of head and neck cancer[42], epithelial-to-mesenchymal transition (EMT) of lung cancer[43], and metastasis of melanoma[44]. In addition, Boiarsky *et al.* reported their single cell RNA-seq analysis on CD138+ cells from MM and premalignant patients where IFN-inducible signatures, including the STAT1 level, are significantly upregulated in MM, but not in precursor conditions[45]. This report is consistent with our finding that HAPLN1 activates STAT1 in MM cells, and HAPLN1-induced IFNβ acts in an autocrine/paracrine manner. Moreover, our analysis of a larger scale clinical trial (CoMMpass) database also demonstrated that higher STAT1 mRNA level correlated with poor PFS of MM patients. Thus, the new function of STAT1 in HAPLN1 matrikine-induced MM cell migration and BM homing expands its emerging context-dependent tumor promoter roles.

Our study also revealed that HAPLN1 matrikine may be a novel dual chemotactic and chemokinetic factor for MM cells. To date, the SDF-1/CXCR4 axis is well established to play a crucial role in MM cell adhesion, migration, and BM homing[46-48]. SDF-1 induces MM cell chemotaxis at low doses but inhibits MM cell migration at high doses, thus promoting MM cell homing in circulation (i.e., low concentrations) but retaining MM cells in the BM niche where SDF-1 is enriched[4]. In contrast, HAPLN1 matrikine increased MM cell migration not only when there was a positive concentration gradient acting as a chemotactic factor but also when concentrations are high without any gradient as a

chemokinetic factor. It is noteworthy that a combination of increased chemotactic and chemokinetic motilities correlates with invasiveness and metastasis of other cancer types, including non-small cell lung cancer cells and others[20,21]. These prior studies support the possibility that dual chemotactic and chemokinetic action of HAPLN1 matrikine contributes to not only BM homing through chemotaxis-mediated migration into the BM niche but also to egress from the BM into the circulation due to high motility when exposed to even higher concentrations of the matrikine in the BM niche, which can result in a vicious cycle of disease dissemination.

We demonstrated that high HAPLN1 levels in BM samples are associated with poor prognosis of newly diagnosed MM patients, supporting its potential use as a prognostic marker and therapeutic target. The current prognostic staging system for MM utilizes the Revised-International Staging System (R-ISS), which can stratify the risk for patients based on protein biomarkers (β_2-microglobulin, albumin and lactate dehydrogenase) and cytogenetic aberrations[34]. Although it is informative on tumor burden and risk assessment, it is not utilized for therapeutic decision-making[49]. Given that the ECM is a major component of the tumor microenvironment, the role of ECM proteins per se as biomarkers remains incompletely understood. Our current study discovered that a tumor microenvironment (TME) factor could be a risk factor in MM pathogenesis. Our previous study also revealed that while HAPLN1 matrikine may induce resistance to multiple therapeutic agents, such as bortezomib, lenalidomide, dexamethasone, and others, it failed to induce resistance to the second generation proteasome inhibitor, carfilzomib and the nuclear export inhibitor, selinexor[14]. These findings combined suggest the possibility that NDMM patients with a high HAPLN1 status may benefit from therapies

that contain either carfilzomib or selinexor or both. These findings also suggest a potential clinical benefit of ablating HAPLN1 matrikine function in MM therapy. However, one caveat is the relatively low number of NDMM patient samples analyzed (n=26) in the current study, especially for the high/ultra-high risk patient group. Another weakness may be the generally low sensitivity of HAPLN1 AlphaLISA. Finally, the roles of full-length HAPLN1 and its matrikine in normal physiological processes in adult humans are currently lacking. Thus, development of a highly sensitive and specific assay to quantify HAPLN1 levels and an assessment of larger cohorts of MM patients are necessary to establish this ECM-derived matrikine as a potential biomarker for predicting poor patient outcomes. Once established, clinical studies could be conducted to test the potential benefits of stratifying NDMM patients to carfilzomib and/or selinexor therapies. Finally, improved knowledge of the role of HAPLN1 and its matrikine in human physiology may shed light on the safety of HAPLN1 matrikine-targeting therapeutics against MM that is currently considered an incurable cancer type.

Methods

Cell culture

RPMI8226 and MM.1S human MM, HMEC-1, HS-5, and 293T cell lines were purchased from the American Tissue Type Culture Collection (Manassas, VA, USA). MM cell lines were cultured at 37°C/5% CO_2 in RPMI-1640 media (Gibco, Rockville, MD, USA) containing 10% fetal bovine serum, 2% GlutaMAX (Gibco, Rockville, MD, USA), 100 U/mL penicillin, and 100 µg/mL streptomycin. HMEC-1 was cultured in MCDB131 media (Gibco, Rockville, MD, USA) containing 10% fetal bovine serum, 2% GlutaMAX, 10 ng/mL epidermal growth factor (EGF), 1 µg/mL hydrocortisone, 100 U/mL penicillin, and 100 µg/mL streptomycin. HS-5 and 293T were cultured in DMEM (Corning, Tewksbury, MA, USA) containing 10% fetal bovine serum, 100 U/mL penicillin, and 100 µg/mL streptomycin. All the cell lines were mycoplasma negative and authenticated by short tandem repeat (STR) genotyping.

Purification of maltose-binding protein (MBP)-tagged proteins

Purification of MBP-PTR1 and MBP proteins was done as described in De Bakshi et al[16]. Briefly, the cDNA sequence encoding the HAPLN1-PTR1 domain (aa 159-253) was inserted into pET28-MBP-TEV plasmid in frame with and downstream of the MBP coding sequence and the resulting plasmid was transformed into the BL21 Rosetta 2 *Escherichia coli* strain. Proteins were induced with 1 mM IPTG followed by purification using amylose resin and elution by 50 mM maltose. To remove potential LPS contamination, the eluted protein fraction was run through Pierce High-Capacity Endotoxin Removal Spin Columns (Thermo Scientific, Waltham, MA, USA) according to the manufacturer's instruction. The

LPS-removed protein fraction was further processed by fast protein liquid chromatography (FPLC) using a size exclusion column, Superose 6 Increase 10/300 GL (Sigma-Aldrich, St. Louis, MO, USA) to obtain highly purified, monomeric and functional recombinant HAPLN1-PTR1 domain. The purity of the protein fragment was assessed by SDS-PAGE analysis and Coomassie staining and the functional activity was ensured by assessing NF-κB activation in MM cell lines via electrophoretic mobility shift assay (EMSA) as described previously[12]. Cells were treated with either 100 nM MBP-PTR1 or MBP alone, unless indicated otherwise.

Adhesion assay

The glass plates (6 mm diameter well) coated with fibronectin (FN, 10 μg/mL) or plated with a confluent monolayer of cells (HMEC-1, HS-5) were prepared one day before assaying for MM cell adhesion. Fibronectin-coated plates were blocked with 1% BSA/PBS for 1 hour. MM cells were pre-stained with CFSE (Thermo Scientific, Waltham, MA, USA) according to the manufacturer's instruction and plated on the glass plate (50,000 cells/well in 1% BSA RPMI1640 media) and incubated for 2 hours at 37°C. After incubation, non-adherent MM cells were washed with PBS twice and fixed with 4% paraformaldehyde. The plates were imaged, and cell number was counted by ImageJ software.

Transwell migration assay

The bottom chambers of Transwell filter chambers (5 μm pores; Corning, Tewksbury, MA, USA) were coated with 10 μg/ml of FN as described previously[50]. Cells (5×10^5 and $1 \times$

10^5 for RPMI8226 and MM.1S, respectively) were pre-stained with CFSE (Thermo Scientific, Waltham, MA, USA) according to the manufacturer's instruction and placed in the upper chamber in 1% BSA RPMI1640 media and incubated for 16 hours at 37 °C. In the bottom chamber, chemoattractants were added in 1% BSA RPMI1640 media. Cells on the bottom of the filter were fixed, and four fields were imaged, and the cell number was counted by ImageJ software. For the co-culture of HS-5 and MM cells, HS-5 cells (5 × 10^4 cells/24-well) were plated in the bottom chamber one day before the migration assay. The media was changed with 1% BSA RPMI1640 media and the Transwell inserts were assembled for the assay.

μ-Slide time-lapse migration assay

The time-lapse migration assays were performed with μ-Slide Chemotaxis (Ibidi GmbH, Planegg, Germany) following the manufacturer's instruction. Briefly, RPMI8226 cells were plated in the complete media in the channel. In the reservoir, the final concentration of 30 nM of MBP or MBP-PTR1 was filled. Images were taken every 10 minutes for 16 hours using a Nikon Eclipse Ti Inverted Microscope (Nikon, Tokyo, Japan) equipped with a CO_2- and temperature-controlled chamber. Images were imported as stacks to ImageJ software and analyzed with the ImageJ plugins, Manual Tracking, and the Chemotaxis and Migration Tools. Individual cells moving at least one cell length were tracked at each cell position in the field throughout the temporal stacks, until the cell could no longer be tracked, e.g., moving out of frame. Calculations of the forward migration index parallel (FMI^{II}) or perpendicular ($FMI^{\perp}$) to the chemotactic gradient were as following[24,25].

$$FMI^{II} = \frac{1}{n}\sum_{i=1}^{n}\frac{y_{i,end}}{d_{i,accum}}$$

$$FMI^{\perp} = \frac{1}{n}\sum_{i=1}^{n}\frac{x_{i,end}}{d_{i,accum}}$$

(i = index of single cells, n = number of cells, $x_{i,end}$, $y_{i,end}$ = coordinates of the cells' endpoints, $d_{i,accum}$ = accumulated distance of the cells' paths)

Primary CD138+ myeloma cell isolation and BM plasma fraction collection

Bone marrow (BM) aspirates from MM patients were obtained in accordance with the University of Wisconsin-Madison Institutional Review Board requirements (HO07403). CD138+ myeloma cells were positively sorted with CD138+ magnetic MACS® beads (Miltenyi Biotec, Bergisch Gladbach, Germany) as described previously[12,51] The BM plasma fraction was collected by centrifuging the BM aspirate and stored at -80°C in multiple microcentrifuge tubes until analysis.

Generation of stable HS-5 cells secreting HAPLN1 matrikine

The cDNA sequence encoding the HAPLN1 fragment (aa 32-354) was inserted into the pSecTag2A (Invitrogen, San Diego, CA, USA) plasmid in frame with the N-terminal Igκ chain leader sequence for protein secretion and the C-terminal *c-Myc* epitope and 6×His tag. The integrity of the resulting construct was sequence verified. HS-5 cells were transfected with pSecTag2A empty vector (EV) or pSecTag2A-HAPLN1-32-354 by Nucleofector kit (Lonza, Walkersville, MD, USA). The cells were treated with 100 μg/mL Zeocin (Thermo Scientific, Waltham, MA, USA) and the stable clones (HS-5/EV and HS-5/H1) were selected by limited dilution and clonal expansion. HAPLN1 knockdown cells were generated by shHAPLN1 (SHCLNG-NM_001884, Sigma-Aldrich, St. Louis, MO, USA) transduction and selected with puromycin.

Western blot (WB) analysis of conditioned media (CM) and cell extracts

CM was prepared by culturing a confluent monolayer of HS-5 cells, in serum-free DMEM at 37°C. After 48-72 hours, the CM was removed and centrifuged at 13,000 *g* for 5 minutes to remove cellular debris. The secreted protein was precipitated by adding 50 µl of 100% trichloroacetic acid (TCA) and 50 µl of 2% deoxycholate (DOC) into 0.5 mL CM and centrifuged at 13,000 *g* for 10 minutes. The pellet was solubilized with 1 M Tris buffer (pH 8.8) and run on denaturing 12.5% SDS-PAGE gel. Dilutions of recombinant human HAPLN1 protein (2608-HP, R&D Systems, Minneapolis, MN, USA) were used for quantification standards. Cell extracts were made using TOTEX buffer, as described previously[52]. Equal amounts of soluble protein were run on denaturing 7.5% SDS-PAGE gel and transferred onto a polyvinylidene fluoride (PVDF) membrane (Millipore, Bedford, MA, USA). The membrane was then incubated with the appropriate antibodies. Antibodies used for the CM were against Myc-tag (clone 9E10, Santa Cruz, Dallas, TX, USA) and HAPLN1 (MAB2608, R&D Systems, Minneapolis, MN, USA). Primary antibodies to pSTAT1 (9167), pSTAT3 (9145), STAT1 (9172), and STAT3 (9139) were purchased from Cell Signaling Technology (Danvers, MA, USA), tubulin from Millipore (DM1A, Bedford, MA, USA) and actin from Sigma-Aldrich (A5441, St. Louis, MO, USA). Immunoblots were analyzed by enhanced chemiluminescence as described by the manufacturer (GE Healthcare, Chicago, IL, USA).

ELISA of HAPLN1 in HS-5 cell conditioned media

Pierce® Streptavidin Coated 96-well Plates (15120, Thermo Fisher Scientific, Waltham, MA, USA) were coated with 4 μg/mL biotinylated anti-HAPLN1 antibody (BAF-2608, R&D Systems, Minneapolis, MN, USA) overnight at 4°C. The plates were washed 3 times with TBS containing 0.05% Tween-20 and blocked with 3% BSA for 1 hour. After washing, the samples were incubated overnight at 4°C. Next day, the plates were washed and incubated with 2 μg/mL detection antibody (MAB-2608, R&D Systems, Minneapolis, MN, USA), for 0.5 hour at room temperature. Plates were washed and incubated with secondary anti-mouse HRP-conjugated antibody (95017-332, Cytiva, Marlborough, MA, USA) diluted 1:5,000 for 0.5 hour. After washing, TMB (34028, Thermo Fisher Scientific, Waltham, MA, USA) was added to the plates and incubated for 15 minutes. The reaction was stopped using 1N H_2SO_4, and absorbance was measured at 450 nm. Dilutions of recombinant human HAPLN1 protein (2608-HP, R&D Systems, Minneapolis, MN, USA) were used for quantification standards.

In vivo bone marrow homing assay

NOD/SCID IL-2Rγ(null) (NSG) mice were injected with HS-5 cells (10^5 cells/10 μL PBS/tibia) by intra-tibial (IT) injection at 6-8 weeks of age. Initial experiments used luciferase-transduced HS-5 cells to confirm the accuracy of the intra-tibial injection (Figure 2.4A). Two weeks after the IT injection, a MM homing assay was conducted as described previously[27,28]. Briefly, MM.1S cells labeled with PKH26 fluorescent cell linkers (Sigma-Aldrich, St. Louis, MO, USA) were inoculated by intra-cardiac (IC) injection (3×10^6 cells/100 μL PBS/mouse). To facilitate the MM engraftment, one day before IC injection, mice were irradiated with a sublethal dose (3 Gy). Three days after MM

engraftment, hind leg bones were harvested, and BM samples were collected by centrifugation[53]. BM samples were incubated with red blood cell lysis buffer containing ammonium chloride and potassium bicarbonate. Subsequently, mononuclear cells were isolated by density gradient centrifugation using Lymphocyte Separation Medium (Corning, Tewksbury, MA, USA) following the manufacturer's instruction and fixed with 4% paraformaldehyde. Mouse femur and tibia BM samples were analyzed by flow cytometry. The injected PKH26 labeled MM cells were cultured for 3 days and harvested at the same time when the mice were sacrificed. The cultured $PKH26^+$ MM cells were analyzed together as a positive control to gate for $PKH26^+$ cells.

Immunohistochemistry (IHC) analysis

Mouse tibiae were fixed in 10% formalin-buffered saline and decalcified. The tissue was paraffin-embedded and sectioned. Sections were deparaffinized in xylene and rehydrated in graded alcohols, and the epitope was retrieved by boiling in citrate buffer (pH 6.0; Vector Laboratories, Burlingame, CA, USA) for 20 minutes. Immunohistochemistry was performed using antibodies against CD138 (clone B-A38, Bio-Rad, Hercules, California, USA) and HLA class 1 ABC (ab225636, Abcam, Cambridge, UK) with the secondary anti-rabbit (Alexa Fluor® 647 Conjugate; CST4414, Cell Signaling Technology, Danvers, MA, USA) and anti-mouse (Alexa Fluor® 488 Conjugate; CST4408, Cell Signaling Technology, Danvers, MA, USA) antibodies. The TrueVIEW Autofluorescence Quenching kit (Vector Laboratories, Burlingame, CA, USA) was used according to the manufacturer's instruction before mounting.

Single-cell cloning of MM cells

Luciferase-labeled MM.1S cells or STAT1 knockdown MM.1S cells were generated by lentiviral transduction. The lentiviral particle was packaged by transfecting pLenti CMV Puro LUC (w168-1)[54], MISSION pLKO.1-shSTAT1, (TRCN0000004267) or MISSION pLKO.1-puro Control Vector (SHC001, Sigma-Aldrich, St. Louis, MO, USA), with packaging plasmids (pCMV-dR8.91, and pCMV-VSV-G) to 293T cells. pLenti CMV Puro LUC (w168-1) was a gift from Eric Campeau and Paul Kaufman (Addgene plasmid #17477). MM.1S cells were spinfected for 60 minutes at 1,200 *g* in the presence of 8 μg/mL polybrene. Transduced cells were selected with puromycin, and the stable clone was selected by limited dilution and clonal expansion. RPMI8226 STAT1 and STAT3 knockout CRISPR/Cas9-edited cell pools were purchased from Synthego Corporation (Redwood City, CA, USA). STAT1 and STAT3 knockout clones were generated by limited dilution and clonal expansion.

Quantitative PCR analysis

Total RNA and genomic DNA from samples were purified by Trizol (Invitrogen, San Diego, CA, USA) according to the manufacturer's instruction. cDNAs were synthesized from the total RNAs using iScript cDNA synthesis kit (Bio-Rad, Hercules, California, USA). QPCR was performed and analyzed using a Bio-Rad CFX Connect real-time system. The absolute copy number of *luciferase* gene was determined by the standard curve using serial dilutions of the plasmids (pLenti CMV Puro LUC w168-1) as quantification standards for *luciferase*. The human-specific primer pair for *HAPLN1* was designed to target the PTR1 domain of HAPLN1. The primer sequences are Luciferase (forward,

TGATTACACCCGAGGGGGAT; reverse, CTCACACACAGTTCGCCTCT), HAPLN1 (forward, TCTCAATTTTCACGAGGCGC; reverse, GCTCTCTGGGCTTTGTGATG), SMA (forward, GTGTTGCCCCTGAAGAGCAT; reverse, GCTGGGACATTGAAAGTCTCA), STAT1 (forward, CTAGTGGAGTGGAAGCGGAG; reverse, CACCACAAACGAGCTCTGAA), STAT3 (forward, CCTCTGCCGGAGAAACAG; reverse, AACACCAAAGTGGCATGTGA), CD44 (forward, TGGCACCCGCTATGTCGAG; reverse, GTAGCAGGGATTCTGTCTG), SDF-1 (forward, TCAGCCTGAGCTACAGATGC ; reverse, CTTTAGCTTCGGGTCAATGC), and ICAM-1 (forward, GGCCGGCCAGCTTATACAC; reverse, TAGACACTTGAGCTCGGGCA).

*M*ining *A*lgorithm for *G*enet*I*c *C*ontrollers (MAGIC) analysis

Differentially expressed genes between GST and GST-PTR1 samples[14] were passed through MAGIC[55] using default settings. Predicted transcription factors and coregulators were ordered by Score and graphed.

STAT1/3-dependent luciferase reporter assay

RPMI8226 cells were transiently transfected with Cignal STAT3 Reporter Kit (CCS-9028L, Qiagen, Hilden, Germany) using Lipofectamine 2000 (Invitrogen, San Diego, CA, USA). The transfected cells were split into a 24-well plate 48 hours after transfection to control for the same transfection efficiency and treated with 100 nM MBP or MBP-PTR1 or 50 ng/mL IL-6 for 24 hours. Cell extracts were incubated with luciferin in a white 96-well plate, and the luminescence was measured by ENSPIRE plate reader (Perkin Elmer, Waltham, MA, USA).

Electrophoretic mobility shift assay (EMSA) and supershift assay

EMSAs to measure STAT1/3 activity in MM cells were performed using ^{32}P-labeled double-stranded DNA probes with the following sequences: 5′-GTCGACATTTCCCGTAAATCGTCGA-3′. Cell extracts were made using TOTEX buffer as described before[12], and extracts were separated on 4% native polyacrylamide gel, dried, and exposed to a phosphor screen (Amersham Biosciences). For super shift assays, 1 µL of anti-STAT1 or anti-STAT3 antibody (9172, 9139, Cell Signaling Technology, Danvers, MA, USA) was added to the cell extract reaction mixture before probes were added.

RNA-sequencing transcriptome analysis

RPMI8226 WT and STAT1 KO clone were treated with 100 nM MBP or MBP-PTR1 for 6 hours in 3 biological replicates run on 3 separate days (GSE237216). The frozen pellets were shipped on dry ice to Genewiz/Azenta (South Plainfield, NJ, USA) for RNA sequencing, RNA extraction, sample QC, library preparations, and sequencing reactions. Briefly, total RNA was extracted using Qiagen RNeasy Plus Universal kit (Qiagen, Hilden, Germany) following the manufacturer's instructions. The RNA sequencing library was prepared using the NEBNext Ultra II RNA Library Prep Kit (New England Biolabs, Ipswich, MA, USA) for Illumina using manufacturer's instructions. Raw sequence data generated from Illumina HiSeq. Reads were aligned to the Homo sapiens GRCh38 reference genome by STAR. Differential expression was analyzed using DESeq2 using count values and Likelihood Ratio Test[56]. Genes with an adjusted P value (P adj) of <0.05 were

subjected to Leiden Clustering with a resolution of 1.0 using custom Python scripts utilizing the leiden tool in Scanpy (PMID: 29409532)[57,58]. For each cluster, the mean expression and standard deviation were plotted per condition. Enrichment score shown in Figure 2.8C were calculated as follows. First, gene lists associated with each pathway in the KEGG database were compared to the list of genes upregulated with MBP-PTR1. Fisher Exact tests for the overlap between lists were performed using custom Python scripts. On a cartesian plot of $\log_{10}$(Odds ratio) vs confidence (-log10(P adj)), the Enrichment Score is calculated as the Pythagorean distance from the origin to each data point on the plot:

$$Score = \sqrt{\log(Odds)^2 + confidence^2}$$

HAPLN1 AlphaLISA assay on patient BM plasma fractions

Bone marrow (BM) aspirates from MM patients were obtained in accordance with the University of Wisconsin-Madison Institutional Review Board requirements (HO07403). Cytogenetic risk was assessed by fluorescence *in situ* hybridization (FISH). The plasma layer of patient BM aspirates was subjected to an amplified luminescent proximity homogenous assay-linked immunosorbent assay (AlphaLISA). First, the IgG level in each BM sample was measured using the Human IgG ELISA kit (BMS2091, Invitrogen, San Diego, CA, USA) following the manufacturer's protocol, with the dilution factor of 1,500,000. Plasma samples were diluted 50 times in PBS and final IgG level was adjusted by adding human IgG isotype control (31154, Invitrogen, San Diego, CA, USA) to match the highest IgG concentration among all the samples analyzed. The balancing of total IgG was necessary because preliminary study indicated that IgG was negatively interfering

with AlphaLISA assay (data not shown). The standard was prepared by serial dilutions of recombinant HAPLN1 (10323-H08H, Sino Biological, Beijing, China) with standard diluent (FBS diluted 50 times in PBS with human IgG isotype control added to match the highest IgG concentration among the samples). The cross-reactivity was tested using recombinant HAPLN3 (H00145864-P01, Abnova, Taipei, Taiwan). The assay was performed using assay buffer (25 mM HEPES, 0.5% BSA, 0.5% Triton X-100, 1 µg/mL Dextran) at room temperature. Diluted patient samples (5 µL) were incubated with 7.5 ng each of 2 primary anti-HAPLN1 antibodies, BAF2608 (R&D systems, Minneapolis, MN, USA) and HPA019105 (Sigma-Aldrich, St. Louis, MO, USA) for 30 min (15 µL total volume). The secondary rabbit IgG acceptor bead (6760002S, Perkin Elmer, Waltham, MA, USA), 1 µg in 10 µL assay buffer, was added and incubated for 1 hour. Subsequently, the streptavidin donor bead (AL159C, Perkin Elmer, Waltham, MA, USA), 1 µg in 25 µL assay buffer, was added, and after 30 min, the samples were measured by ENSPIRE plate reader (Perkin Elmer, Waltham, MA, USA).

The CoMMpass study data

From the IA17 CoMMpass dataset, patients were divided into two groups based on their STAT1 mRNA levels using a TPM cut-off value of 96. The Kaplan-Meier progression-free survival (PFS) curve for the STAT1 high group (n=48) and the low group (n=47) was plotted from the Multiple Myeloma Research Foundation Researcher Gateway. These data were generated as part of the Multiple Myeloma Research Foundation Personalized Medicine Initiatives using the Genospace Population Analytics platform (https://research.themmrf.org and www.themmrf.org).

Statistical analysis

Statistical analysis was performed using the two-tailed Student's t-test. For the analysis of time-lapse microscopy, the two-tailed Mann-Whitney test was used. The log-rank test was used for the Kaplan-Meier survival curve. A P-value of <0.05 was considered statistically significant. The analysis was performed with GraphPad Prism 9 Software (GraphPad Software Inc., La Jolla, CA, USA).

Acknowledgments

The authors thank Dr. Deane F. Mosher (University of Wisconsin-Madison) for the useful discussion on chemotaxis and chemokinesis and Dr. Lixin Rui for advice on STAT analyses. The authors also thank Miyamoto lab members for helpful discussion and Debayan De Bakshi in particular for advice on MBP-PTR1 protein purification; the University of Wisconsin Carbone Cancer Center Flow Cytometry Laboratory, the Experimental Animal Pathology Laboratory (EAPL), and the Small Animal Imaging & Radiotherapy Facility (SAIRF) for use of their facilities and services (supported by P30 CA014520). This work was supported by the National Institutes of Health R01 CA251595 and CA155192 for S.M.; and NIH T32 CA009135 and SciMed Graduate Research Scholars Fellowship at UW-Madison for M.H.

Authorship Contributions

H.Y.C. performed and analyzed the experiments; M.H. performed initial RNA-seq analysis and A.R. performed MAGIC and cluster analyses of all RNA-seq data; N.S.C consented and obtained primary patient samples; H.Y.C. and S.M. were responsible for overall study design; H.Y.C., M.H. and S.M. wrote the manuscript; and all coauthors reviewed, edited, and approved the manuscript.

Disclosure of Conflicts of Interest

The authors declare no conflicts of interest.

References

1. Shain K. Metastatic myeloma? *Blood*. 2012;119(24):5612-5613.

2. Hideshima T, Mitsiades C, Tonon G, Richardson PG, Anderson KC. Understanding multiple myeloma pathogenesis in the bone marrow to identify new therapeutic targets. *Nature reviews Cancer*. 2007;7(8):585-598.

3. Manier S, Sacco A, Leleu X, Ghobrial IM, Roccaro AM. Bone marrow microenvironment in multiple myeloma progression. *Journal of biomedicine & biotechnology*. 2012;2012(6):157496-157495.

4. Alsayed Y, Ngo H, Runnels J, et al. Mechanisms of regulation of CXCR4/SDF-1 (CXCL12)-dependent migration and homing in multiple myeloma. *Blood*. 2007;109(7):2708-2717.

5. Roccaro AM, Sacco A, Purschke WG, et al. SDF-1 inhibition targets the bone marrow niche for cancer therapy. *Cell reports*. 2014;9(1):118-128.

6. Maquart F-X, Pasco S, Ramont L, Hornebeck W, Monboisse J-C. An introduction to matrikines: extracellular matrix-derived peptides which regulate cell activity. Implication in tumor invasion. *Critical reviews in oncology/hematology*. 2004;49(3):199-202.

7. Weathington NM, van Houwelingen AH, Noerager BD, et al. A novel peptide CXCR ligand derived from extracellular matrix degradation during airway inflammation. *Nature medicine*. 2006;12(3):317-323.

8. Hunninghake GW, Davidson JM, Rennard S, Szapiel S, Gadek JE, Crystal RG. Elastin fragments attract macrophage precursors to diseased sites in pulmonary emphysema. *Science*. 1981;212(4497):925-927.

9. Pocza P, Süli-Vargha H, Darvas Z, Falus A. Locally generated VGVAPG and VAPG elastin-derived peptides amplify melanoma invasion via the galectin-3 receptor. *International journal of cancer*. 2008;122(9):1972-1980.

10. Grahovac J, Wells A. Matrikine and matricellular regulators of EGF receptor signaling on cancer cell migration and invasion. *Laboratory investigation; a journal of technical methods and pathology*. 2014;94(1):31-40.

11. Hope C, Foulcer S, Jagodinsky J, et al. Immunoregulatory roles of versican proteolysis in the myeloma microenvironment. *Blood*. 2016;128(5):680-685.

12. Huynh M, Pak C, Markovina S, et al. Hyaluronan and proteoglycan link protein 1 (HAPLN1) activates bortezomib-resistant NF-κB activity and increases drug resistance in multiple myeloma. *Journal of Biological Chemistry*. 2018;293(7):2452-2465.

13. Mark C, Warrick J, Callander NS, Hematti P, Miyamoto S. A Hyaluronan and Proteoglycan Link Protein 1 Matrikine: Role of Matrix Metalloproteinase 2 in Multiple Myeloma NF-κB Activation and Drug Resistance. *Mol Cancer Res*. 2022;20(9):1456-1466.

14. Huynh M, Chang HY, Lisiero DN, et al. HAPLN1 confers multiple myeloma cell resistance to several classes of therapeutic drugs. *PLoS One*. 2022;17(12):e0274704.

15. Spicer AP, Joo A, Bowling RA. A hyaluronan binding link protein gene family whose members are physically linked adjacent to chondroitin sulfate proteoglycan core protein genes: the missing links. *Journal of Biological Chemistry*. 2003;278(23):21083-21091.

16. De Bakshi D, Chen Y-C, Wuerzberger-Davis SM, et al. Ectopic CH60 mediates HAPLN1-induced cell survival signaling in multiple myeloma. *Life Science Alliance*. 2023;6(3):e202201636.

17. Diamond MS, Springer TA. The dynamic regulation of integrin adhesiveness. *Current biology : CB*. 1994;4(6):506-517.

18. Wilkinson PC. Assays of leukocyte locomotion and chemotaxis. *Journal of immunological methods*. 1998;216(1-2):139-153.

19. Wilkinson PC. How do leucocytes perceive chemical gradients? *FEMS microbiology immunology*. 1990;2(5-6):303-311.

20. Tchou-Wong K-M, Fok SYY, Rubin JS, et al. Rapid chemokinetic movement and the invasive potential of lung cancer cells; a functional molecular study. *BMC cancer*. 2006;6(1):151-112.

21. Liu Z, Klominek J. Chemotaxis and chemokinesis of malignant mesothelioma cells to multiple growth factors. *Anticancer Res*. 2004;24(3a):1625-1630.

22. de Gorter DJJ, Reijmers RM, Beuling EA, et al. The small GTPase Ral mediates SDF-1-induced migration of B cells and multiple myeloma cells. *Blood*. 2008;111(7):3364-3372.

23. Zigmond SH, Hirsch JG. Leukocyte locomotion and chemotaxis. New methods for evaluation, and demonstration of a cell-derived chemotactic factor. *The Journal of experimental medicine*. 1973;137(2):387-410.

24. Zengel P, Nguyen-Hoang A, Schildhammer C, Zantl R, Kahl V, Horn E. μ-Slide Chemotaxis: a new chamber for long-term chemotaxis studies. *BMC cell biology*. 2011;12(1):21-14.

25. Tomasova L, Guttenberg Z, Hoffmann B, Merkel R. Advanced 2D/3D cell migration assay for faster evaluation of chemotaxis of slow-moving cells. *PloS one*. 2019;14(7):e0219708.

26. Nguyen Q, Murphy G, Hughes CE, Mort JS, Roughley PJ. Matrix metalloproteinases cleave at two distinct sites on human cartilage link protein. *Biochemical Journal*. 1993;295 (Pt 2)(Pt 2):595-598.

27. Chen Z, Orlowski RZ, Wang M, Kwak L, McCarty N. Osteoblastic niche supports the growth of quiescent multiple myeloma cells. *Blood*. 2014;123(14):2204-2208.

28. Runnels JM, Carlson AL, Pitsillides C, et al. Optical techniques for tracking multiple myeloma engraftment, growth, and response to therapy. *Journal of biomedical optics*. 2011;16(1):011006.

29. Fangazio M, Ladewig E, Gomez K, et al. Genetic mechanisms of HLA-I loss and immune escape in diffuse large B cell lymphoma. *Proceedings of the National Academy of Sciences of the United States of America*. 2021;118(22).

30. Roopra A. MAGIC: A tool for predicting transcription factors and cofactors driving gene sets using ENCODE data. *PLoS Comput Biol*. 2020;16(4):e1007800.

31. Horvath CM, Wen Z, Darnell JE. A STAT protein domain that determines DNA sequence recognition suggests a novel DNA-binding domain. *Genes Dev*. 1995;9(8):984-994.

32. Huynh M, Pak C, Markovina S, et al. Hyaluronan and proteoglycan link protein 1 (HAPLN1) activates bortezomib-resistant NF-κB activity and increases drug resistance in multiple myeloma. *J Biol Chem*. 2018;293(7):2452-2465.

33. Toshchakov V, Jones BW, Perera PY, et al. TLR4, but not TLR2, mediates IFN-beta-induced STAT1alpha/beta-dependent gene expression in macrophages. *Nat Immunol*. 2002;3(4):392-398.

34. Palumbo A, Avet-Loiseau H, Oliva S, et al. Revised International Staging System for Multiple Myeloma: A Report From International Myeloma Working Group. *J Clin Oncol*. 2015;33(26):2863-2869.

35. D'Agostino M, Cairns DA, Lahuerta JJ, et al. Second Revision of the International Staging System (R2-ISS) for Overall Survival in Multiple Myeloma: A European Myeloma Network (EMN) Report Within the HARMONY Project. *J Clin Oncol*. 2022;40(29):3406-3418.

36. Bharti AC, Shishodia S, Reuben JM, et al. Nuclear factor-kappaB and STAT3 are constitutively active in CD138+ cells derived from multiple myeloma patients, and suppression of these transcription factors leads to apoptosis. *Blood*. 2004;103(8):3175-3184.

37. Bollrath J, Greten FR. IKK/NF-kappaB and STAT3 pathways: central signalling hubs in inflammation-mediated tumour promotion and metastasis. *EMBO Rep*. 2009;10(12):1314-1319.

38. Catlett-Falcone R, Landowski TH, Oshiro MM, et al. Constitutive activation of Stat3 signaling confers resistance to apoptosis in human U266 myeloma cells. *Immunity*. 1999;10(1):105-115.

39. Chong PSY, Chng WJ, de Mel S. STAT3: A Promising Therapeutic Target in Multiple Myeloma. *Cancers (Basel)*. 2019;11(5).

40. Malilas W, Koh SS, Kim S, et al. Cancer upregulated gene 2, a novel oncogene, enhances migration and drug resistance of colon cancer cells via STAT1 activation. *International journal of oncology*. 2013;43(4):1111-1116.

41. Kharma B, Baba T, Matsumura N, et al. STAT1 drives tumor progression in serous papillary endometrial cancer. *Cancer Research*. 2014;74(22):6519-6530.

42. Khodarev NN, Beckett M, Labay E, Darga T, Roizman B, Weichselbaum RR. STAT1 is overexpressed in tumors selected for radioresistance and confers protection from radiation in transduced sensitive cells. *Proceedings of the National Academy of Sciences*. 2004;101(6):1714-1719.

43. Kaowinn S, Kaewpiboon C, Koh SS, Krämer OH, Chung Y-H. STAT1-HDAC4 signaling induces epithelial-mesenchymal transition and sphere formation of cancer cells overexpressing the oncogene, CUG2. *Oncology reports*. 2018;40(5):2619-2627.

44. Khodarev NN, Roach P, Pitroda SP, et al. STAT1 pathway mediates amplification of metastatic potential and resistance to therapy. *PloS one*. 2009;4(6):e5821.

45. Boiarsky R, Haradhvala NJ, Alberge JB, et al. Single cell characterization of myeloma and its precursor conditions reveals transcriptional signatures of early tumorigenesis. *Nat Commun*. 2022;13(1):7040.

46. Vila-Coro AJ, Rodríguez-Frade JM, Martín De Ana A, Moreno-Ortíz MC, Martínez-A C, Mellado M. The chemokine SDF-1alpha triggers CXCR4 receptor dimerization and activates the JAK/STAT pathway. *FASEB journal : official publication of the Federation of American Societies for Experimental Biology*. 1999;13(13):1699-1710.

47. Sanz-Rodríguez F, Hidalgo A, Teixidó J. Chemokine stromal cell-derived factor-1alpha modulates VLA-4 integrin-mediated multiple myeloma cell adhesion to CS-1/fibronectin and VCAM-1. *Blood*. 2001;97(2):346-351.

48. Azab AK, Azab F, Blotta S, et al. RhoA and Rac1 GTPases play major and differential roles in stromal cell-derived factor-1-induced cell adhesion and chemotaxis in multiple myeloma. *Blood*. 2009;114(3):619-629.

49. Wallington-Beddoe CT, Mynott RL. Prognostic and predictive biomarker developments in multiple myeloma. *J Hematol Oncol*. 2021;14(1):151.

50. Jung O, Trapp-Stamborski V, Purushothaman A, et al. Heparanase-induced shedding of syndecan-1/CD138 in myeloma and endothelial cells activates VEGFR2 and an invasive phenotype: prevention by novel synstatins. *Oncogenesis*. 2016;5(2):e202-e202.

51. Markovina S, Callander NS, O'Connor SL, et al. Bortezomib-resistant nuclear factor-kappaB activity in multiple myeloma cells. *Molecular cancer research : MCR*. 2008;6(8):1356-1364.

52. O'Connor S, Shumway SD, Amanna IJ, Hayes CE, Miyamoto S. Regulation of constitutive p50/c-Rel activity via proteasome inhibitor-resistant IkappaBalpha degradation in B cells. *Mol Cell Biol*. 2004;24(11):4895-4908.

53. Lwin ST, Edwards CM, Silbermann R. Preclinical animal models of multiple myeloma. *BoneKEy reports*. 2016;5:772.

54. Campeau E, Ruhl VE, Rodier F, et al. A versatile viral system for expression and depletion of proteins in mammalian cells. *PloS one*. 2009;4(8):e6529.

55. Roopra A. MAGIC: A tool for predicting transcription factors and cofactors driving gene sets using ENCODE data. *PLoS computational biology*. 2020;16(4):e1007800.

56. Love MI, Huber W, Anders S. Moderated estimation of fold change and dispersion for RNA-seq data with DESeq2. *Genome Biol*. 2014;15(12):550.

57. Traag VA, Waltman L, van Eck NJ. From Louvain to Leiden: guaranteeing well-connected communities. *Sci Rep*. 2019;9(1):5233.

58. Blondel VD, Guillaume J-L, Lambiotte R, Lefebvre E. Fast unfolding of communities in large networks. *Journal of Statistical Mechanics: Theory and Experiment*. 2008;2008(10):P10008.

Figure 2.1

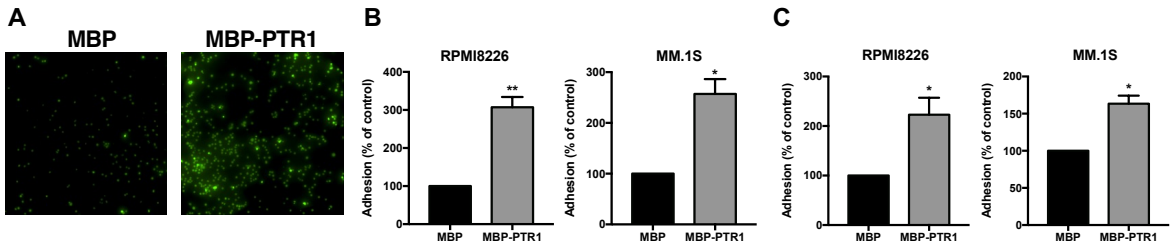

Figure 2.1. HAPLN matrikine increases MM cell adhesion and migration. (A) Microscopy images of RPMI8226 cells adhered to fibronectin-coated plates following incubation with MBP or MBP-PTR1 at 100 nM for 16 hours. (B) Graphs depicting %adhesion of RPMI8226 and MM.1S MM cell lines in response to MBP or MBP-PTR1 (100 nM) normalized to MBP control being set as 100%. (C) Graphs depicting %adhesion of RPMI8226 and MM.1S MM cell lines adhering to endothelial cells (HMEC-1). MM cells were incubated with MBP or MBP-PTR1 at 100 nM for 16 hours prior to the adhesion assay. Experiments were independently repeated 4 times for (B, left) and 3 times for (B, right, and C). Data are expressed as means ± SEM. *, $p < 0.05$; **, $p < 0.01$.

Figure 2.2

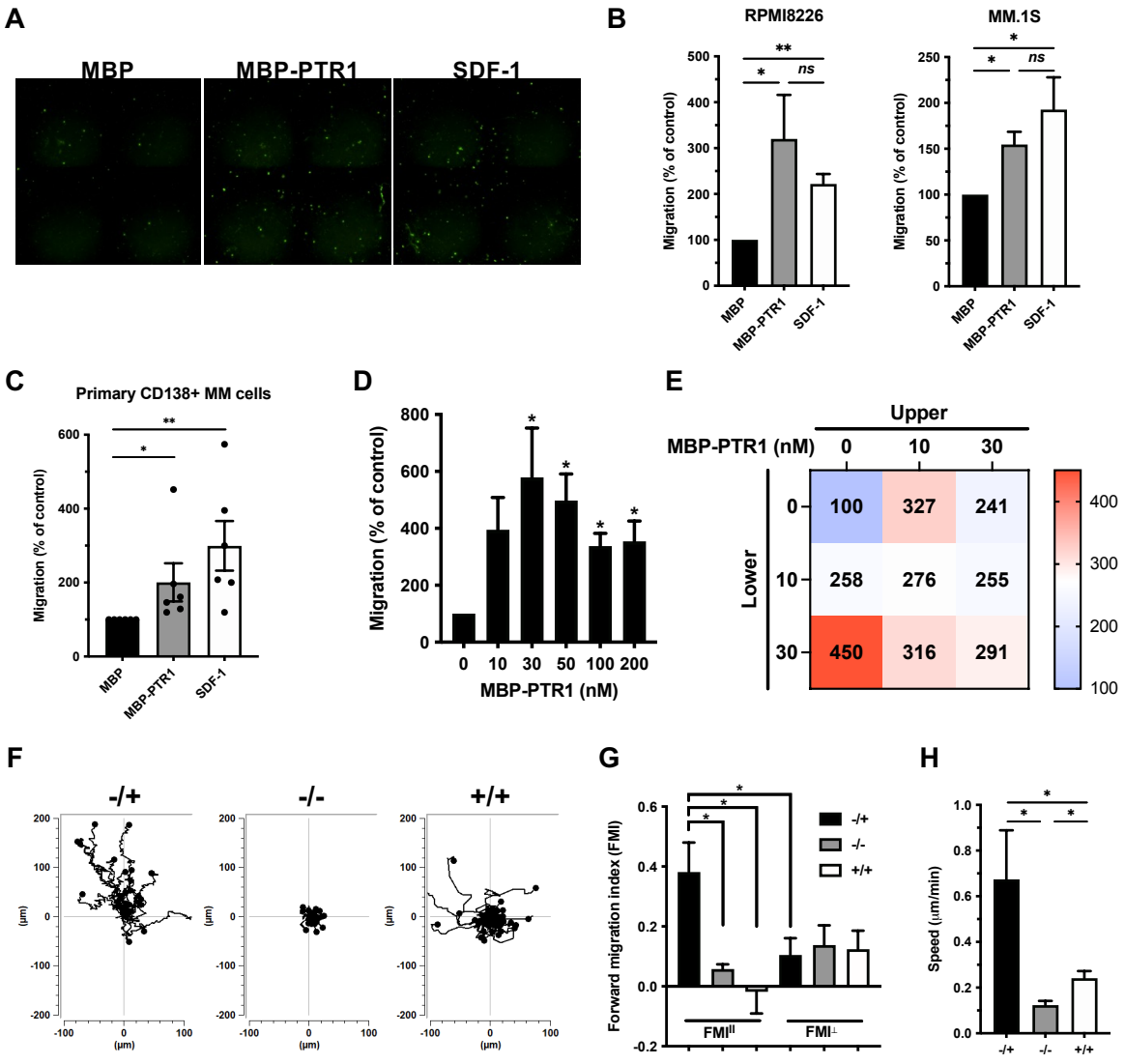

Figure 2.2. HAPLN1-PTR1 induces chemotactic and chemokinetic migration in MM cells. (A) Microscopy images of RPMI8226 cells on Transwell membranes which had migrated from the upper chamber to the lower chamber containing MBP or MBP-PTR1 at 100 nM or SDF-1 at 30 nM after 16 h. (B) Graphs depicting %migration of RPMI8226 and MM.1S MM cells treated as in (A) with MBP control being set as 100%. (C) Graphs depicting %migration of $CD138^{+}$ primary MM cells isolated from 6 patients in response to

MBP, MBP-PTR1, or SDF-1 with MBP control being set as 100%. (D) Graphs depicting %migration of RPMI8226 MM cell lines in response to indicated MBP-PTR1 concentrations in the lower Transwell compartment with the control (0 nM) set as 100%. (E) Migration of RPMI8226 cells in response to indicated MBP-PTR1 concentrations in the upper and lower chambers were quantified with the control (0 nM) set at 100%. (F) Individual cell track trajectories of three groups in time-lapse μ-Slide migration assay using RPMI8226 cells recorded for 16 hours are shown: positive gradient (-/+, 30 nM MBP/MBP-PTR1), negative control (-/-, 30 nM MBP/MBP), and no gradient (+/+, 30 nM MBP-PTR1/MBP-PTR1). The y-axis is parallel to the chemotactic gradient where cell trajectory going up along the y-axis is the migration towards the MBP-PTR1 in the -/+ group. (G) Graphs showing the comparison of averaged $FMI^{||}$ and $FMI^{\perp}$ for each group from (F). (H) Graph showing the comparison of the cell speed from (F). All experiments were independently repeated 3 times for (D and E) and 4 times for (B, G-H). Data are expressed as means ± SEM. *, $p < 0.05$; **, $p < 0.01$; *ns*, not significant.

Figure 2.3

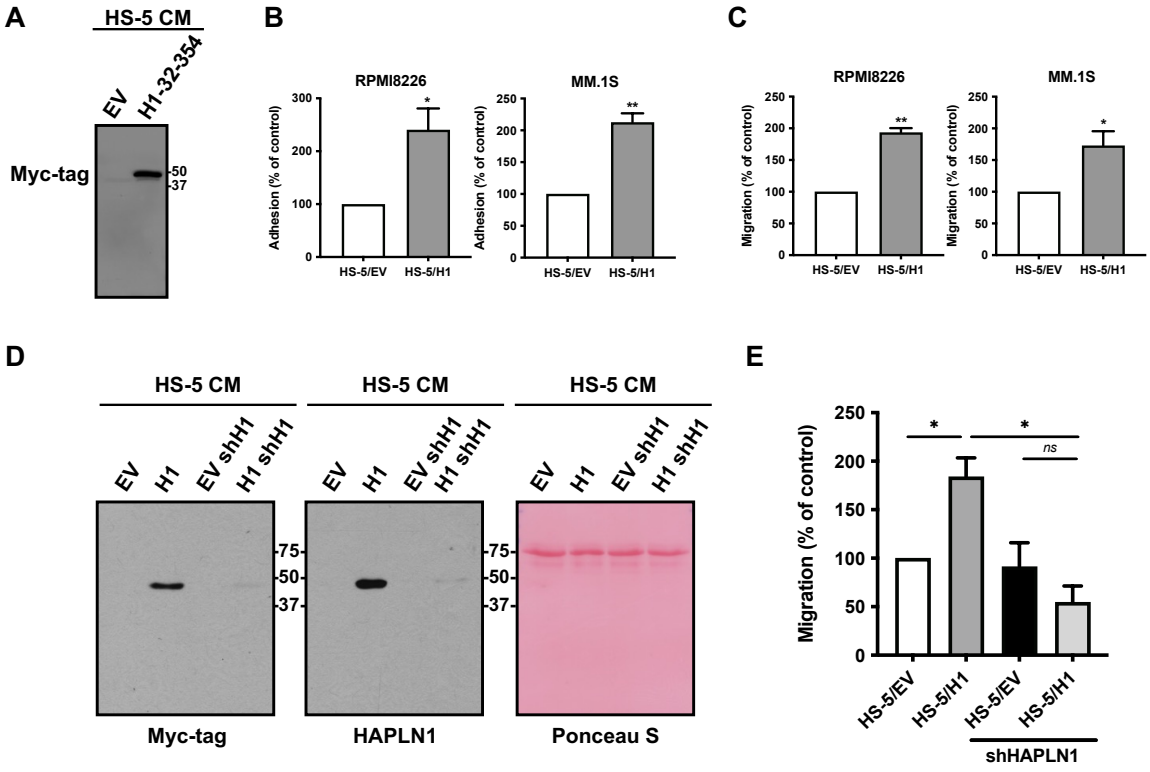

Figure 2.3. MM cells adhere and migrate towards BMSCs secreting HAPLN1 matrikine. (A) Western blot analysis of the conditioned media (CM) of HS5/EV and HS-5/H1 cells using anti-Myc-tag antibody. (B) Graphs showing %adhesion of RPMI8226 and MM.1S MM cell lines to HS-5/EV or HS-5/H1 cells with control HS-5/EV cells set as 100%. (C) Graphs showing %migration of RPMI8226 and MM.1S MM cell lines towards HS-5/EV or HS-5/H1 cells in the bottom Transwell chamber with the HS-5/EV group set as 100%. (D) Western blot analysis of the CM of HS5/EV, HS-5/H1 and HAPLN1 knockdown HS-5 cells using anti-Myc-tag and anti-HAPLN1 antibodies. The Ponceau S stain is shown as a loading control. (E) Graphs showing %migration of RPMI8226 cells to HS5/EV, HS-5/H1 and HAPLN1 knockdown HS-5 cells in the bottom of Transwell

chambers with the HS-5/EV group set as 100%. All experiments were independently repeated 3 times for (B and C, left, and E) and 4 times for (C, right). Data are expressed as means ± SEM. *, $p < 0.05$; **, $p < 0.01$; *ns*, not significant.

Figure 2.4

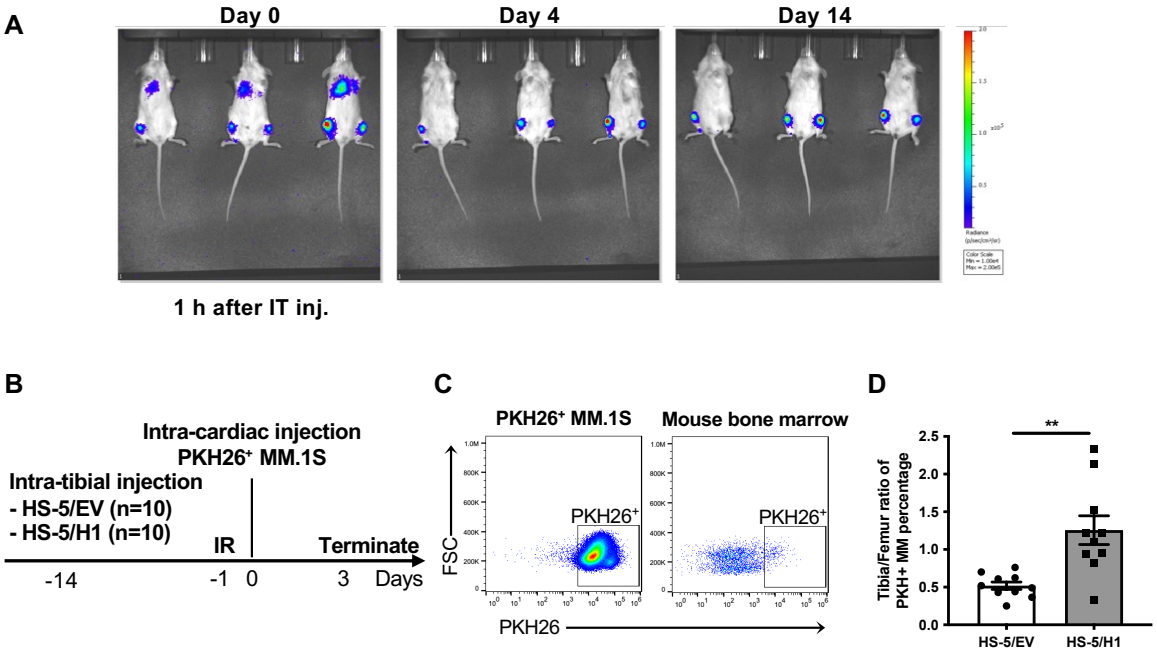

Figure 2.4. HAPLN1 matrikine induces MM cell BM homing *in vivo*. (A) Validation of BMSC intra-tibial (IT) injection. Luciferase-labeled HS-5 cells were injected via the intra-tibial route and imaged by IVIS on indicated days. On Day 0, 1 h after the IT injection, the cells were detected in the tibia and chest area, indicating the injection was rightly done in the bone marrow partially entering the systemic circulation. On Day 4 and 14, the majority of the cells were detected in the tibia and absent in chest areas. Of note, the first mouse was injected only in one leg showing that the majority of the injected cells remained within the injection site. (B) The experimental scheme for (C-D) is depicted. IR refers to sublethal whole-body irradiation at 3 Gy. (C) Representative flow plots and gating strategy of PKH26$^+$ MM.1S cells after cell culture (left) or from BM of mouse. FSC: forward scatter. (D) The percentage of PKH26$^+$ MM cells in the tibia and femur of mice was obtained by

flow cytometry as in (C) and the tibia/femur ratio of $PKH26^+$ MM percentage was plotted. Data are expressed as means ± SEM. **, $p < 0.01$.

Figure 2.5

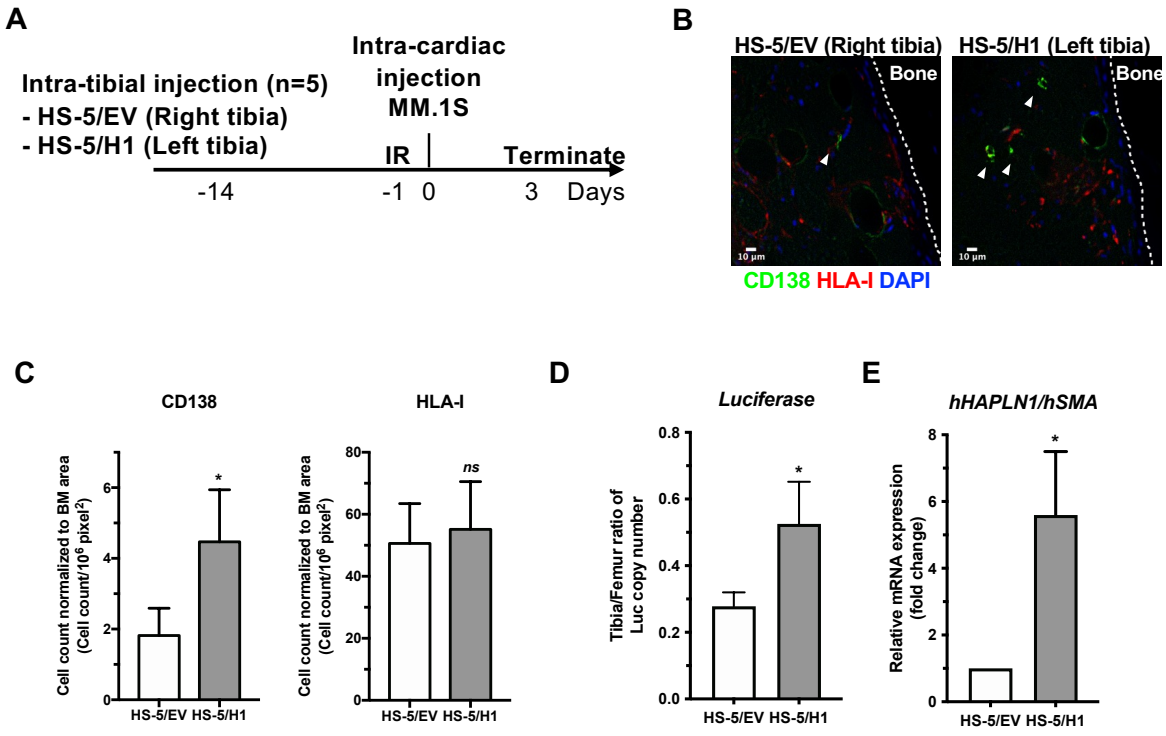

Figure 2.5. MM cells preferentially home to the tibia injected with HAPLN1-secreting BMSCs. (A) The experimental scheme for (B-C) is depicted. (B) IHC images of tibia sections stained for MM cells (CD138, green color), HS-5 cells (HLA-I, red color) or nuclei (DAPI, blue color). The white dotted line indicates the outline of the cortical bone. The white arrowhead indicates $CD138^+$ MM cells. (C) MM or HS-5 cells were counted in the imaged sections, their numbers were then normalized to the BM area from 2-4 sections of each tibia and were averaged and repeated for 5 mice. (D) Fifty ng of total genomic DNA collected from BM of individual mouse tibia and femur (n=5) was used to quantify the *luciferase* copy number using qPCR and *luciferase* gene standard, and the total copy number per tibia was calculated. The tibia/femur ratio of the *luciferase* copy number was plotted. (E) Total RNA was collected from above mouse tibia (n=5) and human *HAPLN1*

mRNA was quantified by qRT-PCR and normalized to human *SMA,* and then fold changes were plotted using HS-5/EV-injected tibia set as 1. Data are expressed as means ± SEM. *, $p < 0.05$; *ns*, not significant.

Figure 2.6

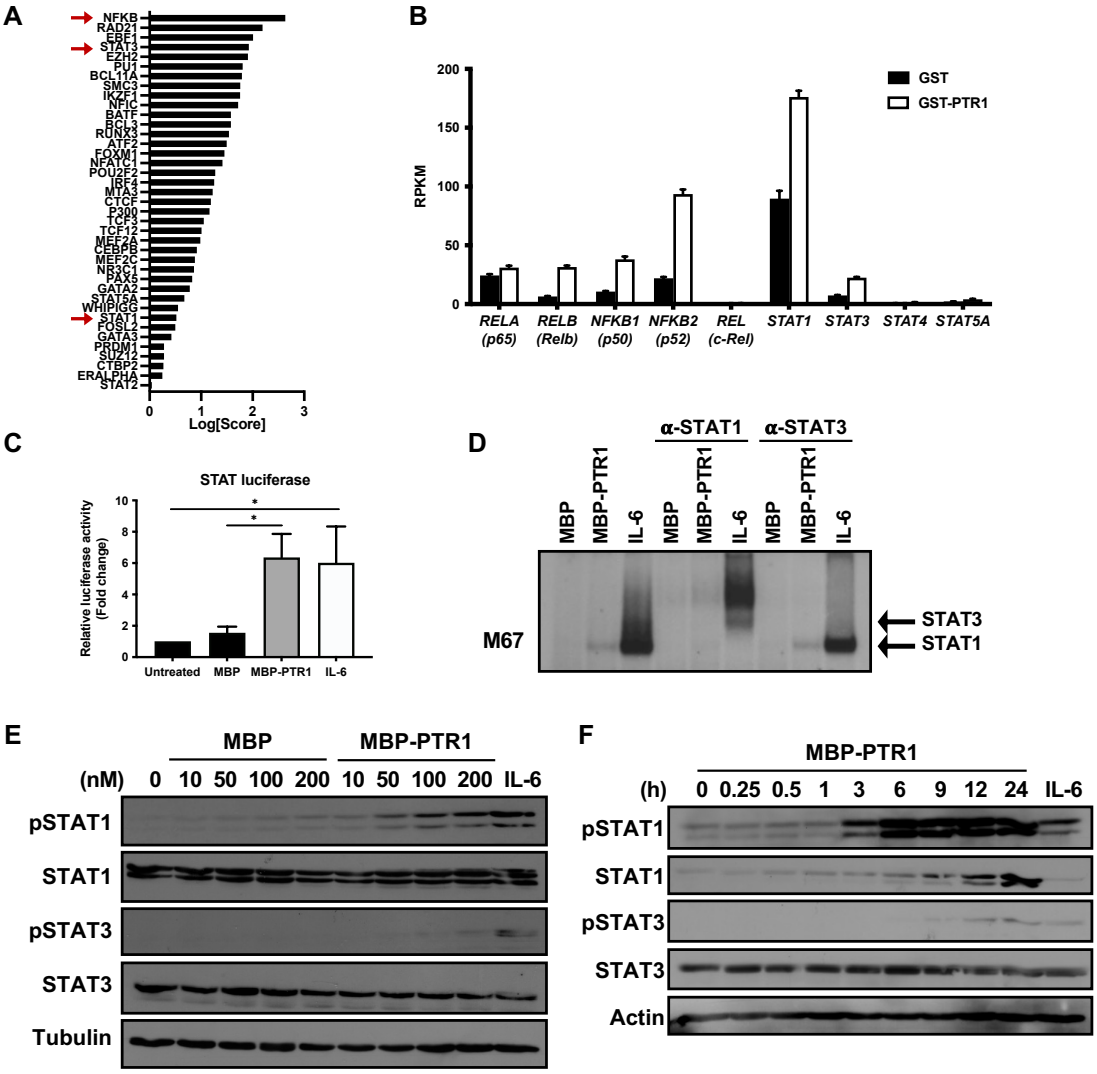

Figure 2.6. HAPLN1 matrikine activates STAT1 in MM cells. (A) The graph depicts MAGIC identified enrichment scores of transcription factors and cofactors in response to PTR1 treatment in RPMI8226 cells. (B) Reads per kilobase million (RPKM) values of indicated genes from the RNA-seq results are plotted. (C) STAT-dependent luciferase reporter activities on RPMI8226 cells with the indicated stimuli are shown. The graph depicts the mean ± SEM of the quantification of 3 independent replicates. (D)

Representative STAT1 and STAT3 supershift analysis of RPMI8226 cells incubated with MBP or MBP-PTR1 (100nM, 6 hours) or IL-6 (50 ng/mL, 15 minutes). (E-F) Representative Western blot analysis on RPMI8226 cells treated with the indicated dose of MBP or MBP-PTR1 for 6 h (E) or 100 nM MBP-PTR1 for the indicated time (F). *, $p < 0.05$.

Figure 2.7

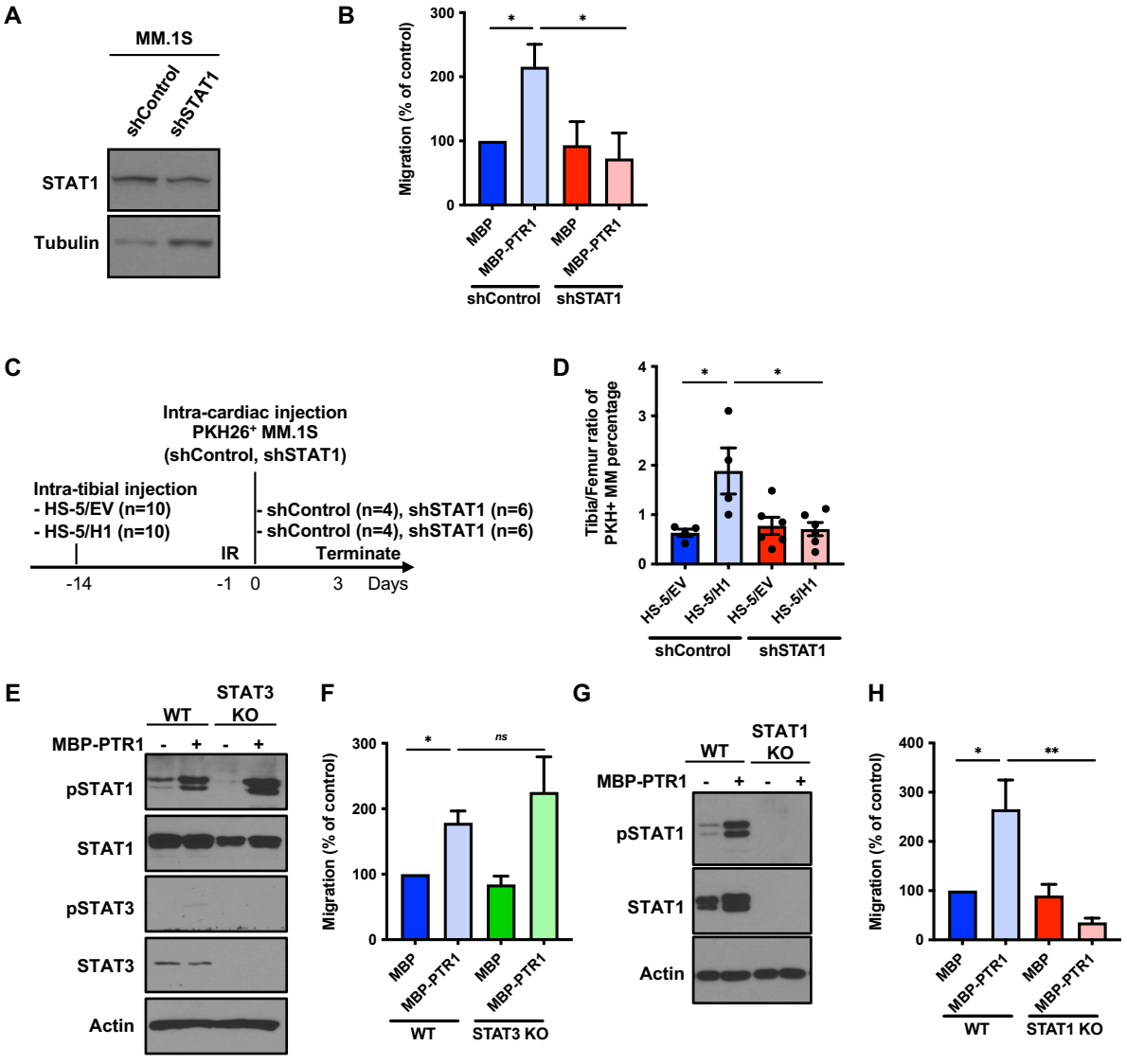

Figure 2.7. STAT1 is required for HAPLN1 matrikine-induced MM cell migration and BM homing. (A) Representative Western blot analysis on MM.1S shControl and shSTAT1 clones probed with STAT1 and tubulin antibodies. (B) Graphs depicting %migration of MM.1S shControl or shSTAT1 clones in response to MBP or MBP-PTR1 with MBP-treated shControl being set as 100%. (C) The experimental scheme for (D) is depicted. (D) The tibia/femur ratio of PKH26$^+$ MM percentage was plotted as in Figure 2.4C. (E)

Representative Western blot analysis of indicated proteins in RPMI8226 WT and STAT3 KO cells treated with 100 nM of MBP or MBP-PTR1 for 6 hours. (F) Graphs depicting %migration of RPMI8226 WT and STAT3 KO cells in response to MBP or MBP-PTR1 (100 nM) with MBP treated WT being set as 100%. (G) Representative Western blot analysis of indicated proteins in RPMI8226 WT and STAT1 KO cells treated with 100 nM of MBP or MBP-PTR1 for 6 hours. (H) Graphs depicting %migration of RPMI8226 WT and STAT1 KO cells in response to MBP or MBP-PTR1 (100 nM) with MBP treated WT being set as 100%. The graph depicts the mean ± SEM of the quantification of 3 independent experiments. *, $p < 0.05$; **, $p < 0.01$; *ns*, not significant.

Figure 2.8

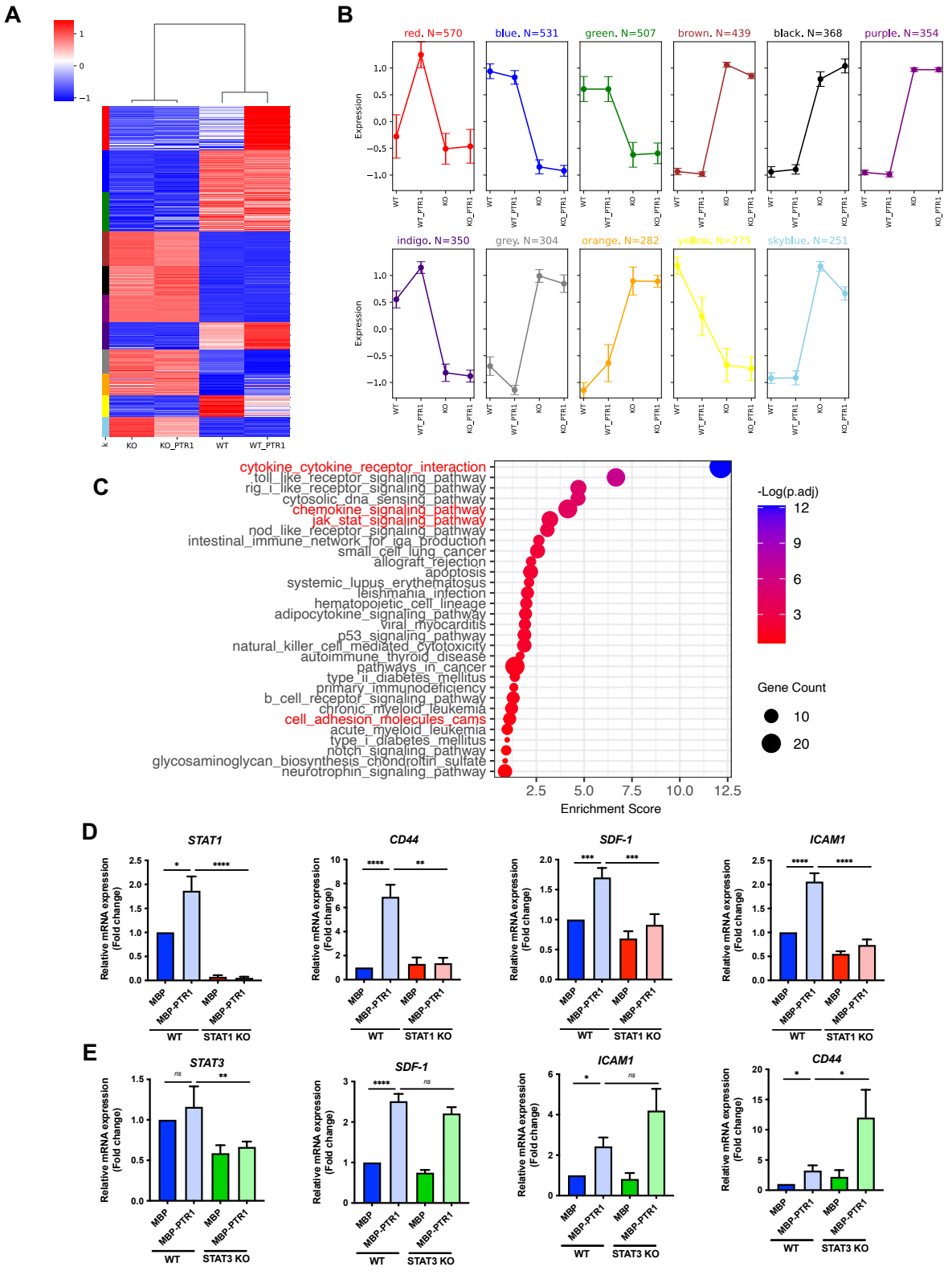
A
1
0
−1
KO
KO_PTR1
WT
WT_PTR1
B
red. N=570
blue. N=531
green. N=507
brown. N=439
black. N=368
purple. N=354
indigo. N=350
grey. N=304
orange. N=282
yellow. N=275
skyblue. N=251
Expression
WT
WT_PTR1
KO
KO_PTR1
C
cytokine_cytokine_receptor_interaction
toll_like_receptor_signaling_pathway
rig_i_like_receptor_signaling_pathway
cytosolic_dna_sensing_pathway
chemokine_signaling_pathway
jak_stat_signaling_pathway
nod_like_receptor_signaling_pathway
intestinal_immune_network_for_iga_production
small_cell_lung_cancer
allograft_rejection
apoptosis
systemic_lupus_erythematosus
leishmania_infection
hematopoietic_cell_lineage
adipocytokine_signaling_pathway
viral_myocarditis
p53_signaling_pathway
natural_killer_cell_mediated_cytotoxicity
autoimmune_thyroid_disease
pathways_in_cancer
type_ii_diabetes_mellitus
primary_immunodeficiency
b_cell_receptor_signaling_pathway
chronic_myeloid_leukemia
cell_adhesion_molecules_cams
acute_myeloid_leukemia
type_i_diabetes_mellitus
notch_signaling_pathway
glycosaminoglycan_biosynthesis_chondroitin_sulfate
neurotrophin_signaling_pathway
2.5
5.0
7.5
10.0
12.5
Enrichment Score
-Log(p.adj)
12
9
6
3
Gene Count
10
20
D
STAT1
CD44
SDF-1
ICAM1
Relative mRNA expression (Fold change)
MBP
MBP-PTR1
WT
STAT1 KO
E
STAT3
SDF-1
ICAM1
CD44
WT
STAT3 KO

Figure 2.8. STAT1 regulates HAPLN1 matrikine-induced migration genes. (A) Heat map of the cluster analysis on differentially expressed genes from the RNA-seq data. (B) Summarized bar graphs showing the 11 clusters. Data are expressed as means ± SD. (C) The dot plot represents the enrichment scores of the top 30 pathways where the size of dot indicates the number of genes enriched for each pathway, and color intensity correlates with the p.adjusted. See Methods for enrichment score calculations. (D-E) RNA levels of indicated genes was quantified by qRT-PCR and normalized to GAPDH and fold change relative to control (MBP in WT cells) were plotted. The graph represents the means ± SEM of 5 biological replicates for (D) and 3 biological replicates for (E), each performed in duplicates. *, $p < 0.05$; **, $p < 0.01$, ***, $p < 0.001$; ****, $p < 0.0001$; *ns*, not significant.

Figure 2.9

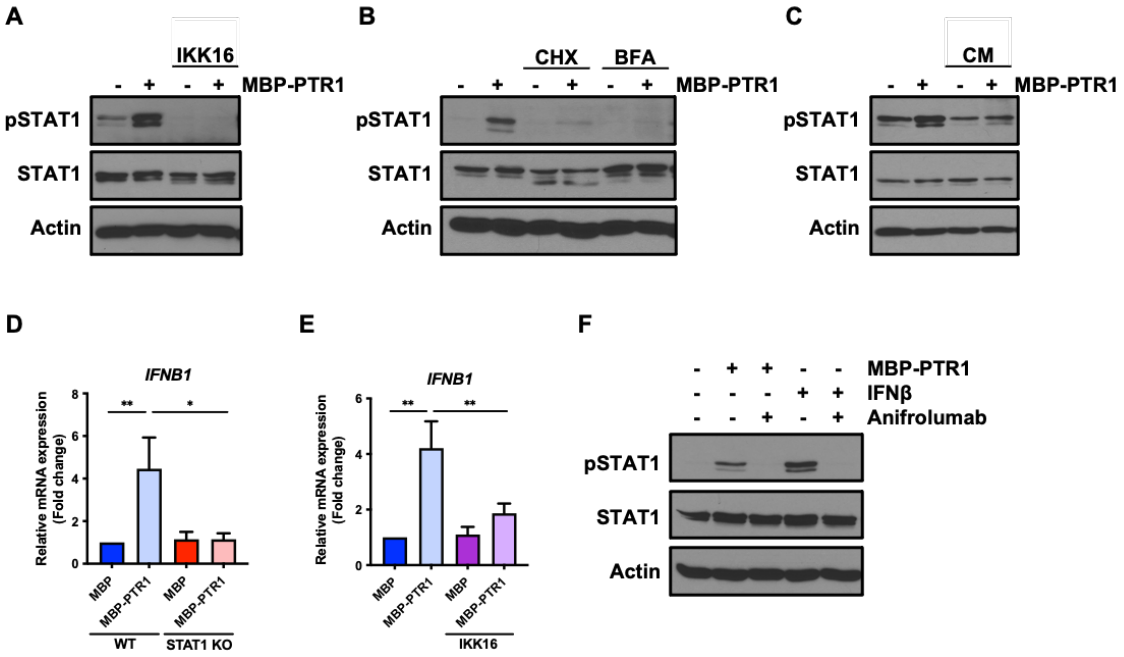

Figure 2.9. Autocrine/paracrine production of IFNβ by NF-κB contributes to HAPLN1 matrikine-induced STAT1 activation. (A) Representative Western blot analysis of indicated proteins in RPMI8226 cells pretreated with IKK16 (10 μM) or DMSO for 10 min and stimulated with 100 nM of MBP or MBP-PTR1 for 6 hours. (B) Representative Western blot analysis of indicated proteins in RPMI8226 cells pretreated for 10 min with cycloheximide (CHX; 20 μg/ml) or brefeldin A (BFA; 3 μg/ml) and stimulated with 100 nM of MBP or MBP-PTR1 for 6 hours. (C) RPMI8226 cells were stimulated with 100 nM of MBP or MBP-PTR1 for 6 hours (lane 1 and 2). RPMI8226 cells were stimulated with 100 nM of MBP or MBP-PTR1 for 5 hours and subsequently washed with fresh media. Conditioned medium (CM) was harvested after a 1-hour incubation of fresh media without MBP or MBP-PTR1. CM was added to fresh RPMI8226 cells for 15 min (lane 3 and 4) and analyzed by Western blotting for the indicated proteins. (D)

RPMI8226 (WT and STAT1 KO) cells were stimulated with 100 nM of MBP or MBP-PTR1 for 6 hours. The *IFNB1* mRNA level was quantified by qRT-PCR and normalized to GAPDH and fold change relative to control (MBP in WT cells) was plotted. (E) RPMI8226 cells were treated as in (A). The mRNA level of *IFNB1* was quantified by qRT-PCR and normalized to GAPDH and fold change relative to control (MBP and DMSO treated cells) was plotted. (F) Representative Western blot analysis of indicated proteins in RPMI8226 cells pretreated with 10 μg/mL of anifrolumab or human IgG for 10 min and stimulated with 100 nM of MBP or MBP-PTR1 for 6 hours or IFNβ (50 pg/mL) for 15 min. The graph represents the means ± SEM of 3 biological replicates for (D-E), each performed in duplicates. *, $p < 0.05$, **, $p < 0.01$.

Figure 2.10

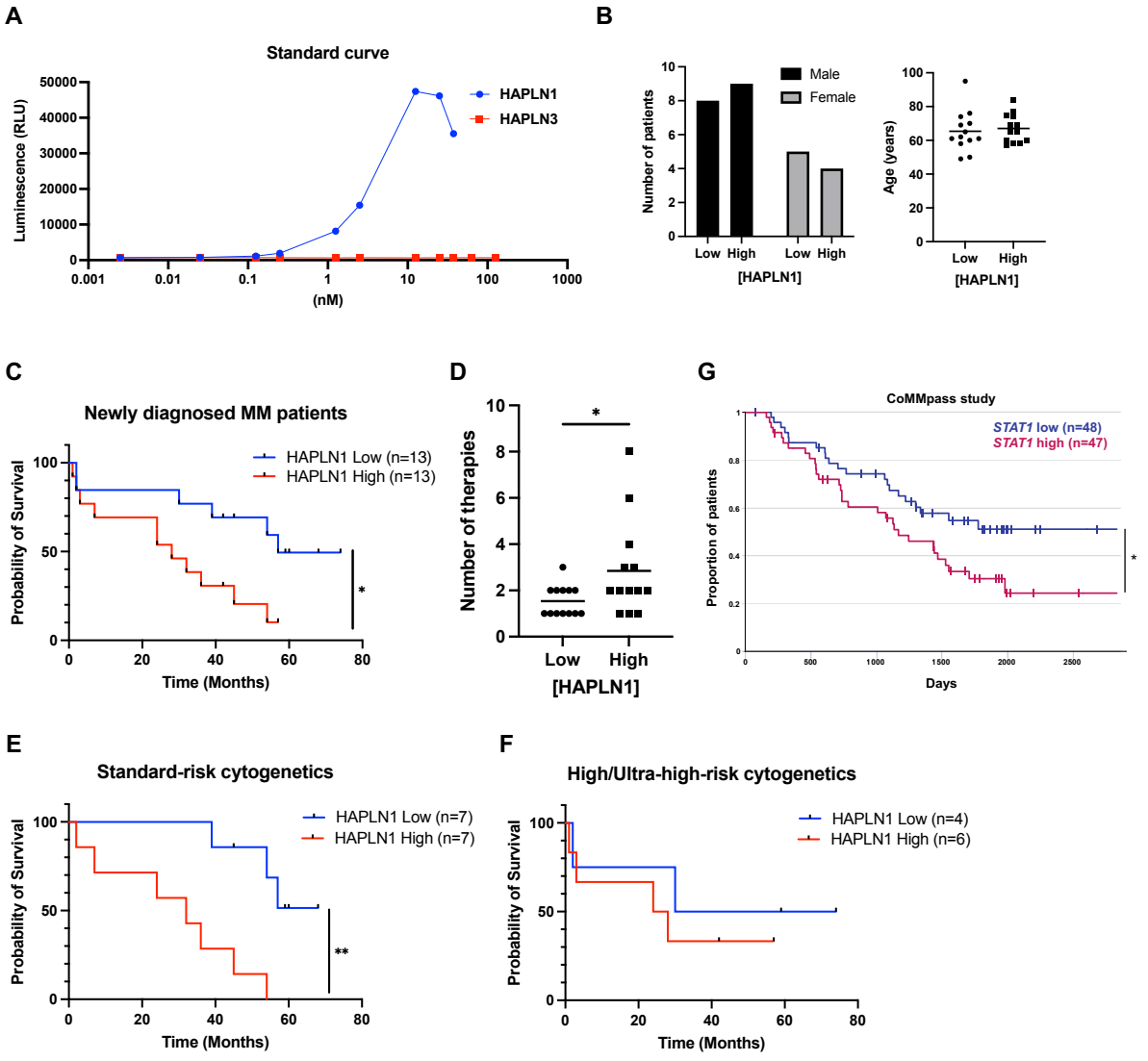

Figure 2.10. High HAPLN1 levels in BM plasma fractions and high *STAT1* mRNA levels in MM cells correlate with poor prognosis of NDMM patients. (A) The standard curve of recombinant HAPLN1 and HAPLN3 by AlphaLISA. Minimal cross-reactivity to HAPLN3 was observed in the assay condition even at a 10x excess concentration. (B) Graph depicting the distribution of sex and age in the HAPLN1 high and low patient groups in Table 2.4. (C) Kaplan-Meier progression-free survival (PFS) curve of the

HAPLN1 high and low groups (n=26). (D) Graph depicting the number of therapies that NDMM patients received during the follow-up. (E) Kaplan-Meier PFS curve of standard cytogenetic risk patients (n=14) separated by HAPLN1 levels. (F) Kaplan-Meier PFS curve of high/ultra-high cytogenetic risk patients (n=10) separated by HAPLN1 levels. (G) Kaplan-Meier PFS curve of *STAT1* high and low groups from the CoMMpass study. *, $p < 0.05$; **, $p < 0.01$.

Table 2.1. List of transcription factors driving genes induced by HAPLN1 matrikine in RPMI8226 MM cells as detected by the MAGIC analysis.

Factor	*Critical ChIP*	*KS statistic*	*Obs Tail Mean*	*Exp Tail Mean*	*Tail Enrichment*	*Raw p*	*Corrected p*	*Score*
NFKB	6.54530669	0.2807431	35.1815127	41.7137979	11.7715788	5.4838E-39	2.7419E-37	430.391889
RAD21	4.30659814	0.11932018	10.1861354	11.0218637	25.3766696	2.1641E-07	7.7288E-07	155.099407
EBF1	7.8215516	0.15116738	25.7923094	31.3995508	10.1996429	1.3202E-11	1.1002E-10	101.573573
STAT3	7.78945995	0.14549345	29.1684577	36.3924389	9.07545231	8.7938E-11	5.4962E-10	84.0381563
EZH2	3.234928	0.19419403	27.836516	42.5649865	4.77996018	7.085E-19	1.1808E-17	80.914256
PU1	5.1502342	0.12640798	21.2137543	26.3001862	9.34131066	3.0418E-08	1.3827E-07	64.0747377
BCL11A	6.04573148	0.19510129	34.7097976	60.9969861	3.64081475	4.7592E-19	1.1898E-17	61.6190477
SMC3	4.68696292	0.11820601	15.9878211	19.7357555	9.5315373	2.9157E-07	9.7191E-07	57.3071583
IKZF1	13.3526104	0.16147157	61.5964912	92.132544	5.03434535	3.5034E-13	4.3792E-12	57.1831243
NFIC	5.25073471	0.15884057	24.0940542	36.9950302	4.7352297	9.0533E-13	9.0533E-12	52.2920499
BATF	5.32278254	0.11676896	30.2658432	41.3692402	6.45163667	4.2654E-07	1.3329E-06	37.9046079
BCL3	6.74636988	0.15027822	31.9802883	54.6122743	3.82611419	1.7856E-11	1.2754E-10	37.8569144
RUNX3	6.88436818	0.08940377	16.8522973	20.3122718	10.7412841	0.00024567	0.00058492	34.7255065
ATF2	7.69754014	0.12822033	25.6187728	40.4857537	4.44639883	1.8086E-08	9.0432E-08	31.318997
FOXM1	9.40233713	0.12061475	27.6756415	43.302642	4.5420286	1.5251E-07	5.8658E-07	28.3044526
NFATC1	10.4608658	0.13996331	35.5513216	70.3858052	3.0411568	5.2064E-10	2.8924E-09	25.9676401
POU2F2	9.3629058	0.11167551	31.2612265	56.1340636	3.51368402	1.5822E-06	4.6534E-06	18.7357747
IRF4	7.16202006	0.10815998	32.0794635	56.8426282	3.59090176	3.7789E-06	1.0497E-05	17.8788679
MTA3	13.7923437	0.12081717	27.8578708	60.7333191	2.6947523	1.4434E-07	6.0142E-07	16.7635813
CTCF	3.8769406	0.07935412	8.98488556	12.4032665	6.25680765	0.00166003	0.00345839	15.3987952
P300	2.77437163	0.09329994	17.7171732	29.2440939	4.0740514	0.00011017	0.00027543	14.5035839
TCF3	8.40615591	0.09397206	30.5820316	59.3857147	3.12348063	9.5606E-05	0.0002516	11.2423342
TCF12	5.94150791	0.08057992	24.7672181	41.127701	4.0276879	0.00133106	0.00302513	10.1467778
MEF2A	6.40152359	0.07965557	36.4441096	61.4131955	3.91913847	0.00157276	0.00341904	9.66496958
CEBPB	4.80577895	0.05654477	15.4201692	19.9573499	7.79724699	0.05453822	0.08796486	8.23148166
MEF2C	8.11488021	0.07667621	49.6025755	92.4303226	3.31637567	0.00265794	0.00531588	7.54284723
NR3C1	7.80499919	0.06750732	38.5552027	61.4993591	4.36078626	0.01178554	0.02182508	7.24345863
PAX5	5.78318766	0.06938323	22.7943829	39.0947254	3.79679802	0.0088249	0.01697097	6.72144621
GATA2	6.03194	0.0578961	23.3087111	33.9277113	5.39000105	0.04581855	0.07636425	6.02122367
STAT5A	9.24860609	0.0580144	34.0913111	55.0467494	4.25369582	0.04511625	0.07778665	4.71775258
WHIPIGG	11.1504468	0.05871475	22.6731897	43.9084243	3.13543105	0.04114682	0.07347647	3.5551139
STAT1	9.55873538	0.0564272	91.9662042	179.162884	3.10939693	0.05536037	0.08650057	3.30522992
FOSL2	6.30505182	0.05111308	28.7374882	48.1289744	3.96392838	0.10537763	0.15966307	3.1584404
GATA3	4.76647081	0.04636683	22.6681247	36.526847	4.27131523	0.17736656	0.23968454	2.64975298

Factor	*Critical ChIP*	*KS statistic*	*Obs Tail Mean*	*Exp Tail Mean*	*Tail Enrichment*	*Raw p*	*Corrected p*	*Score*
PRDM1	11.7633149	0.05097104	79.2439249	194.289492	2.37760936	0.10711234	0.15751815	1.90843427
SUZ12	17.9117707	0.04947767	44.6274849	101.768764	2.56200512	0.12682015	0.18117165	1.90077663
CTBP2	13.1683098	0.0474254	28.4410465	59.8815696	2.80919677	0.15862874	0.22031769	1.84550358
ERALPHA	3.21758498	0.04414241	39.28017	73.4525153	3.29894494	0.22237142	0.29259397	1.76076116
STAT2	13.5089439	0.04344046	86.5307552	247.026163	2.07829571	0.23824257	0.30543919	1.07047866
FOS	3.40643612	0.03190816	14.1483213	27.1649798	3.17387915	0.61490065	0.76862581	0.36272689
ZNF217	13.1118749	0.02802284	39.2074186	82.1531593	2.82590487	0.76829368	0.93694351	0.07993522
JUN	4.90573319	0.02526052	19.2502293	32.7699553	3.84772477	0.86491446	1	0
JUNB	10.9873312	0.02004601	34.196361	68.4471157	2.99682379	0.97737302	1	0
RXRA	19.7756369	0.01234603	43.7135871	120.165459	2.14355832	0.99999508	1	0
BRF2	60.3457987	0.01171055	75.874739	459.308529	1.39576449	0.99999896	1	0
HDAC6	64.4782257	0.00920812	84.1928925	213.595371	2.30125626	1	1	0
NELFE	116.925782	0.0089239	85.8248167	283.754374	1.86722587	1	1	0
NANOG	33.3381245	0.00870787	47.5423245	131.385557	2.13407661	1	1	0
POL3	369.460895	0.0034495	53.9453836	550.874671	1.21711493	1	1	0
BRF1	299.394965	0.00412712	83.2064894	570.288768	1.34165271	1	1	0

Table 2.2. List of genes in the cluster analysis of HAPLN1 matrikine induced genes.

Blue	Green	Skyblue	Brown	Red	Black	Yellow	Orange	Indigo	Grey	Purple
FAT4	IFI6	KCNMB4	THBS2	MARCKS	DDR1	UGT2B4	AK4	PTPRM	HAVCR2	ATP9A
RPS4Y1	PLSCR1	PRAMEF2	SIGLEC7	CD83	ATP2C2	SNCAIP	LIPG	ZFY	TMCC2	IGF2
MEF2C	LGALS9	FLNC	SMYD1	CXCL10	WNT5A	RNF144B	CRTC3	DIAPH2	ELFN2	CDC42EP1
MME	OAS2	TJP3	KIF1A	CD70	SCN4B	TCEAL8	PTPRK	EPHA3	DUSP4	PCARE
INPP5D	ERP29	TGFA	CLDN1	ADPRH	ADARB2	CYTH4	ABTB2	ZC3H12C	ARHGAP39	KEL
LINC01612	SRI	TPRXL	LGR4	MFSD2A	NXN	GULP1	CD59	SOX4	RXRA	SLC13A4
CTNND2	HLA-F	MAP7D2	HABP2	TNFAIP3	SLC16A9	OR2W3	GJC1	GJA1	GPC1	MATN2
DDIT4L	STAT1	TMEM37	MAMLD1	TLR7	LIMS2	PYCARD	FARP1	CYBB	CLDN3	BMP5
CDH2	CCDC112	SMAD6	CCBE1	SIRPA	ELN	CRACDL	FOXP1	ADAMTS2	SPTLC3	MAGEA12
GALNT17	UBE2J2	GLI2	DAB2IP	TNFSF9	ATF7IP2	METRNL	KIDINS220	HRH2	MAL	FAT1
GALNTL6	MRPS26	F13A1	PYGL	GAS7	DPP6	NT5E	FN1	LCP2	IL17RC	EDN3
CTAG2	B4GALT2	ENTPD8	TMEM132B	PTGER4	LY6H	VSIR	ASAP2	SVIL	ARHGEF16	FBLN2
CTNNA3	COX17	LAD1	SLC47A1	IL10	ZNF423	DHCR7	APLP2	WWC3	KRT80	EPAS1
CDH4	CHCHD1	GLDC	LAPTM4B	TNIP1	FAM227A	SPI1	SIX4	CHRM3	WIPI2	CYP24A1
SLFN13	OAS3	ARHGAP22	SALL1	CD86	BIN1	ACSS2	IL2RB	ITPRIPL2	GTF2IRD1	SCRN1
GLUL	HNRNPA1	GFPT2	RSPO2	RIPK2	FZD6	ACAT2	SGMS2	TFAP2B	ERMAP	DMRT3
SHANK2	TSPAN3	ST3GAL5	FREM2	TFRC	LINC01679	ARV1	ATXN1	KCNQ3	NOL4L	DMTN
SPON1	CIAO1	HLTF	GLI3	CD40	PKIG	EVI2B	CIZ1	PRKY	P3H4	PCOLCE2
TLR4	CYCS	PRXL2A	HSPG2	TRAF4	HOXB9	PLIN2	FOXC1	MIR4527HG	FBLN7	LAMA3
CD53	MAGOHB	CLEC18B	SYT12	DENND4A	AGAP14P	SS18L2	NHLRC2	EYA2	H1-0	ALX4
UTRN	ACLY	GSC	RASL11A	CDKN1B	CDCP1	TNFSF4	SFTPA2	ROBO1	ZER1	CD177
GLB1L2	PCNA	BBOX1-AS1	MYLK3	NRP2	MT1A	EPB41L1	SAMSN1	CNTNAP2	PLP2	TLCD4
SCAMP5	MX1	LIPT2-AS1	PLCB4	CCDC28B	PGLYRP4	H2AJ	ANO9	DPY19L2	KRT6C	IL1R1
LINC01432	CASP4	SH3RF3-AS1	FAM171B	PTX3	PRIMA1	TMA7	PDZD8	GRAMD1B	HDAC11	EMP2
LINC02506	IFI44	DUBR	IL34	MT2A	JDP2	EDA	PRRT4	DAPK1	RGS12	KLK1
KCNK1	AIP	PRAMEF4	UNC13B	ELL2	GRK3	NPRL2	BCL7A	SLC35F1	NACC2	RIMBP2
PARM1	ESRRA	ERICH5	LINC00997	MAP3K8	OSBP2	NME3	HIPK2	PIP5K1B	RHOB	MPZL2
FCMR	PARK7	TUFT1	WNT7A	PELI1	TSPAN1	LSM10	ALDOB	IFNLR1	H2AW	EFR3B
SLC4A10	FH	ABTB1	NCKAP1	CD44	KIF19	CCDC86	ABCC4	MYO1E	MRGPRE	ACTL8
SERPINE2	DELE1	LAMB1	SOX13	RAB30	FGF17	TMEM258	ELF3	LONRF3	GAS6-DT	PRRX1
PGM5	ADA2	ALOX5	DNM1	MS4A7	ANKRD29	GCHFR	CMAHP	KIF13A	KIAA1522	GNG12
CD163L1	PPP1R8	FAM41C	NTRK3	CXCR5	ZNF827	NCK2	BASP1	TP53BP2	TSPAN12	OTX2
MEF2C-AS1	SELPLG	F2RL1	NAP1L2	PMAIP1	IGFBP2	APCDD1	TNS3	TGFBI	TTC39B	WFDC1
GCSAML	IFIT1	SLC6A3	CCDC88A	CD36	RORA	ARMCX6	STAT5B	MAP4K4	LGI2	MCTP2
EFNB2	P2RY8	SDC2	OCLN	SGPP2	ZNRF1	CFC1	PALS2	CDK20	TMEM45B	WIPF3
BLNK	PSMG4	CHST14	NLRP13	VAV1	GRTP1	DMAC1	PHKA1	MTAP	PLXND1	ISLR

Blue	Green	Skyblue	Brown	Red	Black	Yellow	Orange	Indigo	Grey	Purple
FERMT3	ACTR5	KCNMB2-AS1	MLC1	LINC02605	FAM43B	RPS14	TTC39C	ADGRE1	CREB3L4	DYSF
GNAI1	RBIS	DIPK1B	ZNRF2P1	DCP1A	CD300C	COMMD3	BNC2	PRPF38A	NEURL3	ANKRD18B
CD37	CBWD5	CALCRL	KCNT2	BCL2	PHLDA1	DPM3	CMTM8	LYSMD2	TSC22D3	DMRT1
SELENOP	MIEF1	GREB1	DGKB	C21orf91	SIM2	TEX264	THUMPD3	LHX3	PPP1R26	ZBTB7C
P2RX6P	EARS2	FGFR3	MAB21L4	PPRC1	LEF1	ANGPTL2	FMR1	CCDC71L	YPEL3	PCDH18
PAGE1	RCC1	IGLON5	TRIM9	ABI1	TNFRSF25	HRH1	ATN1	RCN1	LIMK1	CALML3
GMFG	SCMH1	KAT6B	TOGARAM2	DRAM1	INHBE	C9orf64	ST20-AS1	RUNX2	HBP1	MAGEH1
CARD18	MRM3	HOXB7	DOP1B	DMRTA1	EGFL6	SYVN1	RNF135	PEX5L	PTMS	OLFM1
ILDR2	SNHG4	ACSM3	DPY19L1P1	GRIA4	SEZ6L2	VIPR2	GPAT3	HEG1	VPS37B	MIR205HG
ABCG2	RAN	PINK1	CHRD	NOD2	SMIM35	NUDT2	SETD5	SPART	TUBG2	PITX1
CHN2	MIIP	MAPK11	MYO7B	IL32	SGK1	SQLE	CRACD	HDAC9	AGFG2	AKR1C1
BARX1	SSBP1	CRISP2	ESPN	RFTN1	DUSP9	UQCC3	SPSB1	SH3GL2	ADGRG5	CEP70
KLHL9	OAS1	PPP1R3B	ACOXL	PIM1	MELTF	AURKAIP1	CLIP2	DOCK8	FAM117A	DPYSL3
LY86	NETO1	MTM1	PXDN	PIK3AP1	FAIM	SEC24D	WNT10A	ETF1	NUAK2	BSND
MACROD2	CCDC57	KCTD11	TUBA1A	ZDHHC18	KLHL5	TRMT112	ZNF623	DMD	FGFR2	TMEM179
GPX7	SYF2	TADA3	HRK	CDKN2B	ARHGEF4	RBM38	WDR81	PDGFC	SHANK3	LINC01098
SAR1B	TTC13	BAIAP2-DT	PTPRE	HGF	SKAP1	RNASE6	CHIC1	TEX9	ST6GAL2	PPM1H
ZMAT2	XAF1	CCNI2	EBF4	IL12B	NFATC2	PLAAT3	FAS	EPHB2	CACFD1	PTPRJ
ANKS6	SAMHD1	TMEM270	MID2	IL7	MAPT	RPS21	RAB5A	G3BP1	NAB2	KRT81
ETS1	MACROH2A1	HOXB6	CCDC144NL-AS1	CXCL9	LY6D	LAMTOR4	ARHGAP8	VAV3	MARCHF8	CELSR1
SERPINB6	ACSL4	OR7E14P	DBH	MIR155HG	ALS2CL	MTHFR	SOCS6	PPP2CA	BRD3OS	CSAG1
MSRA	GPD2	GPRC5B	PLEKHA7	CXCL3	ARHGEF10L	NDUFA2	MECP2	GEMIN5	ETV1	PPL
QPCT	ENO1	RHOD	CLIP4	TAF4B	OBSCN	FMN1	PURB	CBWD1	FUT1	ZPLD1
PTP4A2	ATP5F1E	PTPN9	TSC22D1	ACSL1	TMEM72-AS1	PGRMC1	BCL3	AMD1	ARID4A	TLE2
BRINP2	ITCH	SENP7	LPGAT1	IRF1	CHAC1	CD300A	ST8SIA1	CD28	TMPRSS2	KALRN
LINC01192	DUSP23	RALGPS1	ERRFI1	SOCS3	NAT8L	TMEM50A	KIAA1671	CCDC88B	SHMT1	MTA3
PRKCB	XNDC1N	PSMG3-AS1	CNGB1	RELB	NSMF	SHISA2	SLC8B1	SH3RF2	BHLHE40	KSR1
IMPDH2	CIAPIN1	UICLM	PADI4	TNFAIP2	LINC02474	WDR82	LONRF1	FAM53C	ANO8	SATB2
CTNNA1	SLC5A6	C3orf18	DEGS2	IFNGR2	CCDC80	TMEM42	CBX6	UVRAG	MYCN	FYN
RBM47	RAB8A	KRCC1	CEMIP2	BCL6	FHL3	AIG1	TPO	GNB4	NDRG1	OLFM4
C3orf14	NCLN	SMPD5	LOXL1-AS1	NFKB2	ACOT2	EIF4E2	CXCL1	LPXN	ZYX	SLC6A8
CLTA	CD2BP2	GRHL1	PDGFA	CIITA	IQCH	UQCRQ	CNOT10	RYR3-DT	CHST12	RIPK4
TOMM5	THOC3	F2R	RASSF6	RALGAPA2	TESC	STX5	PLAU	IFRD2	CBFA2T3	STK32A
USP4	BCL7B	OR2C1	STRA6	PHAX	KCP	ARHGEF3	KIAA0232	COPS7B	CITED2	CPXM1
DCLK1	TMEM243	ANGPTL4	CD3G	STX4	CXCL6	MPV17L2	TAF1	AGTR1	FRAT1	SFRP5
FADS2	MAT2B	B3GALT9	MYO6	CXCL11	ACSM5	ENTPD6	BMF	CCND1	SLC25A45	SORL1
PLEK2	MRPL58	CLIP1	ADAMTS17	NAMPT	LHX8	TMCO4	WDR31	ROR1	CLUAP1	OLFML2B
CNTN5	GPSM3	LIMA1	KCNH5	NCF2	TLCD5	SCP2	DUSP10	MS4A1	MAP3K9	KRT7

Blue	Green	Skyblue	Brown	Red	Black	Yellow	Orange	Indigo	Grey	Purple
ABRACL	PRELID1	GTSE1-DT	PGBD5	IER5	CCNO	PRKCE	SMC3	PRKD1	PLAG1	MAGEC2
LHFPL1	TNFRSF1B	PCGF2	PKN3	B4GALT1	RNF43	LYL1	CD276	LRRTM3	ZMYM2	ATRNL1
TBL1Y	OXA1L	KBTBD2	GNGT1	NDE1	IL13RA1	ISYNA1	GCNT2	HNRNPAB	CSRP1	NECTIN2
IL3RA	PHC2	CCZ1	FAR2P2	STARD4	PDGFB	TMEM179B	ITGA6	LINC02484	SH3PXD2B	ZNF467
RNF182	USP18	ADAMTS1	RPS6KA2	RPF2	CSRP1-AS1	KRT40	RARRES2	RBMS1	HCG11	SFTPA1
ANTXR2	UBXN1	ZFYVE28	RALGPS2	NFKB1	KLK15	RTN3	S100A1	ANK3	PIP5K1C	KRT5
MAGI2	HERC5	GOLGA2	DNMT3B	MACIR	AMH	ATP6V0B	METTL6	SPP1	KCNJ4	NLGN2
CYSLTR1	SOAT1	CLDN7	SRPX	DOCK10	PRR5	SNU13	PPP1R12A	ZNF518B	RHPN1-AS1	ZFYVE1
TRIM58	KDM4C	DENND6A	TDRD10	C2CD4A	DNMBP	MRPS18C	FDXR	GPR137B	ATP2A3	SOBP
LINC02273	SDHB	H1-10-AS1	RASGEF1A	SEC24A	PTGES	HINT2	ANGEL1	NRIP1	FLYWCH2	C1orf198
JAKMIP2	PIGU	ABHD2	KRT17P5	EBI3	LINC02054	PEF1	REEP3	PLEKHG1	SLC6A9	SLCO3A1
TMEM273	PARP12	ADCY5	NUP62CL	PLXNC1	MRPS25	PAAF1	SUGP2	WDR36	TOR2A	ARHGAP23
ITGA4	PLGRKT	PRDM10	ZIC2	IER3	LINC02593	SH3BGRL3	ATRX	AK2	SLC16A14	ALDH5A1
ARMCX3	NDUFAF2	PACSIN1	KCNJ12	ICAM1	SEMA6B	LTB4R	SLC49A4	SF3A3	CMTM7	CCDC190
LPCAT2	ANKRD39	ABHD8	ABCA3	SIAH2	MST1R	SP2-DT	TIAL1	ZSCAN20	TBC1D10A	SLC6A19
MYO10	PLAAT4	MAN2A2	CHST15	BATF	VGF	OCRL	NBPF15	APTX	BAIAP2	HTR2C
GTPBP6	SH2B1	LINC01503	CYP2U1	BTBD19	GPR157	NANS	SPECC1L	GCNT1	RCOR2	RHOC
CYFIP2	NADK	DOCK11	IQCE	ARAP2	EMID1	GRHPR	NF1	HERPUD1	FUT8	GRB7
PCSK6	PTPN1	ZRANB1	INHBB	CCL3	GATM	NREP	LRRC1	LCP1	NATD1	IL21R
RRAGD	ERVK3-1	VPS33A	FAM102A	RNF180	ADAM8	ALKBH2	ARL8B	POLR1E	ZBTB42	FAM178B
CPED1	ACAD9	WSB2	USP9Y	TASL	FOSL2	MRPS33	ZC3H4	CD74	SMTN	SLC6A15
LINC01480	NDUFAF3	LINC00938	CTPS2	DDI2	FAM120C	VNN1	TTC21B	NPM1	IL6R	CRAT
SSTR3	FARSA	PRTN3	SAMD11	HNRNPH1	ABI3	SPIN2B	MTMR10	DPH2	INVS	OTOGL
FADS1	PPIH	STN1	LINC00574	RAPGEF1	CCR2	TSPAN17	C21orf58	NR3C1	ABHD15	PDZK1IP1
ST3GAL6	AK6	BIVM	THPO	MAML2	OTUD7B	CDK2AP2	CBR3	LINC00623	CAPN10-DT	CERS3
RERGL	UCHL5	ENGASE	H2BC21	RASGEF1B	C2orf74-DT	SLC27A5	C2CD2	ACSL5	SH3RF3	CORO2B
HIGD2A	EPS15	NAA60	TJP1	HK2	HHATL	GNPDA1	TIGD7	ZNF98	LZTS2	KIAA0319
PRRC1	UBE2C	LAMC1	CERS4	TNFAIP6	CMTM6	ARF4	RTN4RL1	RNF138	HERPUD2-AS1	A4GALT
TMX2	CRNDE	MYO9A	MORC4	IKBKE	CDH1	TUBB2B	KDM5C	RBM15B	SLC43A2	PAPLN
CCDC51	RILPL2	TTYH3	PTPN3	IL4I1	DZIP3	CDKN2AIPNL	NECTIN1	ZNF676	PEX1	CGNL1
PSME2	METTL5	SYNE1	TBC1D16	PRRG4	EVL	RWDD1	CLU	YRDC	SPSB2	RAB39B
SERPINI1	DERL3	DYNLT2B	PPP1R13B	DEFB4A	ISM2	MGMT	C1QTNF1	RND3	LRP11	ARL4C
TNFSF11	CCDC12	IL18	PLA2G4D	NFKBIA	TMEM158	NXPH1	KIF26B	KMO	MOAP1	ZCCHC24
MS4A4A	DCX	TANC2	TUBB6	ALCAM	ATP1B1	CCDC127	TNRC6C	USP46	PLCG2	CERCAM
PRPF6	TRIM22	NBL1	KCNK9	LYN	MECOM	FKBP7	BRWD1	NXF3	COL9A3	LAX1
SMCO4	SNHG3	DTNB	SEMA3A	CCL4	ZBTB46	TMSB4X	JOSD1	PRNP	FAM210B	DLG5
SPCS1	NECAP2	NECTIN3-AS1	TUBB3	JUNB	ITGB2	BTBD3	ITPR3	TAGAP	RAB20	PDXK
BTN3A3	ISG15	TFAP2A-AS1	NPAS2	NETO2	BCAS1	MRPL2	ANKRD26	CD47	RASAL1	PRAMEF11

Blue	Green	Skyblue	Brown	Red	Black	Yellow	Orange	Indigo	Grey	Purple
MCTS2	TFCP2	RAB43	EPB41L5	BID	SDHAF4	RPS27L	TOPBP1	MLKL	KLHL24	RIN2
DBN1	CYB561	ZNF594	ZMAT4	PLK3	LYSMD4	OSBPL11	ETS2	OGFRL1	ATP13A3-DT	KRT86
BRMS1	AKAP8	B3GNT4	NLRX1	OPTN	LINC02707	SVOP	JPX	DAPP1	IL10RB	ULK1
SLC25A6	HINT1	PNMA1	RASD2	MMP13	IL4R	CYSTM1	RAB27A	SZRD1	SPATA20	RAF1
LY75	TRANK1	BAZ2B	IQGAP2	NUP153	LINC00880	MGAT1	TCTN1	UBAP2	TRIM61	CCDC102A
BEST3	PELP1	LTBP1	YWHAZ	PPTC7	FOXD2	POLR2G	NKAP	SLC43A3	IFT27	ACVR1C
USP19	FCRLA	C13orf46	NCOA1	TET3	GPSM1	RPS3	KCNH4	EPB41	CIBAR1-DT	FHL1
SIGMAR1	SCAP	ZNF772	CDON	LYAR	LINC01967	SMIM26	CHM	ADSS2	PLEKHO2	LINC01016
MYO1F	MRPL33	FBXO32	FKBP9	CDC42SE2	KIAA0895	DOK6	MKRN2	HARS2	CCDC126	HES1
TRAPPC3	SLC35A4	RASGRF1	FXYD2	SRFBP1	TRIM16L	SDHAF3	TMEM63B	SPATS2L	MARVELD1	PNPLA5
UBE2D2	DHDDS	PAN2	MRC1	ZC3H12A	PPP1R3F	CSRNP1	BBS2	ATAD3A	TMEM164	CDH3
RER1	EFHD2	TNKS2	ESRP1	NUS1	GNB3	PARS2	PRKD3	LINC00944	PTGDR2	CTHRC1
RPL14	GLRX3	SLC7A11	RHOXF1P1	MDFIC	HMGN3	TMEM109	CEBPB-AS1	CLINT1	INAVA	ARHGEF11
SP140	GLRX5	NR2C2	DSP	USP1	TTC8	RAB3A	KCNA2	TOE1	HDGFL2	PRAMEF9
ZNF804A	BMI1	UAP1L1	PTPN12	BIRC3	ZNF558	CX3CR1	STS	MYEF2	TMEM117	ARHGAP15
WAS	TIMM13	SEMA3G	FGD5-AS1	TOPORS	LINC01674	SOCS2-AS1	NRARP	GPR158	DENND10	MAGEF1
FAR2	HSPA1A	LINC02561	TIMP2	NFKBIZ	IGFBP6	ELOF1	RGS16	EMC1	TBC1D9	DBH-AS1
GPAT2	ERH	SLITRK5	FAM133A	SOX2	CACNG6	FDFT1	SEL1L3	NOP16	AJM1	FER
EXOSC3	RPL35A	GPR107	NOTUM	RAPGEF5	FSCN1	MFSD12	GCNT4	RYR2	SLC7A7	ECI2
SLC16A7	POFUT1	MC1R	MARVELD2	OXSR1	PLEKHG3	TMEM59	WDR90	PLAA	TOM1	CNN3
PLEKHG4B	PSMC5	CLDN9	CHEK2P2	ZBED1	TMEM184A	ADRM1	PHYH	LGALS8	SNX30	PLD4
LY9	PDCD2L	TBC1D19	PPP1R14D	STARD5	SDC3	SRP68	PHF2	FAM111B	TOR4A	EFNB1
SORT1	EMG1	ERBIN	UNC119B	PUM1	LRRC75B	NXT1	RAB11FIP3	SLC36A1	FAM107B	LARGE2
STARD3NL	HID1	CCDC186	PLCD3	PIK3CD	GNGT2	ADRB2	BRPF1	PRELID3B	HBA1	FAM169A
SYNDIG1	DMAC2	ANKRD28	H2AC11	INSIG1	NCS1	FUZ	DYRK1A	TTI1	S100A11	BHLHE41
MTHFD2L	DNAJC12	MIAT	CRYBG3	RUNX3	TRAF1	ZNF672	MCM3AP	CDC25A	TMEM9	PTGS1
CAP1	DLGAP1-AS1	KDM6A	FANCD2	ZRANB2	B4GALNT4	SHISAL2A	HIVEP3	RBM22	PRIMPOL	LINC01315
CKAP4	SLC35B1	KBTBD7	MLF1	SLC25A24	CDK18	CAPG	RASSF5	CCNJ	ST3GAL4	ZNF319
BCAT1	UBE2B	VAMP4	LINC02910	ROR2	MAGEA3	SDF2L1	WDR44	TNFRSF14	ADM	SLC15A1
SLC17A9	TRMT2A	SWI5	OPRD1	TFAM	SECTM1	BLK	CUL9	ATAD3B	ZNF385A	ASPHD1
UGT8	CAPZA1	DPY19L2P3	TIMD4	CEP85	KCNK12	DRG1	ZBTB10	ZNF22	PRPSAP2	ENTPD2
TRIP6	NIPA2	SYNE2	UTS2R	EPOP	TPPP3	OSTC	CAV2	CA8	PIK3CG	SULT4A1
MRPL22	GNAS-AS1	SLC2A12	APP	CSF1	TREX2	CRIP1	PPFIBP1	DHX37	ZSCAN30	JDP2-AS1
COX20	POP5	DPY19L1	MAST4	CASP3	SH2D5	VEGFB	GSE1	COA7	PLEKHH3	ELFN1
PRELID2	POLR3K	TCP11L2	NLGN1	GADD45B	CFAP157	SLC52A2	FAM230C	HSPA9	ATP2A1	TXNRD3
MYL1	LARS2	MTMR2	ADARB2-AS1	CRACR2A	ZDHHC11	NAT14	TP53INP1	TM9SF4	ACP6	RAB31
RUFY1	PHAF1	ZNF606	FBXO43	SLFN5	GRAMD4	TRIAP1	TSPOAP1	PSMB2	PAQR4	BCAM
HMGXB3	FOXP4-AS1	ATG7	MGAT3	TPTEP2	APLF	TNFRSF17	SDCBP	FCHSD2	ZBTB7B	NANOS1

Blue	Green	Skyblue	Brown	Red	Black	Yellow	Orange	Indigo	Grey	Purple
ZNF257	MYL12A	ARID3B	GDNF	SERBP1	HECTD2	CYB561D2	RFC3	ZNF639	SIRT3	AIF1L
MFN2	TXNDC15	CITED1	SPINT1	DCK	CD48	MAPKAPK3	SBF1	NFX1	ABCD1	SLC4A4
SLC15A3	DTNBP1	OSBPL5	SLC12A6	ATP13A2	FABP6	TMBIM6	GART	PDCD11	TBKBP1	ASB9
PTER	PDCD6	PATJ	LINC00957	RPIA	ZSWIM4	SPATC1L	CACUL1	NOC2L	SLC16A3	NPTX1
IMMP2L	TNFRSF13B	LRRC37B	EIF2AK1	LTB	THEM5	USP7-AS1	CYP1A1	RCL1	SIGLEC9	CCR10
FAF2	BMP6	TOR1AIP1	IRX4	GRPEL1	FUT2	VPS51	ANKRD11	DNAJC6	ZNF821	LINC00242
APBB1IP	ISOC1	MMP25-AS1	CEP170B	YWHAG	ANKRD36BP2	ACTR8	MTUS2	HNRNPA0	CERK	DHX32
CSTPP1	CAP2	RLIM	SYTL3	CCR1	C15orf48	ZNF675	VDR	NSUN4	BBS9	GNG10
TSPAN7	EBLN3P	SPTB	TRMT2B	ZNF253	NUPR2	RPS26	MACF1	SLC25A33	TSR2	BCAR1
EIF2B3	KLHL6	CKAP2L	MAGEA6	ANKRD33B	CRIP2	TNFAIP8	TGFBR3	MAX	LINC02341	ACTN1
MRPL36	RPSA	S100A9	AOC3	PPM1K	ADAM19	KRTCAP2	PCYT1A	FOXJ3	KIFBP	SH3TC1
RBBP4	SMPDL3B	PAPSS1	KLHL42	CXCL8	RUNX1	TMEM223	PROSER3	GOLT1B	CBX8	FAM3B
SSR1	SNHG21	MAMDC4	FRMPD3	ANKRD30A	GPR153	ATP5MC2	PBX2	TSPAN5	GDPD5	PECR
OSBP	MAPKAPK2	S100A13	COBL	PSD3	NEIL2	EXOSC1	SPAG1	SIDT1	CCDC122	CLDN4
IK	CCT5	NEO1	UBE2QL1	NIBAN1	LINC02870	KLHL21	AHRR	PHF20	PIK3R3	ACADVL
LILRB4	TIMM22	RRAGB	ZFPM1	SH2D3A	CDC42EP4	TRIM52-AS1	OLIG2	EBNA1BP2	SRGAP2D	H2BC11
VDAC1	DDOST	UBP1	AAK1	SELENOT	RGL3	PLPP2	KIAA0753	EXOSC10	ABHD4	ARRDC1
HEMK1	RAD51B	USP28	MAGEB2	OXTR	PNPLA2	INTS5	ADM2	FBXO38	EGLN3	SUMF1
CANX	CYP27B1	SLC2A3	HERPUD2	MMD	TSPAN9	SEC22C	HSD17B1-AS1	CHSY3	FUCA1	GADD45A
SEC61B	CRLS1	APOL4	ADAM22	UTP23	LINC02253	DTWD1	CARD9	SFPQ	ZMYM3	COL18A1
YIPF5	COMMD10	SYP	ODAD3	B3GNT2	GRIN2C	SSU72	SUN1	DCAF1	TP53INP2	CRACR2B
TKT	APMAP	KRT17	MYO7A	CHSY1	LINC01805	ABHD14B	PINCR	DHX30	TMEM65	ZNF542P
SPCS2	RDH11	FCGR2A	SLC25A43	RAPH1	KCNJ11	RPP25L	PCNX4	C1orf109	HCFC1-AS1	CYTH3
TMEM201	SART1	FBXL18	MAN1C1	NFE2L3	FAM83H	SMIM30	BCOR	LINC01145	ZNRF2P2	ILF3-DT
CREB3	LSM11	TBC1D12	AKR1C3	SETBP1	TEAD3	RPL36	SIK3	CTSS	CLMN	FAM124A
TTC1	APOBEC3G	MIB1	ITSN1	IGFBP3	SHF	PREB	MIR503HG	RELA	MAPK3	PLXNB2
NKX2-1	FBXO6	RTL10	LINC02257	WIPF1	FNBP1	EEF1D	CDKN1A	FAM193B	MKS1	ADAM11
TRIM44	ALYREF	HDAC4	PALLD	HNRNPU	SLC16A13	DHCR24	ASB1	WDR77	EPS8L1	MANSC1
UBA7	RNF121	ATXN3	SH3BP4	PPIF	HTATIP2	PLA2G15	TNFRSF10D	LINC00869	RETREG2	SAYSD1
YOD1	KHDRBS1	CARD10	NUP210	SBDS	CDC42BPG	LIN52	RABGAP1	TTC4	ODAD4	SORBS3
PSMB9	MMP24OS	MIR4664	PDE5A	ELOA	WDR59	FRMD3	ATAD2B	GIMAP6	BTBD2	GSTZ1
CD33	RBFA	ANKDD1A	GK5	RNF11	LLGL2	ALG5	SH2B3	AKIRIN1	NIPSNAP1	SLC44A3
TIMM10	BTN3A1	SLC51A	CDK16	NEDD4L	ITGB4	ALG12	GATD1	SEMA3C	BNIP3L	RPS10P7
SEC22B	DPP3-DT	FBXL3	CCDC74B	FMNL3	TEP1	FDX2	CNTNAP1	KAZN	CCNG2	CSTB
STPG1	ELOC	TMEM210	EML5	IFIT3	NPHP3	MYLIP	RBKS	PARP8	RTN4RL2	SCHIP1
CTU2	ATP5MK	MOB1B	HERC2P4	APOL3	MKRN9P	SLC50A1	EML2	NOL7	CTDSP1	PPP4R1
IL12RB1	GNB1	CACNB1	ADCY9	CSNK2A1	POMC	NDUFS4	PHF21A	GGA2	SNX29	SLC27A2
NADSYN1	PSMB8	TRAPPC6B	SKAP2	ZNF267	IQCG	CUTA	GRB14	IFNG-AS1	KRT16	YPEL5

Blue	Green	Skyblue	Brown	Red	Black	Yellow	Orange	Indigo	Grey	Purple
LRRC47	TRMT6	PPP1R12A-AS1	FURIN	IL2RA	MAPK12	PCYT2	TSPAN33	TMEM138	RAD17	LINC01139
APBA1	RUVBL1	LNP1	CEP128	ZFP91	LRG1	FMC1	IRF8	ERLIN1	ZNF836	CSRP2
LARS1	RASSF3	PRDM5	DCLK2	TNFRSF9	CFAP36	SLC25A20	TFE3	SCML1	GATD1-DT	ADAMTSL2
RUBCNL	MRPL47	ZNF429	MICALL2	FAM3C	EMC3-AS1	ATP6V0E1	SEPTIN7	DNAJA1	SH2D3C	ADGRB2
PTMA	ELOVL1	CAMK2N2	MTURN	GTPBP1	COX6C	RPL23A	MAP7D3	CTPS1	PC	EPN2
IL24	HLA-B	ADAM10	BCL9	PGLYRP2	CARMIL1	RPS13	NCOA7	DPP4	ATP23	PCNX2
ARHGAP17	CSNK1G3	P2RY1	SCCPDH	NUAK1	LCAT	SLC25A38	APOBEC3B	WDR55	MCOLN1	RERG
CPNE3	POLR3F	RHPN1	SPIRE1	LARP1	SLC12A4	RPS25	SLC9A1	CLCN6	DSTNP2	LAMA5
CAMK1D	CLNS1A	TAB2	DBNDD1	QKI	MIR548XHG	DPYSL4	PITPNM1	PPP4R1L	FAM214B	KRT13
ZC4H2	MRPL48	TUG1	TBC1D8	TRIP10	SH3BGR	SRC	CDK13	ADPRS	LINC01003	ACP3
UBAP1	COX5A	PTPN21	NOXA1	RAB11A	MARVELD3	ZFP69B	ACTR3C	GIMAP4	LRRN4	EHD3
PLAC8	NFIA	ZHX3	TTC3	CXCL12	LINC02188	CPTP	FBXW2	THG1L	HAGH	AOPEP
EXOSC7	LZTFL1	IRX4-AS1	CRTAP	SMARCA2	CBR3-AS1	MORF4L2-AS1	OSBPL3	TMEM69	FAM167A	PCTP
EAF2	EXOC3	DDX53	DOCK6	CEBPD	IVD	FAM89B	MED12	OXR1	CAPNS1	STMN3
DCAF12	TIPIN	MXRA7	FZD7	PIM2	KIFC2	TNFAIP8L2	RASSF2	HBBP1	FAM78A	CFD
OLMALINC	NDUFB6	SUPT20H	TFDP2	HAPLN3	AMDHD1	RPN1	RBSN	UTP11	KIAA0895L	TMEM231
COA4	CDKN2A	YJEFN3	DLG3	WDR3	SPESP1	BET1	LRRC37A4P	UIMC1	CCM2	AQP3
SLC25A46	MX2	SPEN-AS1	FHOD3	TICAM1	RP9P	RPL19	PCM1	ZNF729	XKR3	BTK
MRPL20	PHLDA2	ARMC8	PLXNB1	HIVEP2	CREB3L1	CYB5B	CUX1	EEF1E1	RNPEPL1	CACNA2D2
ATP10D	NIFK	CBR1-AS1	ACVR1	ARHGEF40	C16orf74	ZCCHC17	C8G	PRKAR2A	PLEC	RNLS
REEP5	TXNDC11	NCOA2	MFHAS1	CCL2	DNAAF8	SEC31A	CNTRL	TDRD7	ENKD1	PANX2
TFB2M	ANO7L1	VTI1A	LINC02064	PITPNB	HOXB4	MPG	B4GALT5	GRWD1	KDM7A-DT	COL4A4
ESYT2	MRPL1	SEPTIN3	LINC02983	GFOD1	TCTN2	PLPP5	EPHA10	RRN3P1	CD72	CFH
NFYC	YBX3	ZBED3	IER5L	AIM2	URGCP	ZFP42	KREMEN2	MCUR1	SCN9A	TNRC18
LINC01606	LAMP3	AEBP1	FAM214A	GSPT1	GINM1	TMC5	NONO	KCTD5	THRA	HEXB
C1orf174	WDR4	RWDD2B	EXT2	MYBPH	EEF1A2	MPC1	CENPE	SP110	TMEM254	LINC01414
DNAJC15	MRPS15	HSPA2	ATE1	SNX20	EGFL7	RPS5	ADD2	ARIH2	TIGD3	NUDCD3
GNE	MMADHC	RAPGEF2	DENND6B	NDUFAF4	INSIG1-DT	MINCR	TRNT1	GALT	NT5DC1	FGFR1
IFI27	ZFAS1	IFT80	C3orf33	TGIF2	SNX8	CHAMP1	TRIP11	ATG12	CCDC50	H2BC4
LARGE1	PFKP	NEDD4	SSBP2	IRF2	DNASE1L3	NOP10	IFNAR1	SMU1	KANK2	LXN
CPSF7	TFAP2C	CENPF	OAT	PSME4	TMEM260	BEX1	MKI67	AKAP17A	CLSTN3	ZBTB4
DPM1	LINC02864	C10orf88B	TRNP1	FAR1	CIB2	MRPS18B	JMY	GIMAP2	ASTE1	EDEM1
COMT	EIF2B4	RNF215	MANBA	ZC3HAV1	SLC27A1	ZFP69	ITSN2	TWNK	CALM1	NFIX
MRPL16	ZNF232	TCP11L1	ZNF318	WWC1	CHST2	ATG4C	NKIRAS1	DDX41	LINC02982	HACL1
ZMPSTE24	UBE2L6	SETDB2	ZNF322	ID2	HSPA6	GORASP1	TMTC1	ZC3H15	ERCC2	SPIRE2
MAGOH	PPP1CA	LINC00662	PHACTR2	IRF9	FHIP2B	BANF1	NCOR2	TMEM106A	ST14	ABCB9
ACO1	ZNF385B	RNF103	EVC	C12orf29	ZNF844	MEA1	MPHOSPH9	CHCHD3	MNX1-AS1	SPIN3
RFT1	BRD8	FOXD2-AS1	ZBED5	MASTL	PFN2	DHRS1	DUSP5	PDE3B	MCM5	TALDO1

Blue	Green	Skyblue	Brown	Red	Black	Yellow	Orange	Indigo	Grey	Purple
RNF145	ABHD5	DYNC1H1	GARS1	ZFP36L1	RTL8A	ZNHIT1	ADCY1	CMPK1	BAK1	RBFOX1
PAM	ERAP1	SMC2	RAVER2	CEBPZ	RGS10	CARD17	TCAF2	CCT2	TKFC	BICD1
MRPL49	MARCHF3	LMTK3	LINGO3	PUM3	PDK3	MRPS34	CELSR3	KCNQ5	USP51	STRADB
DRG2	GNPDA2	MRTFB	LANCL1	EYA1	SLC9A9	TTC22	NIN	HAUS6	PIERCE2	IGSF9
QPRT	JPT2	PAK6	ARHGEF12	CLK4	CHD3	MEAF6	SLC25A25-AS1	KANK1	INPP5K	H2AX
CDC23	FAM32A	LGALSL	TFAP2A	CDK6	ACTR1B	PRANCR	CUL7	TPD52	SERTAD3	PMS2
MIX23	MUTYH	ZFYVE16	PRRT3	IKZF1	IL2RG	NUDT22	AMMECR1	BRD9	BRF1	CCDC69
YTHDF2	SNRK	SNX12	HIBADH	AHCTF1	TNFAIP8L1	NAT1	CEP350	UTP6	TYSND1	SMKR1
ZCCHC7	MBIP	STARD8	C22orf46	IL15RA	PSPH	UNC5A	SEPTIN7P2	ZDHHC5	STBD1	IQSEC1
UAP1	PPP1R14B	CLASP2	ABLIM1	TOP3A	CSNK1E	SLC7A8	TPST1	DEGS1	PSAT1	PLEKHB1
ZBTB8OS	POLR1C	SPTBN1	ENO2	NOL11	RYK	GMPPA	SLC25A53	GAR1	OSBPL6	SLC35G1
DUSP7	NSA2	GDPD3	ACER3	EIF4H	MESP1	RPL26	PPP1R12C	SNRPB2	CASP6	XXYLT1
MED24	EEF2KMT	ZNF714	TSPYL4	KDM2A	LGALS2	RPL28	C1orf21	SREK1IP1	ZXDC	CD4
ARMC6	C18orf21	BRWD3	WNK2	TIPRL	AKR7A3	RBM33-DT	MPRIP	TIMM17A	MKLN1-AS	GLS2
MRPL21	PFDN6	NHLRC4	CAMKV	KPNA6	SLC26A11	FNBP1L	UTY	MNS1	PHYHIP	SERAC1
MANF	SCNM1	EPG5	ID1	GORAB	SLC30A4	VAMP1	LARP4B	LIMD2	ZDHHC4	RSRC1
DMKN	PCBP4	APOOL	NRDE2	FRMD4B	LINC00920	TMEM70	MREG	CPNE8	RXRB	ALDH3A2
SEC23B	LSS	IGF1R	LDAF1	RAB21	C4orf36	RNF207-AS1	FLOT1	MRPS30	TOX2	ADPRHL1
PODXL2	B3GAT3	AVL9	DIP2C	GCH1	U2SURP	SPTSSA	SH3BP5-AS1	SFXN1	MIEF2	CLCN5
ARHGAP30	NUB1	KIAA1109	FMO4	WBP11	MIF4GD-DT	RPL18A	ANKRD10	DENND1B	PIGC	OTUB2
TOMM22	MIR3667HG	CPD	MAPRE3	SYNCRIP	FBXL19-AS1	TMEM101	CASP8	NUFIP1	FZD1	PCCB
JCHAIN	HSPA4	SIPA1L2	AFAP1L2	COMMD5	CMTM4	ABCB6	GDI1	MIR646HG	MEF2D	LTBP4
LINC01194	SRSF4	CD109-AS1	CEP68	ZNF598	PTBP2	CEP41	ASAP1	HMGCS1	ORAI3	MBTPS1
ZNF296	ARFGAP3	H2AC17	ITGA3	BCL2A1	ATP6V1E2	RPS12	SHOC2	MTA2	RTN4IP1	BRD3
PGD	PLAAT2	SLC38A6	CAPN7	LINC02397	TFCP2L1	PRMT5	DTNA	SDHD	ZNF395	DONSON
SNRNP40	BST2		FBXO3	PIGV	ETFDH	AKIP1	EPIC1	PNRC2	ARL15	XPC
MORC1	RHEB		ZNF12	YTHDF1	H4C14	RPL41	RDX	PWWP2A	PIP5KL1	DIRAS1
DDAH1	SHFL		NUMBL	MPI	BBC3	MRPL43	KLHL11	RAPGEF6	FRAT2	SHANK1
SNX2	PPIE		PIK3CB	DUSP2	TXNRD2	RPS16	CREBBP	FBXW11	TRAM2-AS1	LRP1
TBC1D9B	PPIP5K1		AKR1C2	SVIL-AS1	NSMAF	TRPM2	STX6	TIGAR	MISP3	CD151
RPL26L1	NASP		EFNA5	CD274	TBXAS1	RPS15A	PDCL	NME6	MXD4	ZNF516
ERGIC1	SORD		INKA2	SLU7	LINC01655	MIEN1	VHL	LUZP1	H1-10	TMC8
LRRC59	SUB1		CRBN	NCOA5	LINC02444	RBM4	VPS41	HNRNPR	SDC1	BTG2
RPL11	SLC15A4		SELENON	MB21D2	PLEKHF1	IDH3G	ADGRL1-AS1	CHMP5	CD63-AS1	CXCR3
RPL22	THNSL1		KAT2B	CTNND1	BICDL1	AP3S1	SETD1B	PPIP5K2	PJA1	ZNF219
HIGD1A	GNAS		L1CAM	NOL10	PPP1R16A	MRPL10	LRRC8B	ZCCHC10	C14orf93	FEZ2
RARS1	USE1		MEGF6	PANK3	SMG6	MRPL45	ACADSB	EMC6	IFT22	SOS2
MIR3147HG	MRPL37		PDCD6IP	BRIX1	ADSS1	GNAI2	TOGARAM1	DCTPP1	ADCK2	MYO5B

Blue	Green	Skyblue	Brown	Red	Black	Yellow	Orange	Indigo	Grey	Purple
MED8	TIMM9		NRCAM	RBM17	KLF9	OST4	PDE4D	BOD1	ZNF561-AS1	PREX1
NOP9	PHB2		MGST3	CRLF3	RECQL4	RAB1B	RAB9A	ME1	CREBL2	EVI5L
RTF2	STIP1		NPTXR	WDR75	H2AC13	LINC01123	SBF2	TMEM165	PKP2	RPH3AL
F2RL3	PPAT		MAP7	NAA50	GLTP	KDELR3	RRAD	VDAC2	SNX24	CA11
PHF5A	APEX1		MTPN	CYB5R2	ARID3A	CYBA	MED13L	DOHH	MAP10	MCMBP
POMGNT2	MIB2		ABL1	IFIT5	LHPP	MRPS31	CHST7	GBA2	MYL12B	FBF1
DANCR	RBL1		HLCS	CNOT9	HAS3	ANG	POMK	HLA-DMA	MESP2	RPUSD3
FAU	CORO1C		EDIL3	STK38L	INF2	MAMDC2	POGZ	MRPS35	MFSD13A	CEP164
RCE1	DEK		GARS1-DT	USP15	MMP17	SPON2	KCNA3	KCNAB2	SERPINE1	ZP3
TMEM218	SSR3		BOLA1	IGFBP4	REEP6	RPLP0	PRRC2A	QRSL1	MMP15	FUCA2
ZNF90	RELT		MGAT5B	PDE4B	MOK	SNAI3	ORC2	KTI12	TPRN	HMG20B
TAF12	ARL3		NGB	UTP20	THBS3		HOMER1	ZNF716	ITGB5	NIBAN2
RAB30-DT	MED19		MAGEA10	BTG1	NDNF		MAP3K4-AS1	CAPN2	NPDC1	ANKRA2
PYGB	PARP9		MYO1C	MCL1	LINC01881		SIN3B	NLE1	SCARB1	LSP1
CLP1	RPS20		DCLRE1A	LYRM7	CFAP73		MYO1B	MYD88	TST	WDSUB1
ASMTL	TNFRSF8		TMEM250	UTP25	TMSB4Y		ATF4	RIOK2	ZNF362	BBS10
MGLL	COPZ1		PLPPR2	IFIT2	SLC9A3R2		CCDC174	ZNF589	ARPC4	PIERCE1
SEC61G	SAMD10		FOXO4	BMS1	ST6GALNAC6		DBR1	ERAP2	BAZ2B-AS1	ITM2C
LMAN1	IDH3B		SPINT1-AS1	NRROS	CC2D1A			GAL	CBX4	FAM53B
SOCS2	MRPS18A		ATP2B4	MYB	TRIM68			ATP10A	TMEM242	TIMP1
GMPPB	PINK1-AS		CIC	GBP1	GUCY1B1			COL27A1	TOB1	FZR1
TIMM8B	DNAJC1		SLAIN1	GTF2I	IFT88			LINC01229	PMM1	XYLT2
FKBP11	ANXA2R-OT1		LBH	ATAD1	MLXIP			CALHM6	SOX8	H2AZ2
POLR2K	GPR89A		DCAF6	HELB	NPW			PML	IFT43	SNTA1
ICMT	HLA-C		KIF26A	RAB3IP	FUNDC1			RBMY3AP	HDAC5	FLYWCH1
EIF3G	THAP12		SLC4A11	PIP4K2A	COCH			TMX1	SRD5A3	UBTD1
PROB1	MFSD3		ZNF768	PHACTR1	TCEA3			AATF	NSMCE3	TEX19
DTX4	SHISA5		MAGI3	NUDCD1	PPP1R26-AS1			DNAJC11	NANOS3	MEGF8
MUS81	CCDC9		TAF9B	FAM13A	FCGBP			EYA3	TRAPPC9	EPHX1
ARHGDIB	B2M		PTPRF	BYSL	CBX7			MRTO4	MARCHF9	KLF13
ZNRD2	TYMSOS		TCIRG1	TNFSF10	ARVCF			LRP8	PPT2	NCK1
WIPI1	ACOT8		C4orf50	GMEB1	TMEM54			MYBBP1A	JAGN1	STK33
PFDN1	NOPCHAP1		CADM1	DDX21	CPNE2			BNIP1	KIFC3	GIHCG
ACY3	CDC42EP5		NBR1	RFFL	CHTF18			GNL2	HMCES	RPGRIP1L
SRP19	PGAM1		LMLN	URB2	TNFRSF12A			FLI1	SPIN4	ASB2
CLPTM1L	PDIA2		RNF183	USP3	FIBCD1			UBE2D3	SLC2A8	SLC38A7
TEKT4P2	PA2G4		BUB3	PRKCD	H4C12			ARL6IP5	PIGS	GGCT
PTPN23	RAD54L		TBC1D5	TRIM25	ADAMTSL5			SP140L	TMEM53	H3C10

Blue	Green	Skyblue	Brown	Red	Black	Yellow	Orange	Indigo	Grey	Purple
MILR1	DOCK2		PLXNA3	MITD1	NMU			CCDC47	TPMT	KAZALD1
ABCG1	NIPAL3		LDHD	NFKBIE	MRM2			OGFR	LASP1	DYNC1LI1
MZB1	APBB2		CARD11	NABP1	PACS2			NOL6		PTPN4
SCD	IFI44L		SRPK2	MOB3C	LINC02595			EIF2S1		LGALS9C
LYPLA2	EXOSC4		H2BC20P	PAK1IP1	FBXL22			ABCF2		METTL27
RAD9A	LAPTM5		YPEL2	TEX261	KCNH2			ZNF124		RTL8C
DPYD	RHOA		PNPLA8	THOC1	CD3E			HSH2D		FABP1
ZNF826P	MAP3K5		C1orf56	PATL1	RABL6			ZNF35		CGN
GANAB	FAM86B2		ZYG11B	AMER1	ZNF571-AS1			CCDC71		DOCK9
LMAN2	NMI		ZFP90	NOL9	SLC44A2			ALAS1		CETN2
RAP1A	SSR2		DSCAM	MTMR4	SAPCD2			NMNAT1		ALS2
RPL29	TMEM175		PRKACA	MIR3142HG	RIMS3			STX12		REXO5
NBEAP1	SLC38A5		MSX1	ZNF330	SMARCD3			PRKAG2		CBFA2T2
CMTM3	FADS3		KC6	MYC	SH3BP1			FAM98A		IRF2BPL
FDPS	NUDT5		DCPS	DDX58	RASSF4			EIF3J		KIF1B
PABPC4	LIPE		ITGB1	SLC11A2	DDIT3			MFAP3		TATDN2
HNRNPUL2	GCSH		B4GALNT1	MLLT1	TFEB			RNF31		PFKL
NOC4L	CADPS2		TTC30A	IFNB1	RAB33B-AS1			ANKHD1		BIK
RNF144A	CAV1		TCAF1	ZBTB17	BEND6			CHUK		DARS2
PUSL1	TPRKB		TAX1BP1	EIF4A1	ZNF75A			ACO2		FMNL1
SKP1	CELF2		SGSM2	ZNF346	MSANTD3			TXNIP		VGLL4
SPATA24	MESD		DVL3	TNFRSF10B	INTS1			ZNF622		EPCAM
PGM1	ATG3		ZNF862	LYRM4	LAT2			NIP7		WDR19
NHP2	TRPT1		OGA	RRP7A	TSSK6			TP53RK		PBXIP1
SMIM4	IFFO2		DSTYK	MAK16	TWSG1			TAF7		CRYBB1
LINC01138	GPATCH11		TRIM59	NFKBIB	CNN3-DT			CLPB		BEGAIN
PITHD1	EHD1		ADD3	PRAG1	GNRHR2			RBM27		FGD3
LZIC	ZNF740		SNX16	ZHX2	RASA2			MIER2		WNT7B
MHENCR	CAAP1		PRICKLE3	G0S2	AASDH			RAB22A		NF2
OTUB1	SNHG19		ODF2	ZNF195	COX18			NDUFA9		WASHC5
FGD5	BEND4		NLRP5	MGRN1	ZFTA			SEC24C		NAIF1
BTF3L4	GRPEL2		ATG2A	BAIAP2L1	WARS2-AS1			RINT1		HSPB8
SRM	SMARCC1		ARHGAP42	QTRT2	MTA1-DT			ENTPD1		SCAPER
NDFIP1	KCNAB1		CLBA1	NR4A3	CTSB			SPTLC1		UBL3
TM2D3	LINC01128		ALPK1	CCNL2	C5orf34			STKLD1		SLC1A5
MACO1	VAMP8		ATP6V0E2	SNRNP27	LYSMD1			SF1		AMPD2
SF3B2	RPL36AL		TGFB3	ZDHHC21	ITPKC			LINC00519		S100A3
CR2	SNX5		KHDRBS3	CILK1	BBS4			SLC25A28		BRK1

Blue	Green	Skyblue	Brown	Red	Black	Yellow	Orange	Indigo	Grey	Purple
CCNG1	KCNK6		ERI2	AGPAT5	FMNL1-DT			HSPA8		FLNA
RAB26	UBE2V1		NPC1	BAP1	SH3PXD2A			PSMB8-AS1		SPINDOC
CYB5R4	ATF1		PLEKHG2	SLC22A23	SEC61A2			C1QL3		SESN2
RACK1	SRRT		ZEB1-AS1	PRR3	LINC02132			AASDHPPT		CCDC34
TEX14	LTO1		TPPP	FASTKD5	EML6			CDC37L1-DT		UBXN2A
DIAPH1	UFC1		MPP1	ZNF620	PLS1			DGUOK-AS1		NDUFA10
HARS1	POLR2C		MNT	WNT5B	SIRT5			ANKHD1-EIF4EBP3		BMP1
ENPP4	ZNF232-AS1		SPC24	GTPBP4	MAN1B1-DT			PORCN-DT		VPS52
CNTF	TMEM161A		USP9X	PAICS	C7orf25			C9orf72		MICALL1
ANAPC15	C1D		CRELD1	RAB12	C11orf71			PMF1-BGLAP		ZBTB11-AS1
MYOM2	LRRC41		VSTM4	CFLAR	PTS					PIR
TUSC2	IFFO1		KAT14	TERF2	CFAP298					FOXJ2
RPS6	GALNT10		PRDM4	NOP2	CTTN					COBLL1
LDLRAD3	ERP44		JARID2	EMSLR	MNX1					PXK
FKBP2	PANK4		CDA	RGS1	ENC1					
RAC2	IFI35		HPSE	ZFP36	HMGB3					
PNP	RABEPK		FCER2	NUP62	NAGLU					
DCTN4	LINC02009		MROH6	NAV2	PLPP3					
CYP51A1	RPL27A		UROS	ASPHD2	FAM222A					
SELENOK	SELENOS		SHTN1	RTCB	LRRC3					
NCEH1	ELP6		BACE2	CAB39	PPP6R2					
KARS1	VAC14		POC1B	PLEK	RAB15					
ZSCAN16-AS1	LY6E		PPP2R5C	GLS	HBA2					
LAMTOR1	IP6K1		TRAF5	SLC44A5	MYO5C					
PSMF1	HYAL2		POMZP3	OGFOD1	BCYRN1					
CYP2J2	CHFR		GPAA1	PLD6	COG8					
SYK	ANXA6		FAM25BP	OTUD4	ASRGL1					
NUDC	SCAMP2		NBPF3	UBAP2L	NDRG4					
CD99	PDIA3		KRT83	PARP14						
TPBG	CRLF2		PSORS1C1	SINHCAF						
CHRAC1	MLX		LCLAT1	RRP7BP						
CEACAM21	DMAP1		ERCC6L	GNL3						
DHX34	PPP1R11		KRT6B	ADAP1						
ARPC5	DNTTIP1		GBE1	EI24						
ZNF436-AS1	TRIM27		NGLY1	SLC16A1						
RSU1	MAPK9		SEMA4D	ICE1						
CTNNBL1	FJX1		DTX1	TMEM39A						
DNAH14	RPL21		PPP1R18	PLCL2						

Blue	Green	Skyblue	Brown	Red	Black	Yellow	Orange	Indigo	Grey	Purple
TMED9	HERC6		TMEM237	PFDN2						
MRPS12	GPR89B		UBALD2	EMSY						
SPRED1	IL17RB		FAM126A	GABPB1						
MLEC	FAM241A		SNTB2	POLR1B						
ALDH1L2	SHROOM3		ACACB	PANK2						
XK	NOP58		STXBP5	RRP12						
AAR2	EEF1B2		EIF3J-DT	RNF19A						
EIF3I	DUS1L		ZDHHC20	UTP15						
SEC61A1	MGST1		EIF4E3	DCAF13						
GLT8D1	SNRPD1		SMAP1	PRMT1						
GASK1A	RPP30		CPPED1	PTPN2						
MPHOSPH6	PSMB10		H2AC6	DGKE						
TCAIM	RTRAF		SELENOW	TCF4						
PSME1	ARSA		LINC00052	PPARGC1B						
UTP4	PDIA5		MAST3	RFX5						
TM9SF3	KPNA1		ANLN	OASL						
PNO1	NRDC		ENDOV	SH2D4A						
ARHGDIA	IRF7		PEX11A	DIP2B						
TMED5	NDC1		ARHGEF9	NFKBID						
MPDU1	RNF125		AGGF1	SNX11						
ITGB7	ITGAL		TBC1D14	MTF1						
NUDCD2	UROD		LINC01278	ING3						
FTSJ3	MRS2		SMARCC2	MAML1						
VKORC1L1	UBLCP1		TNRC6B	TRIM21						
CGREF1	RPL37		PALD1	KLHL18						
TRAM1	CDK11B		TMEM178B	FARS2						
SMIM12	RRS1		DLGAP4	RASA1						
RRP9	STEAP3		TRAPPC13	PGAM5						
STOML2	OPN3		PLXNA2	PPP2R1B						
ORMDL1	DENND2D		NIPA1	GMFB						
SNIP1	TAPBPL		TTC28-AS1	ANKRD40						
VCP	PSMA5		FGFRL1	DTX3L						
TUT1	SLC35E1		ZNF829	MAP4						
MTFP1	CCDC138		MAPK13	PSME3						
EMC7	RBCK1		PPM1B	TNIP2						
CASP1	CNOT8		WASF1	PDSS1						
MTG2	PISD		HNRNPLL	ZNFX1						
PRPF19	ZW10		ITPKB	TRIM26						

Blue	Green	Skyblue	Brown	Red	Black	Yellow	Orange	Indigo	Grey	Purple
NT5DC2	GLCE		SEMA4B	HOOK1						
SLC35F4	MVD		CDCA7L	RPRD1B						
TPK1	EIF3K		NUF2	IFI16						
ERI3	BCS1L		SNHG20	NCL						
ATPAF1	RBFOX2		DHRS2	MRTFA						
HSBP1	RCHY1		REPS2	ZNF506						
FEN1	BHLHA15		TMEM106B	TIFA						
TMED7	DYNLT3		PXN	IFIH1						
ATP1A3	SNORD3B-1		ARL6IP1	KCTD12						
NANP	AK3		RNF13	SMOX						
EIF3M	CDC42		ABCA2	IMP4						
CRNKL1	THTPA		BUB1	CCND2						
MON1A	CAMKK2		GLIS2	RPUSD4						
SPCS3	NDUFS6		H2BC8	RAB24						
KIF9	HSPE1		ETV5	SPATA2						
EIF1AD	SPRYD3		PPP2R5A	RND1						
MKNK1	LMNB1		STRBP	ZNF430						
ANO10	NDUFB3		TMEM63C	WAKMAR2						
SHISA4	IRF1-AS1		ADCY6	ARPP19						
PDIA6	UQCRH		STXBP1	DSE						
CNTNAP3	CUTC		COA1	GBP3						
FCHSD1	RTN2		PKNOX1	IPO7						
DCAKD	RPL38		POMT1	SLCO5A1						
INTS4	DRAP1			SMG5						
SULT1A1	NSUN5			RIOK1						
SPRY4	ZDHHC3			NUP153-AS1						
CCNC	INTS11			STX11						
PEX14	SMYD5			EIF4G2						
GNG5	CCDC187			ELOVL7						
TAF9	SNRNP70			ZNF670						
WDR74	C5orf15			SGTB						
NACA	POLD4			NR1D2						
EMC8	CAMLG			NXF1						
TRIT1	TIGD2			MAFF						
PAQR7	MAN2A1			SNHG1						
SRA1	RAE1			CRIM1						
ZNF682	GSTO1			TAP1						
MTUS1	QDPR			GRAMD2B						

Blue	Green	Skyblue	Brown	Red	Black	Yellow	Orange	Indigo	Grey	Purple
PSMA3	UBE2N			FANCL						
AHCY	EMB			TMA16						
EXO5	SDHAF2			EML4						
EVI2A	MRPL4			HNRNPK						
POLR1H	CSTF3			DENR						
RMDN3	RAB6A			NAA15						
PIGO	NAA80			PLAGL2						
WASF2	SLC10A7			ZNF492						
MUL1	PURA			METTL2B						
POLR3H	ALG1			CYLD						
GSTK1	FAM27B			CCL5						
SYS1	ZNF408			DHX16						
IDI1	MRPS23			SMURF1						
TRPC4AP	SIL1			ASNSD1						
SIRT2	SIRT6			MMACHC						
SF3A1	ACADM			TRAFD1						
RSAD1	BMPR2			HDAC2						
EIF2B2	MRPL24			AGFG1						
ALDH18A1	CYB5RL			HIVEP1						
RANBP6	DNAJC8			ICAM2						
LINC01358	SNHG8			IPO5						
TRIM7-AS2	NARS2			WDR12						
UBIAD1	CKS2			IMPA1						
GPATCH3	CUEDC2			SLC39A1						
SGF29	TMCO1			UBE2V2						
GTF2B	IVNS1ABP			POLR3A						
DDN-AS1	ATF5			PHLPP1						
ZNF593	ATP5IF1			YARS2						
RPS8	GON7			PCNX3						
ZFYVE9	ZNF433-AS1			NEK4						
CACNA2D3	SACS			MACC1						
CCDC163	TMEM97			RBM6						
MTMR8	PURPL			MTOR						
BIN2	SF3A2			TRIM69						
STT3A	MLLT10			MAT2A						
MAPRE1	PSMA7			GPBP1						
KRT10-AS1	DCTN3			CLUHP3						
TXNL1	FABP5			CSNK1A1						

Blue	Green	Skyblue	Brown	Red	Black	Yellow	Orange	Indigo	Grey	Purple
SLC22A5	ODC1			TOMM70						
PHYKPL	ACACA			TMEM120B						
EMC1-AS1	SAR1A			CPEB3						
DNAJC3	AKAP8L			PEAK1						
FXYD5	PLA2G4A			MCTP1						
CISD2	TMEM126A			BNIP2						
C5orf63	GNB1L			NOC3L						
HLA-DOB	SMARCD1			SLC9A8						
ASAH2B	TCP1			RNF19B						
IFITM2	MRPL14			CDK17						
C5orf24	MT1X			CSF2RB						
PNOC	CALU			SPTY2D1						
LINC01531	RGS19			CCDC59						
SF3B5	CYP20A1			SRRM1						
ERO1B	ARF1			SFMBT2						
C11orf98				ST8SIA4						
HM13				CCDC66						
NETO1-DT				TVP23B						
GAREM1				ENTPD1-AS1						
M6PR				PBRM1						
EIF6				FAM210A						
UCHL3				TANK						
CDH18				NAGK						
TBL2				EML2-AS1						
SMIM27				SDC4						
SLC2A1				CSGALNACT1						
NRBP2				LACTB						
CHI3L2				PLEKHM2						
SLC8A1-AS1				XRN2						
TMEM80				MRPS11						
ERCC6L2-AS1				IGHMBP2						
EMBP1				THUMPD2						
EEF1A1				SLC2A6						
CSTF1				NLRP7						
PIGL				COPS2						
ALOX5AP				SDAD1						
MIR4500HG				TIMM23						
BATF3				LPIN1						

Blue	Green	Skyblue	Brown	Red	Black	Yellow	Orange	Indigo	Grey	Purple
ZNF341				EDC4						
				KLF5						
				PTP4A1						
				E2F3						
				UMPS						
				RNGTT						
				NOCT						
				ELL						
				ITPRID2						
				STEAP1B						
				THADA						
				ZNF268						
				HEATR1						
				SLC7A6						
				ATP2A2						
				GRINA						
				HLA-DRA						
				TOM1L1						
				AEN						
				MITF						
				ZNF669						
				MIS12						
				NOB1						
				NOP56						
				PPM1F						
				KCMF1						
				RPS6KC1						
				RRP15						
				SETD2						
				PROX1						
				LSM12						
				SAMD9L						
				ZFYVE27						
				PEA15						
				TDG						
				SUPV3L1						
				IPPK						
				NOTCH2						

Blue	Green	Skyblue	Brown	Red	Black	Yellow	Orange	Indigo	Grey	Purple
				RBM39						
				NOLC1						

Table 2.3. Gene set enrichment analysis (GSEA) using KEGG pathways of the differentially expressed genes between control and STAT1 KO MM cells stimulated with HAPLN1 matrikine.

Term	*Pathway Genes*	*Overlap*	*raw p*	*adjusted p*	*Score*
CYTOKINE_CYTOKINE_RECEPTOR_INTERACTION	106	29	4.5648E-15	7.8058E-13	12.1411937
TOLL_LIKE_RECEPTOR_SIGNALING_PATHWAY	71	18	2.8936E-09	2.474E-07	6.66106492
RIG_I_LIKE_RECEPTOR_SIGNALING_PATHWAY	52	13	5.5596E-07	2.3767E-05	4.69944011
CYTOSOLIC_DNA_SENSING_PATHWAY	36	11	4.5994E-07	2.6217E-05	4.68053052
CHEMOKINE_SIGNALING_PATHWAY	118	19	2.3072E-06	7.8905E-05	4.14671407
JAK_STAT_SIGNALING_PATHWAY	82	14	2.4955E-05	0.00071121	3.21022545
NOD_LIKE_RECEPTOR_SIGNALING_PATHWAY	46	10	4.2673E-05	0.00104244	3.07657261
INTESTINAL_IMMUNE_NETWORK_FOR_IGA_PRODUCTION	19	6	0.00016821	0.00359558	2.6316797
SMALL_CELL_LUNG_CANCER	64	11	0.00017205	0.00326898	2.56435872
ALLOGRAFT_REJECTION	16	5	0.00063794	0.009917	2.22524833
APOPTOSIS	71	11	0.00044007	0.00752525	2.20036175
SYSTEMIC_LUPUS_ERYTHEMATOSUS	17	5	0.00086909	0.01238452	2.12191889
LEISHMANIA_INFECTION	44	8	0.00089543	0.01177834	2.03828143
HEMATOPOIETIC_CELL_LINEAGE	36	7	0.0012374	0.01410632	1.97647153
ADIPOCYTOKINE_SIGNALING_PATHWAY	46	8	0.00121395	0.01482748	1.93607636
VIRAL_MYOCARDITIS	38	7	0.00172471	0.01638476	1.90539386
P53_SIGNALING_PATHWAY	59	9	0.00160886	0.01618322	1.87867419
NATURAL_KILLER_CELL_MEDIATED_CYTOTOXICITY	70	10	0.0015093	0.01613064	1.87031887
AUTOIMMUNE_THYROID_DISEASE	15	4	0.00434874	0.03913866	1.65481458
PATHWAYS_IN_CANCER	220	20	0.00528655	0.04519997	1.38127202
TYPE_II_DIABETES_MELLITUS	27	5	0.00769	0.06261854	1.37563393
PRIMARY_IMMUNODEFICIENCY	19	4	0.01063853	0.07909513	1.32482362
B_CELL_RECEPTOR_SIGNALING_PATHWAY	62	8	0.00816474	0.06346227	1.29082058
CHRONIC_MYELOID_LEUKEMIA	65	8	0.01078747	0.07686071	1.204873
CELL_ADHESION_MOLECULES_CAMS	68	8	0.01398645	0.09566734	1.10855068
ACUTE_MYELOID_LEUKEMIA	47	6	0.02190413	0.13872619	0.98083187
TYPE_I_DIABETES_MELLITUS	16	3	0.03659446	0.19555165	0.97674503
NOTCH_SIGNALING_PATHWAY	37	5	0.02830947	0.16692828	0.92630213
GLYCOSAMINOGLYCAN_BIOSYNTHESIS_CHONDROITIN_SULFATE	18	3	0.04977049	0.23640985	0.87421199
NEUROTROPHIN_SIGNALING_PATHWAY	100	10	0.02686156	0.16404738	0.86246399
EPITHELIAL_CELL_SIGNALING_IN_HELICOBACTER_PYLORI_INFECTION	53	6	0.0370699	0.19208946	0.82850686
T_CELL_RECEPTOR_SIGNALING_PATHWAY	79	8	0.03165908	0.18045676	0.82723984
MELANOMA	42	5	0.04571426	0.22334681	0.78594642

Term	*Pathway Genes*	*Overlap*	*raw p*	*adjusted p*	*Score*
PROSTATE_CANCER	69	7	0.04260001	0.21425298	0.7611339

Table 2.4. Newly diagnosed MM Patient Characteristics.

	All	Low	High
Patient Characteristics			
Median age	65	62	65
Gender, No. (%)			
Male	17 (65.4%)	8 (61.5%)	9 (69.2%)
Female	9 (34.6%)	5 (38.5%)	4 (30.8%)
Cytogenetic risk (No. of patients)			
Standard	14	7	7
High	7	2	5
Ultra-high	3	2	1
Not assessed	2	2	0
Median follow-up time (months)	51	59	45
HAPLN1 concentration (μg/mL)			
Mean ± SD	0.71 ± 0.80	0.36 ± 0.05	1.06 ± 1.03
Median progression-free survival (months)	42	57	28
Hazard ratio			3.027
[95% CI]			[1.135-8.072]
p-value (log-rank)			0.0164

Chapter III

Discussion & Future Perspectives

DISCUSSION

The aim of this thesis was to elucidate the role of hyaluronan and proteoglycan link protein 1 (HAPLN1) in multiple myeloma (MM) disease. In particular, I worked to identify a malignant phenotype induced by HAPLN1 and delineate the molecular mechanism through which HAPLN1 exerts this malignant action. MM is currently considered an incurable disease, manifesting continuous spread of malignant plasma cells in the bone marrow (BM)[1]. MM cells are highly dependent on the BM microenvironment which activates multiple cellular pathways, protecting these cells from apoptosis and inducing drug resistance[2,3]. The nature of the disease being already spread to multiple sites at the time of diagnosis prevents any surgical interventions, undermining any treatment[4]. In order to understand the role of HAPLN1 in MM, it is essential to investigate its function in MM biology and clarify the cellular and molecular mechanisms involved. In this thesis, I aimed to elucidate how the HAPLN1 matrikine functions in MM through the following goals: 1) to test if HAPLN1 matrikine is a novel BM homing factor and 2) to test if HAPLN1 is a prognostic marker.

The Miyamoto lab previously showed that HAPLN1 can induce resistance to bortezomib, one of the frontline MM therapies, and activate bortezomib-resistant NF-κB signaling in MM cells[5]. Here, I contributed to testing whether the HAPLN1 matrikine can induce drug resistance to several classes of MM drugs. The term ‘matrikine’ was defined as a proteolytically digested product of an ECM protein that can regulate cellular activities[6]. Our lab previously demonstrated that fragments of HAPLN1 containing all domains or the two PTR domains were detected in the BM aspirate of relapsed/refractory MM patients[5]. Moreover, the detection of these fragments correlated with the patients

having progressive disease, an unfavorable category of treatment response criteria[7]. However, the role of HAPLN1-derived matrikine in MM is not well understood. We used a recombinant protein of a specific HAPLN1 domain, PTR1, as a representative HAPLN1-derived matrikine. HAPLN1 can induce MM cell survival in the presence of different classes of FDA-approved drugs for MM chemotherapy. We found that HAPLN1 can increase the expression of anti-apoptotic genes (e.g., *BCL2, BCL2L1, BCL2A, BIRC2, BIRC3, CFLAR (c-FLIP) and IER3 (IEX-1L)*) that are known to be NF-κB target genes. Furthermore, from an RNA-seq analysis, the *multi-drug resistance (MDR)* family genes that are previously reported to be involved in drug resistance were also found to be upregulated. Indeed, the drug efflux pump function was increased after HAPLN1 incubation suggesting a dual mode of HAPLN1-induced drug resistance by inducing the expression of both anti-apoptotic genes and drug efflux pump genes. The data therefore support HAPLN1 as a multi-drug resistance inducer in MM cells.

My study also revealed that the matrikine can cause MM cell BM homing. Again, I used a recombinant PTR1 domain as a representative HAPLN1 matrikine. This peptide was sufficient to induce MM cell adhesion and both chemotactic and chemokinetic migration *in vitro*. In addition, I developed a human BMSC (HS-5) cell model that stably expresses and secretes an MMP-cleaved product of HAPLN1, HAPLN1-32-354. This cell model (HS-5/H1) also induced MM cell migration *in vitro* and importantly BM homing *in vivo*. I observed MM cells preferentially home to HS-5/H1 cell-injected tibia compared to the control HS-5/EV tibia. The magnitude of increase in MM cell homing to the HS-5/H1 cell-injected tibia was comparable in three independent assays using flow cytometry, IHC, and qPCR quantifications. Lastly, I identified that the HAPLN1 matrikine can activate

STAT1 signaling which can regulate MM cell migration and BM homing. In summary, the fragments from the ECM protein HAPLN1 attract MM cells to the BM via STAT1 activation, supporting its newly identified role in MM homing, dissemination, and disease progression.

Our studies support the role of HAPLN1 as an inducer of drug resistance and a BM homing factor in MM. Given its pathogenic role in MM, I hypothesized that the HAPLN1 level could serve as a prognostic and/or diagnostic marker in MM patients. Using AlphaLISA, I collected preliminary data on HAPLN1 concentrations in patient BM samples and grouped the patients into two groups based on a median cut-off value. Significantly, high HAPLN1 concentrations correlated with poor patient outcomes, confirming our hypothesis. Specifically, patients with high HAPLN1 levels (average 1.06 μg/mL, n=13) exhibited worse progression-free survival (hazard ratio, 3.027) and a higher number of therapies compared to the low HAPLN1 group (Table 2.4 and Figure 2.10). Moreover, when the patients were stratified based on the presence of high/ultra-high risk or standard risk cytogenetic markers, patients with standard risk showed a stark difference in PFS (hazard ratio, 5.861), while patients with high/ultra-high risk did not exhibit a significant difference in PFS. It is possible that MM cells harboring cell-intrinsic high/ultra-high-risk alterations may not require cell-extrinsic factors to increase drug resistance. Cell-extrinsic factors, unlike cell-intrinsic genetic alterations, are overlooked in the risk assessment of MM patients. To our knowledge, using an ECM protein as a biomarker of disease progression is unprecedented in MM. These findings are encouraging and warrant further investigation into the potential of HAPLN1 as a prognostic marker in MM patients.

FUTURE PERSPECTIVES

Determining HAPLN1 levels in MM patients

I demonstrated that high HAPLN1 levels in BM samples are associated with poor prognosis in newly diagnosed MM patients. I measured the HAPLN1 concentration in BM aspirates from MM patients in 26 newly diagnosed MM patients with relevant clinical data. Upon acquiring patient BM aspirates, I centrifuged the sample and collected the plasma fraction to measure the soluble HAPLN1 protein concentration in the BM. I attempted several antibody-based assays, including 1) immunoprecipitation (IP)-Western blot, 2) ELISA, and 3) immunoassay with different detection systems, named AlphaLISA. In my research, to find suitable antibodies, I first screened commercially available HAPLN1-reactive antibodies. The main challenge with antibody-based assays on MM samples was the excessive amount of monoclonal antibodies produced by MM cells. Fetal bovine serum (FBS), used as a control or standard diluent, contains ~180 µg/ml immunoglobulin G (IgG)[8], whereas newly diagnosed MM patients have ≥30 mg/mL of monoclonal immunoglobulin in the blood and also likely in BM samples. The presence of monoclonal antibodies in patient samples interfered with the IP pull-down, increased noise in the ELISA and hindered antigen-antibody binding in the AlphaLISA. For IP experiments, I initially attempted to preclear the sample with protein A/G/L or a size exclusion spin column to remove immunoglobulins. However, both methods were unsuccessful in clearing excess monoclonal immunoglobulins or resulted in the loss of HAPLN1 protein in the spin column, respectively. In-house ELISA was unsuccessful due to sensitivity issues, as the linear range achieved for HAPLN1 was between 0.5-2 µg/ml HAPLN1, which was not sensitive enough to reliably measure the patient samples. Finally, I

employed AlphaLISA, an immunoassay with a unique secondary detection antibody that does not require washing steps. Initially, I encountered significant signal interference, leading to negative values when calculated from the standard curve. To address this issue, I adjusted the standard and all the samples to the same human IgG concentration. After measuring human IgG concentration using a commercially available human IgG ELISA kit, I spiked the samples with human IgG so that all the samples had the same final concentration of IgG antibodies. With the optimized assay protocol, I measured BM aspirates from newly diagnosed MM patients who had not undergone treatment or transplant. Using AlphaLISA, I acquired preliminary data on HAPLN1 concentrations in patient BM samples and demonstrated high HAPLN1 concentrations correlated with poor patient outcomes.

Although my preliminary data showed promising results of HAPLN1 as a prognostic marker, especially for standard risk NDMM patients, there are some caveats related to this assay. I tested two pairs of anti-HAPLN1 antibodies: the first pair targeted the PTR1 domain only, while the second pair targeted both the PTR1 domain and N-terminal sequence (immunogen sequence 16-75 amino acid residues). These antibody pairs displayed different magnitudes of readouts against the standard. The difference in magnitude could be due to the proximity of the two antibodies that is necessary for the AlphaLISA to work or different antibody species (mouse monoclonal vs rabbit polyclonal). Despite the differing magnitudes of reactivity, the relative concentration trend between these two paired antibody assays remained consistent, further supporting the detection of HAPLN1 in these assays. Additionally, the PTR domain shares a considerable degree of homology throughout the PTR domain superfamily with 30-40% sequence identity in

PTR domains[9]. Therefore, we decided to use a pair of antibodies against the PTR1 domain and N-terminal region to specifically detect HAPLN1, and not other PTR-containing proteins. It was surprising to observe that HAPLN1 levels have the potential to predict clinical outcomes as a prognostic marker. However, we cannot rule out the possibility of antibody cross-reactivity with other PTR domain superfamily members. Further optimization of the assay and a larger sample size are thus warranted. These finding may provide new perspectives on patient stratification for different MM therapy approaches.

Defining the role of HAPLN1 in the non-cancerous BM microenvironment and other types of cancer cells

Although work on HAPLN1-knockout mice suggest a critical role of HAPLN1 in promoting the proper formation of cartilage, bone, heart, and brain during embryonic development[10–12], its role in adult mice or humans remains undefined. In addition to its role in MM pathology, there may be potential physiological roles for HAPLN1 matrikine. I have developed an immunoassay to quantify the HAPLN1 level in BM aspirates. Currently, the sample size of normal BM is too small to draw any conclusions. However, preliminary data on BM aspirates from healthy donors showed no statistically significant difference in the HAPLN1 level between MM patients and healthy donors. The HAPLN1 concentration exhibited varied levels showing heterogeneity in both healthy donors and MM patients. This finding suggests that the soluble HAPLN1 molecule exists in normal BM and possibly functions not only in the malignant plasma cells but also under physiological conditions. Furthermore, as hematopoietic stem cells (HSCs) employ the

same BM homing mechanism as plasma cells, it would be interesting to investigate the function of HAPLN1 matrikine in BM homing of HSCs and normal plasma cells.

Moreover, MM cells utilize common molecular pathways for homing to the BM similar to HSCs and other types of cancer cells that form BM metastases[13]. In a recent publication, the Miyamoto lab identified the receptor of HAPLN1 matrikine, the CH60-TLR4 complex, as a mediator of inflammation signaling[14]. This result suggests that the degradation of local extracellular matrix, which is an indispensable step in cancer dissemination, BM injury or stress, may act as damage-associated molecular patterns (DAMPs)[15]. HAPLN1 overexpression has been reported to correlate with poor survival prognosis in several cancer types, such as gastric cancer and pancreatic cancer, without a clear mechanism[16,17]. It would be of great interest to apply the mechanisms learned from MM cell homing to these cell types and investigate whether the HAPLN1 matrikine plays a role in HSC physiology and HAPLN1 overexpressing cancers. Thus, an improved understanding of the normal roles of HAPLN1 and its matrikine in normal BM physiology and other processes will be critical for the development of HAPLN1 matrikine-targeting therapeutics against MM and possibly several other cancer types.

Elucidating the mechanism of HAPLN1-mediating signaling

I have discovered a novel role of STAT1 in MM migration and BM homing. In the context of MM, previous studies on STAT family members in MM have mainly focused on STAT3. In line with this, my collaborator's bioinformatics analysis revealed STAT3 as a potential master regulator of HAPLN1 signaling. Surprisingly, on the contrary to the well-established oncogenic role of STAT3 signaling, my biochemical analyses showed STAT1

to be activated instead of STAT3. Although STAT1 is well-known for its tumor suppressor function in various types of cancers[18], its role in oncogenesis is context-dependent[19]. My data support the activation of STAT1 by HAPLN1 matrikine, leading to increased MM cell homing to the BM and the subsequent seeding of circulating MM cells into a more protective microenvironment, ultimately resulting in MM disease progression. These findings support that STAT1 can act as an oncogenic signaling inducer in MM disease in response to HAPLN1 matrikine exposure. Additionally, ongoing clinical trials aim to combine the JAK1/2 inhibitor ruxolitinib with the treatment regimen for heavily treated relapsed MM patients[20]. These findings strongly suggest that inhibition of BM homing and/or the STAT pathway may overcome drug resistance and improve the prognosis of MM.

To further clarify the migratory phenotype induced by HAPLN1, downstream effectors were screened from the RNA-seq analysis (e.g., SDF-1, CD44, ICAM-1). However, it is yet to be elucidated whether these genes are directly or indirectly regulated by STAT1 or NF-κB. This finding can be further investigated by ChIP-seq analysis of STAT1 and NF-κB (p65, p50). Additionally, the genes of interest from the migratory gene set can be verified. For instance, we observed that HAPLN1 matrikine can induce migration-related genes including SDF-1. It would be logical to test whether HAPLN1-induced MM migration is mediated through the SDF-1/CXCR4 axis, despite the distinct migration phenotype displayed by SDF-1 and HAPLN1, i.e., chemotaxis only by the former versus a combination of chemotaxis and chemokinesis by the latter. This hypothesis can also be verified using inhibitors, neutralizing antibodies or genetic ablation.

Confirming the role of HAPLN1 in drug resistance *in vivo*

MM is currently considered incurable because most patients relapse or become refractory by developing drug resistance to multiple therapies. Even patients who achieve a complete response to therapy eventually relapse, indicating the persistence of remnant MM cells. Therefore, eradicating the minimal residual disease (MRD) is crucial for a cure[21,22]. Undoubtedly, achieving MRD-negativity is associated with better clinical outcomes. MRD-negative status is defined as the absence of clonal plasma cells, and this depends on the sensitivity of the detection method. Currently, next-generation flow cytometry (NGF) and next-generation sequencing (NGS) are used, with the sensitivity to detect one MM cell in 10^5 cells and in 10^6 cells, respectively[23]. Conceptually, MRD can be explained by cancer stem cells (CSCs)[24]. In this model, after initial treatment, bulk cancer cells will die, but resistant CSCs will survive. Given that HAPLN1 is capable of inducing multidrug resistance in MM *in vitro*, it is plausible to investigate the role of HAPLN1 in cancer stemness and multi-drug resistance *in vivo*. I established a mouse MM xenograft model using intracardiac and intratibial injections, and it is of great interest to conduct an orthotopic *in vivo* study. Furthermore, my current studies have focused on measuring BM homing of MM cells 3 days post-inoculation. Investigating the long-term biology of HAPLN1 in MM, such as tumor growth, would be of great interest. In my preliminary 3-week-observation, I found that HAPLN1-conditioned tibia showed larger tumor burden, which was proportional to the BM homing. This result indicates that the increased tumor burden observed at 3 weeks was primarily due to the enhanced homing of MM cells to the HAPLN1-conditioned tibia, rather than the role of HAPLN1 in tumor

growth or proliferation, neither of which has been observed in both *in vitro* and *in vivo* xenograft studies[5,14]. However further optimization of this experiment is needed, for example, determining the optimal cell number for injection, drug dosage, and employing more robust cell labeling. It would be of great interest to conduct additional *in vivo* studies to confirm the role of HAPLN1 in multi-drug resistance, cancer stemness and/or MRD phenotypes.

HAPLN1 as a drug target

Because BM homing plays a pivotal role in MM disease progression and drug resistance, HAPLN1 matrikine could serve as a potential target for future therapeutic interventions. Small-scale clinical trials (phase I/II) have been conducted to target MM BM homing, specifically focusing on the SDF-1/CXCR4 axis. Thus far, blockade of the SDF-1/CXCR4 axis using CXCR4 antagonist (AMD3100)[25], anti-CXCR4 monoclonal antibody[26], and a SDF-1 neutralizing oligonucleotide[27] has shown to be effective in chemosensitization. These chemosensitizing agents have demonstrated clinical benefits when combined with conventional MM chemotherapies. In a phase II trial in relapsed/refractory MM patients, where 70% of patients had prior bortezomib treatment, the combination of AMD3100 and bortezomib resulted in an overall response rate (partial response or better) of 48.5% and a median progression-free survival (PFS) of 12.6 months. Comparing the median PFS to prior studies in relapsed/refractory MM patients treated with bortezomib and dexamethasone (8.08 months)[28], the combination of AMD3100 improved PFS by 4.6 months. One plausible mechanism for chemosensitization is the blockade of SDF-1/CXCR4 action, which inhibits MM cell

interaction with the BM microenvironment and mobilizes MM cells from the protective BM niche into circulation where MM cells become more sensitive to conventional therapies as they lose the protection afforded by the BM tumor microenvironment[29]. However, since SDF-1 plays a critical role in the regulation of hematopoietic stem cells (HSCs) and immune cells, such as B cells, T cells, monocytes, granulocytes, dendritic cells, basophils, and NK cells, an increase of these cells in the patient peripheral blood was observed in the trials after CXCR4 inhibition. Thus, larger trials are warranted to further evaluate the efficacy of the therapy and potential unwanted side effects.

Regarding the HAPLN1 matrikine, we previously demonstrated its direct role in inducing drug resistance in MM cells via NF-κB[30]. Inhibition of HAPLN1 matrikine action could promote drug sensitization in MM cells via two independent mechanisms: directly increasing their drug sensitivity by inhibition of NF-κB signaling and indirectly reducing their BM homing to retain MM cells in circulation where they are more vulnerable to drug effects. Thus, HAPLN1 seems a plausible target to prevent drug resistance in MM and prevent MM cells from homing to chemoprotective BM niches. Therefore, targeting the soluble HAPLN1 protein using neutralizing antibody or inhibitors of the CH60-TLR4 receptor complex maybe be developed. However, it is important to identify specific features of HAPLN1 matrikine that can be therapeutically targeted, distinct from those involved in its normal physiological roles to avoid currently unforeseen unwanted toxicities. Protein folding and structures of both the full-length protein and its cleaved fragments are pivotal for the development of matrikine-specific drugs.

Currently, MM is considered incurable because most patients relapse and become refractory to treatments. The majority of patients relapse, and with the successive lines

of therapy, their remissions become shorter, resulting in poorer survival[31]. In addition, from an economic perspective, MM imposes a significant burden, with the average cost of MM-related healthcare of $670,561 per patient ($34,610 per patient per month)[32]. We previously reported that HAPLN1 matrikine is unable to induce resistance in MM cells to carfilzomib and selinexor[30]. In this study, I have demonstrated that higher HAPLN1 levels correlated with a poor prognosis, particularly in newly diagnosed MM patients with standard cytogenetic risk and required more therapies than the low HAPLN1 patients. These findings altogether suggest that screening HAPLN1 levels in newly diagnosed MM patients may have potential therapeutic and financial benefits. HAPLN1 screening could help predict the course of therapy and guide therapeutic decision-making. For instance, standard risk patients with high HAPLN1 levels may benefit from therapies that include carfilzomib, selinexor, or both, and avoid other standard therapies that may be less effective and can incur significant financial burdens. Ultimately, HAPLN1 screening may help reduce the economic burden of therapies and improve patient outcomes. Overall, the potential use of HAPLN1 levels in BM aspirates as a prognostic marker and drug target opens the door to the more effective and personalized medicine in the treatment of MM patients.

REFERENCES

1. Bianchi, G. & Anderson, K. C. Understanding biology to tackle the disease: Multiple myeloma from bench to bedside, and back. *CA A Cancer J. Clin.* **64**, 422–444 (2014).

2. Hallek, M., Bergsagel, P. L. & Anderson, K. C. Multiple myeloma: increasing evidence for a multistep transformation process. *Blood* **91**, 3–21 (1998).

3. Noonan, K. & Borrello, I. The immune microenvironment of myeloma. *Cancer Microenviron.* **4**, 313–323 (2011).

4. Röllig, C., Knop, S. & Bornhäuser, M. Multiple myeloma. *The Lancet* **385**, 2197–2208 (2015).

5. Huynh, M. *et al.* Hyaluronan and proteoglycan link protein 1 (HAPLN1) activates bortezomib-resistant NF-κB activity and increases drug resistance in multiple myeloma. *J. Biological Chem.* **293**, 2452–2465 (2018).

6. Maquart, F.-X., Pasco, S., Ramont, L., Hornebeck, W. & Monboisse, J.-C. An introduction to matrikines: extracellular matrix-derived peptides which regulate cell activity. Implication in tumor invasion. *Crit. Rev. Oncol. Hematol.* **49**, 199–202 (2004).

7. Rajkumar, S. V. *et al.* Consensus recommendations for the uniform reporting of clinical trials: report of the International Myeloma Workshop Consensus Panel 1. *Blood* **117**, 4691–4695 (2011).

8. Cheever, M., Versteegen, R. & Master, A. A Method for Differentiating Fetal Bovine Serum from Newborn Calf Serum. *Bioprocess. J.* **16**, (2017).

9. Blundell, C. D. *et al.* Towards a Structure for a TSG-6·Hyaluronan Complex by Modeling and NMR Spectroscopy INSIGHTS INTO OTHER MEMBERS OF THE LINK MODULE SUPERFAMILY*. *J. Biological Chem.* **280**, 18189–18201 (2005).

10. Carulli, D. *et al.* Animals lacking link protein have attenuated perineuronal nets and persistent plasticity. *Brain* **133**, 2331–2347 (2010).

11. Wirrig, E. E. *et al.* Cartilage link protein 1 (Crtl1), an extracellular matrix component playing an important role in heart development. *Dev. Biology* **310**, 291–303 (2007).

12. Watanabe, H. & Yamada, Y. Mice lacking link protein develop dwarfism and craniofacial abnormalities. *Nat. Genet.* **21**, 225–229 (1999).

13. Mishra, A., Shiozawa, Y., Pienta, K. J. & Taichman, R. S. Homing of cancer cells to the bone. *Cancer Microenviron.* **4**, 221–35 (2011).

14. Bakshi, D. D. *et al.* Ectopic CH60 mediates HAPLN1-induced cell survival signaling in multiple myeloma. *Life Sci. Alliance* **6**, e202201636 (2023).

15. Frevert, C. W., Felgenhauer, J., Wygrecka, M., Nastase, M. V. & Schaefer, L. Danger-Associated Molecular Patterns Derived From the Extracellular Matrix Provide Temporal Control of Innate Immunity. *J. Histochem. Cytochem.* **66**, 213–227 (2018).

16. Zhang, T. *et al.* Cancer-associated fibroblasts-derived HAPLN1 promotes tumour invasion through extracellular matrix remodeling in gastric cancer. *Gastric Cancer* **25**, 346–359 (2022).

17. Wiedmann, L. *et al.* HAPLN1 is a driver for peritoneal carcinomatosis in pancreatic cancer. *bioRxiv* 2022.05.30.493185 (2022) doi:10.1101/2022.05.30.493185.

18. Zhang, Y. & Liu, Z. STAT1 in cancer: friend or foe? *Discovery medicine* **24**, 19–29 (2017).

19. Adámková, L., Soucková, K. & Kovarík, J. Transcription protein STAT1: biology and relation to cancer. *Folia biologica* **53**, 1–6 (2007).

20. Berenson, J. R. *et al.* Ruxolitinib and methylprednisolone for treatment of patients with relapsed/refractory multiple myeloma. *Br. J. Haematol.* **200**, 722–730 (2022).

21. Kumar, S. *et al.* International Myeloma Working Group consensus criteria for response and minimal residual disease assessment in multiple myeloma. *The Lancet Oncol.* **17**, e328–e346 (2016).

22. Bravo-Pérez, C. *et al.* Minimal Residual Disease in Multiple Myeloma: Something Old, Something New. *Cancers* **13**, 4332 (2021).

23. Yee, A. J. & Raje, N. Minimal residual disease in multiple myeloma: why, when, where. *Hematology* **2021**, 37–45 (2021).

24. Ghiaur, G., Gerber, J. & Jones, R. J. Concise Review: Cancer Stem Cells and Minimal Residual Disease. *STEM CELLS* **30**, 89–93 (2012).

25. Ghobrial, I. M. *et al.* Phase I/II trial of the CXCR4 inhibitor plerixafor in combination with bortezomib as a chemosensitization strategy in relapsed/refractory multiple myeloma. *Am. J. Hematol.* **94**, 1244–1253 (2019).

26. Ghobrial, I. M. *et al.* A Phase Ib/II Trial of the First-in-Class Anti-CXCR4 Antibody Ulocuplumab in Combination with Lenalidomide or Bortezomib Plus Dexamethasone in Relapsed Multiple Myeloma. *Clin. Cancer Res.* **26**, 344–353 (2020).

27. Ludwig, H. *et al.* Olaptesed pegol, an anti-CXCL12/SDF-1 Spiegelmer, alone and with bortezomib-dexamethasone in relapsed/refractory multiple myeloma: a Phase IIa Study. *Leukemia* **31**, 997–1000 (2017).

28. San-Miguel, J. F. *et al.* Panobinostat plus bortezomib and dexamethasone versus placebo plus bortezomib and dexamethasone in patients with relapsed or relapsed and

refractory multiple myeloma: a multicentre, randomised, double-blind phase 3 trial. *The Lancet Oncol.* **15**, 1195–1206 (2014).

29. Roccaro, A. M. *et al.* SDF-1 inhibition targets the bone marrow niche for cancer therapy. *Cell Reports* **9**, 118–128 (2014).

30. Huynh, M. *et al.* HAPLN1 confers multiple myeloma cell resistance to several classes of therapeutic drugs. *PLOS ONE* **17**, e0274704 (2022).

31. Yong, K. *et al.* Multiple myeloma: patient outcomes in real-world practice. *Br. J. Haematol.* **175**, 252–264 (2016).

32. Jagannath, S. *et al.* Healthcare Costs of Multiple Myeloma Patients with Four or More Prior Lines of Therapy, Including Triple-Class Exposure in the United States. *Oncol. Ther.* **10**, 411–420 (2022).

Figure 3.1

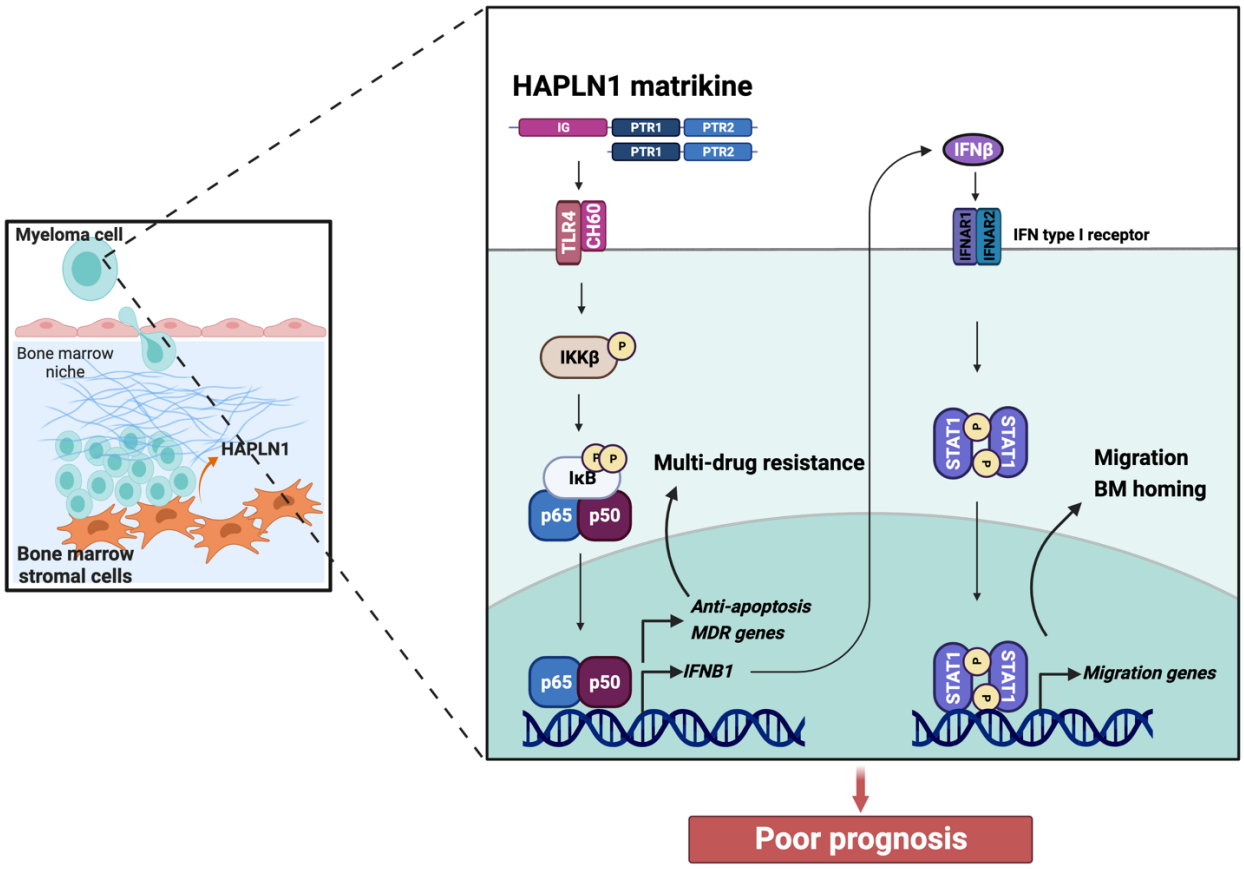

Figure 3.1. Schematic of the proposed role of HAPLN1 in multiple myeloma (MM). Bone marrow stromal cells (BMSCs) secrete HAPLN1. HAPLN1 fragments containing PTR1/PTR2 domain(s) induce the NF-κB pathway via the CH60-TLR4 complex. Newly synthesized, secreted factor(s) can subsequently activate the STAT1 pathway inducing MM cell migration and bone marrow (BM) homing, ultimately leading to a poor prognosis.

Appendix:

HAPLN1 confers multiple myeloma cell resistance to several classes of therapeutic drugs

---

This Chapter has been accepted for publication:
Mailee Huynh, Hae Yeun Chang, Dominique N. Lisiero, Irene M. Ong, Trinayan Kashyap, Natalie S. Callander, Shigeki Miyamoto. PLOS ONE 17, e0274704 (2022)

Contributions: Figures 1B-D & Table S1 were performed by I.M.O. Figures 2 & 6 were performed by M.H and H.Y.C. Figure 4E was performed by M.H and D.N.L. Figure 5 was performed by H.Y.C. All remaining experiments were performed by M.H.

Abstract

Multiple myeloma (MM), a malignant plasma cell infiltration of the bone marrow, is generally considered incurable: resistance to multiple therapeutic drugs inevitably arises from tumor cell-intrinsic and tumor microenvironment (TME)-mediated mechanisms. Here we report that the proteoglycan tandem repeat 1 (PTR1) domain of the TME matrix protein, hyaluronan and proteoglycan link protein 1 (HAPLN1), induces a host of cell survival genes in MM cells and variable resistance to different classes of clinical drugs, including certain proteasome inhibitors, steroids, immunomodulatory drugs, and DNA damaging agents, in several MM cell lines tested. Collectively, our study identifies HAPLN1 as an extracellular matrix factor that can simultaneously confer MM cell resistance to multiple therapeutic drugs.

Introduction

Multiple myeloma (MM) is a hematopoietic malignancy characterized by the unrestrained proliferation and accumulation of antibody secreting plasma cells in the bone marrow [55]. In the United States, MM represents ~11% of all hematological cancers and is increasing in incidence in the US (e.g., 14,400 in 1996 to 34,920 estimated in 2021) [56]. Since the first documented case of MM in 1844, the treatments available for MM have improved considerably [57], from early success with L-phenylalanine mustard (melphalan), an alkylating agent [58,59] with addition of a corticosteroid, such as prednisone or dexamethasone [60] to highly active, more targeted agents such as the immunomodulatory drugs (IMiDs; thalidomide, lenalidomide and pomalidomide) [61-64], proteasome inhibitors (PIs; bortezomib, ixazomib, and carfilzomib) [65-67], and monoclonal antibodies (daratumumab, elotuzumab and isatuximab). Other agents, including alkylating agents (cyclophosphamide) and DNA-damaging agents (doxorubicin and bendamustine), are also employed at times in MM therapy. More recently, a selective inhibitor of nuclear export (XPO1), selinexor in combination with dexamethasone, demonstrated efficacy in MM patients previously resistant to five classes of therapies (penta-refractory) [68-71]. Drugs under development include novel agents such as cereblon E3 ligase modulator (CELMoD) such as iberdomide, the BCL2 inhibitor (venetoclax) and bispecific T cell engagers [72-74]. Finally, the recently FDA approved chimeric antigen receptor (CAR)-T cell therapy against B cell maturation antigen (BCMA) has shown promising results in relapsed/refractory MM patients. Yet patients continue to relapse [75]. Despite the vast array of currently available therapies, MM is still generally considered incurable with a median survival of 5-7 years after diagnosis. Therefore, there is a critical need to

understand factors that contribute to therapy resistance and key signaling and regulatory pathways involved in therapy resistance to improve clinical outcomes [55,57,71,76].

Data from sequencing efforts confirmed that MM is a highly genetically heterogeneous disease. Often observed are aberrant genetic changes in critical pathways such as: nuclear factor-kappaB (NF-κB), β-catenin, insulin-like growth factor receptor (IGFR), mitogen-activated protein kinases (MAPK), AKT, KRAS, JAK/STAT and many more [77-79]. Alterations of these various pathways to induce their constitutive activation or hyperactivation is often implicated in mediating MM cell survival and drug resistance. The complex bone marrow (BM) tumor microenvironment (TME) is also an essential component of MM pathogenesis and has been the focus of intense research efforts. It is recognized that direct and indirect interactions with different cell types, such as bone marrow stromal cells (BMSCs) and the extracellular matrix (ECM) augment MM cell growth, survival, migration, and drug resistance [80-82]. Drug resistance (DR) through the TME can be divided by two major subgroups: soluble factor mediated (SFM-DR) and cell adhesion mediated (CAM-DR). SFM-DR involves soluble cell-derived cytokines, growth factors and chemokines that act on MM cells to promote growth and survival [83]. CAM-DR is dependent on the adhesive contacts of MM cells directly to BMSCs or ECM proteins. The adhesion of MM cells through molecules, such as VLA-4 or CD44, and direct contact of myeloma cells to BMSCs allow MM cells to survive the cytotoxic effects of anti-cancer therapy [83]. Like cell-intrinsic genetic alterations, SFM-DR and CAM-DR commonly deregulate key survival signaling pathways in MM cells. Numerous ECM proteins and glycosaminoglycans (GAGs) undergo enzymatic cleavage resulting in the release of peptides (matrikines) that exert biological activities, which are usually different

from those of the full-length molecules. The liberated matrikines may interact with specific receptors on the cell surface to activate several signaling pathways leading to increased migration, proliferation, or cell adhesion [84,85]. However, whether matrikines cause drug resistance in MM remains obscure.

We previously reported that HAPLN1 is secreted by patient-derived bone marrow stromal cells, and HAPLN1 fragments containing proteoglycan tandem repeat 1 and 2 (PTR1/2) are present in MM patient bone marrow plasma or soluble fraction [31]. HAPLN1-PTR1 is sufficient to activate bortezomib-resistant NF-κB activity and confer bortezomib-resistance survival of MM cells [31]. Because the NF-κB pathway plays a pivotal role in MM biology, there has been a persistent attempt to target NF-κB signaling and its effectors in anti-myeloma therapy, such as monoclonal antibodies against BAFF and BCMA, and small molecule inhibitors against NIK and IKK, among others [86]. In addition, blockade of PD-L1, a downstream effector of NF-κB signaling, is heavily investigated [87,88]. Whether HAPLN1-PTR1 can also induce resistance to other MM therapeutic drugs remain untested.

In this study, we report that HAPLN1-PTR1 induces a constellation of survival genes, and confer MM cell resistance to multiple classes of therapeutic agents used in MM treatment. Our study reveals a novel mechanism of matrikine-mediated drug resistance in MM, which could represent a novel biomarker and/or therapeutic target for MM disease.

Material and Methods

Cell line culture

RPMI8226, MM.1S, NCI-H929, and U266 human MM cell lines were obtained from American Type Culture Collection (ATCC). L363 cell line was obtained from Dr. Lixin Rui. All MM cell lines were cultured at 37°C/5% CO_2 in RPMI1640 containing 10% FBS, 2% glutamax (Gibco) + 1% penicillin/streptomycin. These cells were checked for mycoplasma contamination by Universal Mycoplasma Detection Kit (30-1012K, ATCC) and confirmed to be negative.

Antibodies and reagents

Antibodies against IκBα (C-21), IκBβ (C-20) were obtained from Santa Cruz Biotechnology and antibody against tubulin (CP06) purchased from Calbiochem, recombinant human TNFα (654205, EMD Millipore), cycloheximide (C7698, Sigma-Aldrich), and leptomycin B (87081-35-4, Cayman Chemicals). Bortezomib (S1013), ixazomib citrate (S2181), carfilzomib (S2853), melphalan (S8266), and bendamustine (S1212) were purchased from Selleckchem. Dexamethasone (D4902), doxorubicin (D1515), and lenalidomide (CDS022536) were purchased from Sigma-Aldrich. Selinexor (KPT-330) was provided by Dr. Trinayan Kashyap (Karyopharm). MTT (3-(4,5-dimethylthiazol-2-yl)-2,5-diphenyltetrazolium bromide) (M6494) was purchased from Thermo-Fisher Scientific.

Purification and expression of GST-Tagged proteins

The details of GST-fused HAPLN1-PTR1 and assessment of bacterial LPS

contamination have been published [89]. Briefly, pGEX6p-1 plasmid-based expression constructs were transformed into BL21 Rosetta 2 *Escherichia coli* strain and induced with 1 mM IPTG followed by lysis and purification by glutathione-agarose beads (G4510, Pierce) and elution by 50 mM reduced glutathione at pH 8.0.

Electrophoretic mobility shift assays (EMSA)

EMSA to measure NF-κB activity in MM cell lines were performed as previously described [90]. Briefly, cell extracts were made using TOTEX buffer, as previously described [48] and 10 μg of extracts were separated on 4% native polyacrylamide gel, dried, and exposed to phosphor screen (Amersham Biosciences) followed by quantitation of NF-κB DNA-binding through ImageQuant software (GE Healthcare). Each NF-κB lane was normalized to Oct-1 values from the same sample and then to the vehicle treated control values for each experiment to derive fold induction.

SDS-PAGE and immunoblot (IB) analysis

Myeloma cell lines were pelleted and lysed in TOTEX buffer, as previously described [48]. Equal amounts (100 μg) of soluble protein were run on denaturing 10 or 12.5% SDS-PAGE gel and transferred onto a polyvinylidene fluoride or nitrocellulose membrane (GE Healthcare). The membrane was then incubated with the appropriate antibodies as described previously [48]. Immunoblots were analyzed by enhanced chemiluminescence as described by the manufacturer (GE Healthcare).

Immunofluorescence and ImageStream cytometry

For immunofluorescence, IκBα antibody (E130, Abcam), 5 mM DRAQ5 (564902, BD Biosciences), anti-rabbit IgG (H+L), F(ab')2 fragment (Alexa Fluor® 488 Conjugate), and viability stain (Fixable Viability Dye eFluor 780) were purchased from Thermo-Fisher Scientific. RPMI8226 cells (2 x 10^6) were treated with or without 10 μM selinexor for 45 min at 37°C. Cells were stained with fixable viability dye eF780 for 15 min at room temperature and subsequently fixed with 4% paraformaldehyde for 10 min. The eBioscience Foxp3 transcription factor staining buffer set (Thermo-Fisher Scientific) was used to permeabilize and stain cells with an IκBα antibody (1:50), followed by F(ab')2 Fragment (1:1000) in permeabilization buffer with 1.5% goat serum for 45 min. Nuclear DNA was labeled with DRAQ5 (1:1000) immediately preceding acquisition on the Imagestream X Mark II Imaging Flow Cytometer. Images were acquired based on circularity (Area vs. Aspect Ratio in the brightfield channel) and exclusion of the eF780 fixable viability dye. Following acquisition, IDEAS software was used to measure the degree of IκBα nuclear translocation. Similarity scores were calculated for at least 1,000 cells. The similarity score is a log-transformed Pearson's correlation coefficient between the pixel values of two image pairs to measure the pixel intensity correlation between the IκBα and DRAQ5 images and gives the degree to which the IκBα signal is localized to the nucleus.

RNA-Sequencing

Total RNA was isolated from RPMI8226 cells treated with GST-PTR1 or GST control for 6 hours in 3 biological replicates following a standard protocol with TRIzol reagent (15596-018, Thermo-Fisher). Full RNA-Seq workflow service (including library

preparation, sequencing, and data QC) was provided by ProteinCT Biotechnologies (Madison, WI).

GSEA analysis using KEGG pathways of RNA-Seq data

Gene set enrichment analysis (GSEA) was performed by calculating a ranked vector as sign(FoldChange)*1/p-value and submitted to the GSEA Ranked. The statistical significance was determined by 1,000 gene set permutations [91]. The latest KEGG pathway [92] database was used for the GSEA analysis. Analyses and plots were performed and generated using R statistical package.

Quantitative RT-PCR (qRT-PCR) analysis

Total RNAs from treated cells were purified by a Nucleospin RNA II column (740955, Clontech) according to the manufacturer's instruction. cDNAs were synthesized from the total RNAs using iScript cDNA synthesis kit (1708891, Bio-Rad). qRT-PCR was performed and analyzed using a Bio-Rad CFX Connect real-time system. Relative expression was determined by ΔΔCt calculation. The mRNA levels of the samples were normalized to GAPDH mRNA levels and shown as fold induction relative to GST-treated control samples. The primers for qRT-PCR analysis were: IL-8 (forward, 5'-tgcagctctgtgtgaagg-3'; reverse, 5'-ctcagccctcttcaaaaac-3'), IL-10 (forward, 5'-aggatcagctggacaacttg-3'; reverse, 5'-gatgtctgggtcttggttctc-3'), BCL2A1 (forward, 5'-tacaggctggctcaggactat-3'; reverse, 5'-cgcaacattttgtagcactctg-3'), Bcl-2 (forward, 5'-ggtggggtcatgtgtgtgg-3'; reverse, 5'-cggttcaggtactcagtcatcc-3'), and Bcl-XL (forward, 5'-gagctggtggttgactttctc-3'; reverse, 5'-tccatctccgattcagtccct-3').

Cell viability assay

For the MTT assay, 10^4-10^5 cells per well were plated in triplicate in a 96-well clear bottom microassay plate and assayed per manufacturer's instructions. Cells containing formazan (MTT) were dissolved in 50-75 µL DMSO and the formazan concentration was measured by absorbance at 540 nm. For the 10-day cell viability assessment, 5×10^4 cells per well were plated in a 24-well plate and cultured for 10 days. A trypan blue assay was carried out every 2 days to assess the effect of lenalidomide on cells. The number of viable cells were counted using a hemocytometer every 2 days. The assays were run in technical triplicate with GST-PTR1 treatment and the data were normalized to mean of GST control. Then, the means of three independent biological replicates were averaged to determine the mean and SD reported. The following concentrations of drugs were used:

Table 1. Drug concentrations for cell viability assay.

	RPMI8226	MM.1S	H929	L363	U266
Bortezomib	10 nM	10 nM	10 nM	10 nM	10 nM
Ixazomib	100 nM	100 nM	100 nM	100 nM	100 nM
Carfilzomib	100 nM	100 nM	100 nM	100 nM	100 nM
Dexamethasone	100 µM	100 µM	100 µM	100 µM	100 µM
Melphalan	10 µM	10 µM	10 µM	10 µM	10 µM
Doxorubicin	2 µM	0.5 µM	2 µM	2 µM	3 µM
Bendamustine	250 µM	50 µM	250 µM	250 µM	250 µM
Lenalidomide	1 µM	1 µM	1 µM	1 µM	1 µM
Selinexor	100 nM	100 nM	100 nM	100 nM	100 nM

Flow cytometric analysis of rhodamine 123 efflux

Rhodamine 123 (Rh123) was obtained from Abcam (ab275545); propidium iodide (PI) from Thermo-Fisher Scientific (ICN19545825). RPMI8226 cells pretreated with 100 nM GST-PTR1 or GST for 24 hr were stained with rhodamine 123 (10 nM) at 37 °C for 60 min. Samples were analyzed by flow cytometry. The ratio of rhodamine 123 mean fluorescent intensity (MFI) was assessed.

Statistical analysis

The unpaired two-sided Student's t-test was used to compare two independent groups. Two-way ANOVA analysis with multiple comparisons test was used to compare PI curves and IκB degradation curves. A p-value of <0.05 was considered statistically significant. The analysis was performed with GraphPad Prism Software (GraphPad Software Inc.).

Results

HAPLN1-PTR1 induces a host of cell survival genes in RPMI8226 MM cells

We previously demonstrated that the PTR1 domain of HAPLN1 (HAPLN1-PTR1), produced as a recombinant glutathione-S-transferase (GST) fusion (GST-PTR1), induces pro-survival NF-κB signaling in a manner resistant to the PI bortezomib and confers resistance to this clinical drug in several human MM cell lines tested relative to GST negative control [31]. To gain insights into global transcriptional changes induced by HAPLN1-PTR1 in MM cells, we performed RNA-Seq analysis of RPMI8226 cells exposed to 100 nM GST-PTR1 for 6 hr using GST exposed cells as a negative control (GSE202672). We measured bacterial LPS contamination using highly sensitive Limulus Amebocyte Lysate assay and confirmed that it was a few orders of magnitude below that which is detectable by NF-κB EMSA assay in these cells as before [31]. We performed RNA-Seq analysis in three biological replicates, which clustered well for upregulated and downregulated genes (Fig 1A), and found that HAPLN1-PTR1 reproducibly induced $\geq$2-fold changes in mRNA levels of >1400 genes (Fig 1B). As expected, many NF-κB regulated genes defined by Staudt et al. [93] were detected in the GST-PTR1-upregulated gene category when compared to GST control (highlighted red in Fig 1B). Gene Set Enrichment Analysis (GSEA) [91] of GST-PTR1 RNA-Seq data identified multiple positive regulated disease pathways or phenotypes significantly correlated with GST-PTR1 treatment (Fig 1C and S1 Table) [92]. Consistent with the gene signature, GST-PTR1 treatment displayed a significant correlation to the induction of NF-κB signaling by the GSEA analysis (Fig 1D). GSEA also identified TNF signaling, JAK/STAT signaling, and immunity related changes (Fig 1C and S1 Table). Notably, NF-κB regulated genes

included a host of anti-apoptotic genes, such as *BCL2, BCL2L1, BCL2A, BIRC2, BIRC3, CFLAR (c-FLIP) and IER3 (IEX-1L)* (Fig 1E), as well as certain immune cytokines, such as IL-8 and IL-10. We confirmed the induction of some of these genes by qRT-PCR analysis (e.g., *BCL2A1,* 284-fold; *IL-8*, 224-fold; and *IL-10*, 153-fold) (Fig 1F).

HAPLN1-PTR1 induces RPMI8226 MM cell resistance to multiple therapeutic drugs

Induction of a host of anti-apoptotic genes by GST-PTR1 suggested the possibility that HAPLN1-PTR1 might induce resistance of MM cells to not only bortezomib but also to other clinically employed FDA-approved drugs. To evaluate this hypothesis, we investigated whether GST-PTR1 could increase RPMI8226 MM cell survival in the presence of different classes of FDA-approved MM therapeutics. These included other PIs (carfilzomib, ixazomib), a glucocorticoid (dexamethasone), DNA damaging agents (melphalan, doxorubicin, bendamustine), an IMiD (lenalidomide), and a nuclear export inhibitor (selinexor). We first exposed RPMI8226 cells to varying concentrations of these drugs and identified drug doses that would yield ~50-80% toxicity using MTT assays at 24-hours (PIs, doxorubicin), 2 days (bendamustine), or 3 days (dexamethasone, melphalan, selinexor), or longer 10-day growth assay (lenalidomide). IMiD-induced toxicity is known to manifest much more slowly than that induced by other cytotoxic MM drugs [94]. The cells were then treated with 100 nM GST-PTR1 or GST in the presence of these MM drugs. These toxicity assays demonstrated that GST-PTR1 caused significant resistance of RPMI8226 MM cells to all the drugs tested, except for carfilzomib and selinexor (Fig 2). GST-PTR1 alone without the drugs did not affect the growth of the MM cells. These results demonstrate that HAPLN1-PTR1 is capable of inducing RPMI8226

cell resistance to multiple MM drugs.

HAPLN1-PTR1 induces clinical PI resistant NF-κB activation in RPMI8226 MM cells

We previously showed that HAPLN1-PTR1 induces bortezomib-resistant NF-κB signaling, which was correlated with bortezomib resistance in RPMI8226 cells [31]. The finding that GST-PTR1 can cause resistance to ixazomib but not carfilzomib in the above study could be related to the ability of the latter to inhibit NF-κB signaling induced by HAPLN1-PTR1 but not by the former. To test this hypothesis, we treated RPMI8226 cells at different concentrations of ixazomib and carfilzomib, in the presence of GST-PTR1 or GST control. To demonstrate the efficacy of these PIs, the cells were also treated in parallel with TNFα, a canonical NF-κB inducer that involves the 26S proteasome-mediated IκBα degradation to activate NF-κB. The cell samples were then analyzed by EMSA using an Igκ-κB probe with Oct-1 binding serving as a loading control. Similar to the case with bortezomib, NF-κB activation by GST-PTR1 was not inhibited by ixazomib or carfilzomib up to 30 nM (Fig 3A-D). Significant NF-κB inhibition was only evident at 100 nM of these PIs. In contrast, significant inhibition of NF-κB activation by TNFα was evident at 30 nM of ixasomib and 10 nM for carfilzomib. The degree of inhibition was significantly greater for TNFα than that observed for GST-PTR1 at the varying PIs concentrations analyzed (Fig 3A-D). These results suggest that, similar to bortezomib [31], NF-κB activation by HAPLN1-PTR1 is significantly more resistant to both ixazomib and carfilzomib relative to TNFα-induced activation. HAPLN1-PTR1 can reduce the MM cell toxicity of both bortezomib and ixazomib, but not carfilzomib, indicating that the latter drug escapes resistance mediated by HAPLN1-PTR1 despite its inability to inhibit NF-κB

activation.

Selinexor inhibits HAPLN1-PTR1-induced IκBα degradation and NF-κB activation

We previously demonstrated that NF-κB activation by HAPLN1-PTR1 involves PI-resistant degradation of IκBα and PI-sensitive IκBβ degradation [31]. Of these, inhibition of IκBα degradation by selinexor was reported to be critical for its clinical efficacy [95]. We and others also reported that IκBα, but not IκBβ, contains a nuclear export sequence (NES), critical for nuclear export of inactive NF-κB-IκBα complexes to the cytoplasm via the nuclear export receptor XPO1/CRM1 [96,97]. We further reported that the nuclear export inhibitor Leptomycin B (LMB) or a mutation of IκBα-NES can prevent PI resistant IκBα degradation via nuclear sequestration and inhibit atypical bortezomib-resistant NF-κB activity [98]. Because both selinexor and LMB are specific, chemically distinct inhibitors of XPO1, we tested whether the ability of selinexor to overcome HAPLN1-PTR1-mediated drug resistance was related to its ability to prevent HAPLN1-PTR1-induced IκBα degradation and associated NF-κB activation. RPMI8226 cells were exposed to GST-PTR1 in the presence of cycloheximide to block new IκBα synthesis to specifically determine the impact of its degradation induced by the ligand with and without selinexor. We previously demonstrated that IκBα levels are not altered by three-hour treatment with cycloheximide in RPMI8226 cells [31]. GST-PTR1 induced near complete degradation of IκBα within 1 hour, which was inhibited by selinexor (Fig 4A-B). This resulted in partial inhibition of NF-κB activation induced by GST-PTR1 (Fig 4C); the remaining activation is likely arising from degradation of IκBβ, which is insensitive to selinexor (Fig 4A-B) but sensitive to bortezomib [31]. Indeed, this possibility was confirmed by addition of both

selinexor and bortezomib that caused near complete NF-κB inhibition induced by GST-PTR1 (Fig 4D). As expected, selinexor caused nuclear accumulation of IκBα, like LMB treatment (Fig 4E). These results support the hypothesis that selinexor can block HAPLN1-PTR1-induced IκBα degradation via its nuclear sequestration causing inhibition of IκBα-associated NF-κB activation to overcome the survival effects induced by HAPLN1-PTR1 in MM cells. Moreover, these results provide additional molecular details potentially underlying the marked clinical synergy with the combination of selinexor and PIs [99].

HAPLN1-PTR1 also induces expression of *multi-drug resistance (MDR)* genes and function in RPMI8226 cells

While the above studies focused on the potential role of NF-kB-regulated antiapoptotic genes induced by HAPLN1-PTR1, our RNA-seq analysis also identified various *MDR* family genes were also upregulated after GST-PTR1 treatment (Fig 5A). Moreover, using the drug efflux pump substrate, rhodamine 123, showed that GST-PTR1 also significantly upregulated MDR efflux function (Fig 5B-C). These results suggest a dual mode of HAPLN1-induced drug resistance mechanism by inducing the expression of both anti-apoptotic genes and drug efflux pump *MDR* genes.

HAPLN1-PTR1 induces variable levels of drug resistance in several myeloma cell lines

To determine whether the drug resistance phenotype induced by HAPLN1-PTR1 in RPMI8226 cells is not limited to this MM cell line alone, we exposed several other MM

cell lines to different clinical drugs in the presence of GST-PTR1 or GST as control. As in the RPMI8226 cell study, these studies were performed in biological triplicates, each performed in three technical replicates. The results are summarized in Fig 6, which demonstrated that GST-PTR1 was able to induce variable but significant resistance to multiple classes of MM therapeutic drugs in different MM cell lines. Again, as in the case for RPMI8226 cells, GST-PTR1 failed to induce resistance to carfilzomib in all cell lines tested and to selinexor in most lines. Overall, our results identify HAPLN1-PTR1 as a novel extracellular matrix factor capable of inducing resistance in MM cells to multiple classes of MM therapeutics with notable exceptions.

Discussion

In the present study, we tested whether HAPLN1 acts as a drug resistance factor in MM cells against different classes of therapeutic drugs. We previously showed that HAPLN1 can initiate bortezomib-resistant NF-κB activity in MM cells and bortezomib-resistant cell survival [31]. We now performed an RNA-seq analysis of RPMI8226 MM cell line exposed to HAPLN1-PTR1 and found that this ligand induces significant changes in the transcriptomic landscape in these MM cells. These changes included induction of a group of anti-apoptotic genes that are known targets of NF-κB, among many other genes. Because these changes in expression of anti-apoptotic genes may increase the death threshold of MM cells, we tested whether HAPLN1-PTR1 could also increase resistance of MM cells to other clinically employed MM therapeutics. Indeed, this ligand was able to variably increase MM cell resistance to many of the currently employed drugs, including PIs, glucocorticoids, DNA damaging agents, and IMiDs, in several MM cell lines tested. HAPLN1 also induced the expression of a host of *MDR* genes and drug efflux functions of MM cells. These results therefore support HAPLN1 as a novel ECM-derived inducer of multi-drug resistance in MM cells.

Interestingly, HAPLN1 was found to mediate resistance to apoptosis induced by bortezomib and ixazomib, but not by carfilzomib. We found that HAPLN1-PTR1-induced NF-κB activity was highly resistant to all the PIs tested, including carfilzomib, thus further demonstrating the induction of NF-κB activation by HAPLN1 proceeds via an atypical PI-resistant mechanism. Nevertheless, HAPLN1-PTR1 was unable to induce resistance to the apoptosis caused by carfilzomib in any of the MM cell lines tested even though it did so against bortezomib and ixazomib in almost all cell lines tested. The difference in

HAPLN1-mediated survival could potentially be attributed to differences in pharmacological properties of the PIs. Bortezomib and ixazomib are chemically related (peptide boronates) and are both reversible inhibitors of the proteasome [100]. In contrast, carfilzomib has a different chemical structure based on four amino acids and irreversibly binds to the proteasome via an epoxyketone pharmacophore [101]. Furthermore, a regimen of carfilzomib and dexamethasone was shown to be clinically superior to bortezomib and dexamethasone in patients with relapsed MM in a large phase III randomized trial [102]. Indeed, NF-κB activation induced by HAPLN1-PTR1 was also resistant to oprozomib, another irreversible epoxyketone structured PI [100], but it was still unable to cause resistance to this PI similar to carfilzomib (S1 Fig). Other than sharing the similar chemical structure, carfilzomib and oprozomib differ in their selectivity against target proteasome β subunits, i.e., carfilzomib inhibits β5/2/1, oprozomib inhibits only β5 [100]. This finding suggests that HAPLN1 can induce drug resistance only against reversible PIs, but irreversible PIs can overcome HAPLN1-induced survival effects. It is therefore likely that prolonged proteasome inhibition, possibly only with irreversible PIs, can overcome HAPLN1 effects.

The differences in sensitivities to HAPLN1-induced drug resistance may also be due to differences in the resistance mechanisms of different PIs. Unlike bortezomib, whose various resistance mechanisms including NF-κB signaling have been described in the literature [103-109], the mechanisms of resistance to other PIs are not well defined. It is possible that other signaling pathways induced by HAPLN1, such as the JAK/STAT pathway identified by the KEGG analysis of our RNA-seq data, might be playing a role in mediating differential effects against different PIs. In patients, carfilzomib shows clinical

efficacy against MM resistant to bortezomib, thus demonstrating that this second generation PI is capable of overcoming the mechanism(s) of bortezomib resistance [110]. Besse et al, demonstrated that PI's difference in the β subunit selectivity exerts the differential cytotoxic effect, namely, co-inhibition of β5/β2 subunits has the most cytotoxicity which can be achieved by high dose carfilzomib, while bortezomib can only abrogate β5/β1 [111]. Moreover, bortezomib and carfilzomib resistant MM cell lines manifest different *PSMB5* mutation status and MDR gene expression. Unlike bortezomib resistant cell lines, carfilzomib resistant MM cells have wild-type *PSMB5*, but overexpress the drug efflux pump ABCB1/MDR1 [111,112]. Interestingly, we also observed induction of a host of MDR gene family members in response to HAPLN1 stimulation of MM cells but ABCB1/MDR1 was not among those induced. Thus, further studies are required to define the mechanism by which the irreversible PI carfilzomib overcomes HAPLN1-induced survival effects in MM cells.

Similar to carfilzomib, selinexor also overcame HAPLN1-induced survival effects in most MM cell lines analyzed. Selinexor is an oral first-in-class selective inhibitor of XPO1-mediated nuclear export (SINE) compound [95]. This inhibitor was able to abolish HAPLN1-PTR1 induced IκBα degradation by forcing nuclear retention and accumulation of IκBα. This result is consistent with our previous findings that PI-resistant IκBα degradation requires the presence of IκBα in the cytoplasm and thus its nuclear accumulation induced by XPO1/CRM1 inhibitors prevents its degradation [113]. Consequently, selinexor suppressed HAPLN1-induced NF-κB activation. Prior studies have found that cytotoxic effects of selinexor against MM cells (and other cancer types) depend, at least part, on IκBα [114]. Thus, through the inhibition of IκBα nuclear export,

selinexor appears to overcome the HAPLN1-induced NF-κB signaling and effects on survival. Selinexor has been previously shown to inhibit NF-κB transcriptional activity in different cancer and inflammatory models [115-117]. However, selinexor also affects multiple additional key molecular targets, such as p53, p21, p27, STAT1, and STAT3 [118-121], which may also contribute to overcoming the survival effects conferred by HAPLN1.

GSEA analysis of RNA-Seq data also showed that HAPLN1 is not only linked to pathways related to drug resistance but it may have a wider role in orchestrating the intra-tumoral inflammatory milieu and balancing anti-tumor immunity. These results pointed to increased expression of pathways correlated to T cell-mediated immunity and anti-viral responses. This correlation is intriguing in view of recent findings showing that the regulated proteolysis of the tolerogenic versican (VCAN) generates a matrikine, versikine, with opposing, immunostimulatory activities [122,123]. VCAN proteolysis correlates with T-cell infiltration in both hematopoietic and solid tumors and versikine triggers a type-I interferon response in myeloid cells, an essential component of the “T-cell inflamed” TME [124,125]. Notably, HAPLN1 is a critical component of VCAN-ECM and like HAPLN1, VCAN/versikine contains two related PTR-domains. Taken together, these findings point to coordinated roles of PTR-containing proteins in regulating drug resistance and tumor immunity. It seems plausible that distinct components of the MM TME contribute diverse PTR-containing matrikines. It would be of great interest to determine whether the levels of such matrikines vary through MM disease progression and whether their levels could be predictive of therapy resistance and possibly immune microenvironment. Individualized therapeutic approaches using the HAPLN1 level in patient plasma as a prognostic marker need to be further tested in well-designed clinical settings. Such an

approach would require the development of an assay to quantify HAPLN1 matrikine levels in patient samples.

Conclusions

The data presented here demonstrate that a HAPLN1 matrikine can induce resistance in MM cells to different classes of therapeutic agents. This matrikine induces many changes in cell signaling and gene expression in MM cells, including an activation of NF-κB signaling and induction of many cell survival genes, multi-drug resistance genes, and immune-related genes. Our study thus reveals an unappreicated mechanism of drug resistance in MM cells, suggesting that the HAPLN1 matrikine may be a novel biomarker and/or therapeutic target for this currently incurable disease.

Acknowledgements

We thank the members of the Miyamoto lab for their helpful comments on the project and the manuscript, Sean McIlwain for sharing his scripts used in biostatistic analysis.

References

1. Shain K. Metastatic myeloma? *Blood*. 2012;119(24):5612-5613.

2. Hideshima T, Mitsiades C, Tonon G, Richardson PG, Anderson KC. Understanding multiple myeloma pathogenesis in the bone marrow to identify new therapeutic targets. *Nature reviews Cancer*. 2007;7(8):585-598.

3. Manier S, Sacco A, Leleu X, Ghobrial IM, Roccaro AM. Bone marrow microenvironment in multiple myeloma progression. *Journal of biomedicine & biotechnology*. 2012;2012(6):157496-157495.

4. Alsayed Y, Ngo H, Runnels J, et al. Mechanisms of regulation of CXCR4/SDF-1 (CXCL12)-dependent migration and homing in multiple myeloma. *Blood*. 2007;109(7):2708-2717.

5. Roccaro AM, Sacco A, Purschke WG, et al. SDF-1 inhibition targets the bone marrow niche for cancer therapy. *Cell reports*. 2014;9(1):118-128.

6. Maquart F-X, Pasco S, Ramont L, Hornebeck W, Monboisse J-C. An introduction to matrikines: extracellular matrix-derived peptides which regulate cell activity. Implication in tumor invasion. *Critical reviews in oncology/hematology*. 2004;49(3):199-202.

7. Weathington NM, van Houwelingen AH, Noerager BD, et al. A novel peptide CXCR ligand derived from extracellular matrix degradation during airway inflammation. *Nature medicine*. 2006;12(3):317-323.

8. Hunninghake GW, Davidson JM, Rennard S, Szapiel S, Gadek JE, Crystal RG. Elastin fragments attract macrophage precursors to diseased sites in pulmonary emphysema. *Science*. 1981;212(4497):925-927.

9. Pocza P, Süli-Vargha H, Darvas Z, Falus A. Locally generated VGVAPG and VAPG elastin-derived peptides amplify melanoma invasion via the galectin-3 receptor. *International journal of cancer*. 2008;122(9):1972-1980.

10. Grahovac J, Wells A. Matrikine and matricellular regulators of EGF receptor signaling on cancer cell migration and invasion. *Laboratory investigation; a journal of technical methods and pathology*. 2014;94(1):31-40.

11. Huynh M, Pak C, Markovina S, et al. Hyaluronan and proteoglycan link protein 1 (HAPLN1) activates bortezomib-resistant NF-κB activity and increases drug resistance in multiple myeloma. *Journal of Biological Chemistry*. 2018;293(7):2452-2465.

12. Mark C, Warrick J, Callander NS, Hematti P, Miyamoto S. A Hyaluronan and Proteoglycan Link Protein 1 Matrikine: Role of Matrix Metalloproteinase 2 in Multiple Myeloma NF-κB Activation and Drug Resistance. *Mol Cancer Res*. 2022;20(9):1456-1466.

13. Huynh M, Chang HY, Lisiero DN, et al. HAPLN1 confers multiple myeloma cell resistance to several classes of therapeutic drugs. *PLoS One*. 2022;17(12):e0274704.

14. Spicer AP, Joo A, Bowling RA. A hyaluronan binding link protein gene family whose members are physically linked adjacent to chondroitin sulfate proteoglycan core protein genes: the missing links. *Journal of Biological Chemistry*. 2003;278(23):21083-21091.

15. De Bakshi D, Chen Y-C, Wuerzberger-Davis SM, et al. Ectopic CH60 mediates HAPLN1-induced cell survival signaling in multiple myeloma. *Life Science Alliance*. 2023;6(3):e202201636.

16. Diamond MS, Springer TA. The dynamic regulation of integrin adhesiveness. *Current biology : CB*. 1994;4(6):506-517.

17. Wilkinson PC. Assays of leukocyte locomotion and chemotaxis. *Journal of immunological methods*. 1998;216(1-2):139-153.

18. Wilkinson PC. How do leucocytes perceive chemical gradients? *FEMS microbiology immunology*. 1990;2(5-6):303-311.

19. Tchou-Wong K-M, Fok SYY, Rubin JS, et al. Rapid chemokinetic movement and the invasive potential of lung cancer cells; a functional molecular study. *BMC cancer*. 2006;6(1):151-112.

20. Liu Z, Klominek J. Chemotaxis and chemokinesis of malignant mesothelioma cells to multiple growth factors. *Anticancer Res*. 2004;24(3a):1625-1630.

21. de Gorter DJJ, Reijmers RM, Beuling EA, et al. The small GTPase Ral mediates SDF-1-induced migration of B cells and multiple myeloma cells. *Blood*. 2008;111(7):3364-3372.

22. Zigmond SH, Hirsch JG. Leukocyte locomotion and chemotaxis. New methods for evaluation, and demonstration of a cell-derived chemotactic factor. *The Journal of experimental medicine*. 1973;137(2):387-410.

23. Zengel P, Nguyen-Hoang A, Schildhammer C, Zantl R, Kahl V, Horn E. μ-Slide Chemotaxis: a new chamber for long-term chemotaxis studies. *BMC cell biology*. 2011;12(1):21-14.

24. Tomasova L, Guttenberg Z, Hoffmann B, Merkel R. Advanced 2D/3D cell migration assay for faster evaluation of chemotaxis of slow-moving cells. *PloS one*. 2019;14(7):e0219708.

25. Nguyen Q, Murphy G, Hughes CE, Mort JS, Roughley PJ. Matrix metalloproteinases cleave at two distinct sites on human cartilage link protein. *Biochemical Journal*. 1993;295 (Pt 2)(Pt 2):595-598.

26. Chen Z, Orlowski RZ, Wang M, Kwak L, McCarty N. Osteoblastic niche supports the growth of quiescent multiple myeloma cells. *Blood*. 2014;123(14):2204-2208.

27. Runnels JM, Carlson AL, Pitsillides C, et al. Optical techniques for tracking multiple myeloma engraftment, growth, and response to therapy. *Journal of biomedical optics*. 2011;16(1):011006.

28. Fangazio M, Ladewig E, Gomez K, et al. Genetic mechanisms of HLA-I loss and immune escape in diffuse large B cell lymphoma. *Proceedings of the National Academy of Sciences of the United States of America*. 2021;118(22).

29. Roopra A. MAGIC: A tool for predicting transcription factors and cofactors driving gene sets using ENCODE data. *PLoS Comput Biol*. 2020;16(4):e1007800.

30. Horvath CM, Wen Z, Darnell JE. A STAT protein domain that determines DNA sequence recognition suggests a novel DNA-binding domain. *Genes Dev*. 1995;9(8):984-994.

31. Huynh M, Pak C, Markovina S, et al. Hyaluronan and proteoglycan link protein 1 (HAPLN1) activates bortezomib-resistant NF-κB activity and increases drug resistance in multiple myeloma. *J Biol Chem*. 2018;293(7):2452-2465.

32. Bharti AC, Shishodia S, Reuben JM, et al. Nuclear factor-kappaB and STAT3 are constitutively active in CD138+ cells derived from multiple myeloma patients, and suppression of these transcription factors leads to apoptosis. *Blood*. 2004;103(8):3175-3184.

33. Bollrath J, Greten FR. IKK/NF-kappaB and STAT3 pathways: central signalling hubs in inflammation-mediated tumour promotion and metastasis. *EMBO Rep*. 2009;10(12):1314-1319.

34. Catlett-Falcone R, Landowski TH, Oshiro MM, et al. Constitutive activation of Stat3 signaling confers resistance to apoptosis in human U266 myeloma cells. *Immunity*. 1999;10(1):105-115.

35. Chong PSY, Chng WJ, de Mel S. STAT3: A Promising Therapeutic Target in Multiple Myeloma. *Cancers (Basel)*. 2019;11(5).

36. Malilas W, Koh SS, Kim S, et al. Cancer upregulated gene 2, a novel oncogene, enhances migration and drug resistance of colon cancer cells via STAT1 activation. *International journal of oncology*. 2013;43(4):1111-1116.

37. Kharma B, Baba T, Matsumura N, et al. STAT1 drives tumor progression in serous papillary endometrial cancer. *Cancer Research*. 2014;74(22):6519-6530.

38. Khodarev NN, Beckett M, Labay E, Darga T, Roizman B, Weichselbaum RR. STAT1 is overexpressed in tumors selected for radioresistance and confers protection from radiation in transduced sensitive cells. *Proceedings of the National Academy of Sciences*. 2004;101(6):1714-1719.

39. Kaowinn S, Kaewpiboon C, Koh SS, Krämer OH, Chung Y-H. STAT1-HDAC4 signaling induces epithelial-mesenchymal transition and sphere formation of cancer cells overexpressing the oncogene, CUG2. *Oncology reports*. 2018;40(5):2619-2627.

40. Khodarev NN, Roach P, Pitroda SP, et al. STAT1 pathway mediates amplification of metastatic potential and resistance to therapy. *PloS one*. 2009;4(6):e5821.

41. Vila-Coro AJ, Rodríguez-Frade JM, Martín De Ana A, Moreno-Ortíz MC, Martínez-A C, Mellado M. The chemokine SDF-1alpha triggers CXCR4 receptor dimerization and activates the JAK/STAT pathway. *FASEB journal : official publication of the Federation of American Societies for Experimental Biology*. 1999;13(13):1699-1710.

42. Sanz-Rodríguez F, Hidalgo A, Teixidó J. Chemokine stromal cell-derived factor-1alpha modulates VLA-4 integrin-mediated multiple myeloma cell adhesion to CS-1/fibronectin and VCAM-1. *Blood*. 2001;97(2):346-351.

43. Azab AK, Azab F, Blotta S, et al. RhoA and Rac1 GTPases play major and differential roles in stromal cell-derived factor-1-induced cell adhesion and chemotaxis in multiple myeloma. *Blood*. 2009;114(3):619-629.

44. Palumbo A, Avet-Loiseau H, Oliva S, et al. Revised International Staging System for Multiple Myeloma: A Report From International Myeloma Working Group. *J Clin Oncol*. 2015;33(26):2863-2869.

45. Wallington-Beddoe CT, Mynott RL. Prognostic and predictive biomarker developments in multiple myeloma. *J Hematol Oncol*. 2021;14(1):151.

46. Jung O, Trapp-Stamborski V, Purushothaman A, et al. Heparanase-induced shedding of syndecan-1/CD138 in myeloma and endothelial cells activates VEGFR2 and an invasive phenotype: prevention by novel synstatins. *Oncogenesis*. 2016;5(2):e202-e202.

47. Markovina S, Callander NS, O'Connor SL, et al. Bortezomib-resistant nuclear factor-kappaB activity in multiple myeloma cells. *Molecular cancer research : MCR*. 2008;6(8):1356-1364.

48. O'Connor S, Shumway SD, Amanna IJ, Hayes CE, Miyamoto S. Regulation of constitutive p50/c-Rel activity via proteasome inhibitor-resistant IkappaBalpha degradation in B cells. *Mol Cell Biol*. 2004;24(11):4895-4908.

49. Lwin ST, Edwards CM, Silbermann R. Preclinical animal models of multiple myeloma. *BoneKEy reports*. 2016;5:772.

50. Campeau E, Ruhl VE, Rodier F, et al. A versatile viral system for expression and depletion of proteins in mammalian cells. *PloS one*. 2009;4(8):e6529.

51. Roopra A. MAGIC: A tool for predicting transcription factors and cofactors driving gene sets using ENCODE data. *PLoS computational biology*. 2020;16(4):e1007800.

52. Love MI, Huber W, Anders S. Moderated estimation of fold change and dispersion for RNA-seq data with DESeq2. *Genome Biol*. 2014;15(12):550.

53. Traag VA, Waltman L, van Eck NJ. From Louvain to Leiden: guaranteeing well-connected communities. *Sci Rep*. 2019;9(1):5233.

54. Blondel VD, Guillaume J-L, Lambiotte R, Lefebvre E. Fast unfolding of communities in large networks. *Journal of Statistical Mechanics: Theory and Experiment*. 2008;2008(10):P10008.

55. Bianchi G, Anderson KC. Understanding biology to tackle the disease: Multiple myeloma from bench to bedside, and back. *CA: a cancer journal for clinicians*. 2014;64(6):422-444.

56. Society AC. Cancer Facts & Figures 2022. Atlanta: American Cancer Society; 2022.

57. Kyle RA, Rajkumar SV. Multiple myeloma. *Blood*. 2008;111(6):2962-2972.

58. De Bergsagel DE, Migliore PJ, Griffith KM. MYELOMA PROTEINS AND THE CLINICAL RESPONSE TO MELPHALAN THERAPY. *Science*. 1965;148(3668):376-377.

59. Hoogstraten B, Sheehe PR, Cuttner J, et al. Melphalan in multiple myeloma. *Blood*. 1967;30(1):74-83.

60. Pasquali S, Maqueo J, Vela J, et al. Combination chemotherapy versus melphalan plus prednisone as treatment for multiple myeloma: an overview of 6,633 patients from 27 randomized trials. *Journal of Clinical Oncology*. 2016;16(12):3832-3842.

61. Barlogie B, Shaughnessy J, Zangari M, Tricot G. High-dose therapy and immunomodulatory drugs in multiple myeloma. *Seminars in oncology*. 2002;29(6 Suppl 17):26-33.

62. Teo SK. Properties of thalidomide and its analogues: implications for anticancer therapy. *AAPS J*. 2005;7(1):E14-19.

63. Mazumder A, Jagannath S. Thalidomide and lenalidomide in multiple myeloma. *Best Pract Res Clin Haematol*. 2006;19(4):769-780.

64. Lacy MQ, McCurdy AR. Pomalidomide. *Blood*. 2013;122(14):2305-2309.

65. Moreau P, Richardson PG, Cavo M, et al. Proteasome inhibitors in multiple myeloma: 10 years later. *Blood*. 2012;120(5):947-959.

66. Lawasut P, Chauhan D, Laubach J, et al. New proteasome inhibitors in myeloma. *Curr Hematol Malig Rep*. 2012;7(4):258-266.

67. Richardson PG, Barlogie B, Berenson J, et al. A phase 2 study of bortezomib in relapsed, refractory myeloma. *N Engl J Med*. 2003;348(26):2609-2617.

68. Mimura N, Hideshima T, Anderson KC. Novel therapeutic strategies for multiple myeloma. *Exp Hematol*. 2015;43(8):732-741.

69. Naymagon L, Abdul-Hay M. Novel agents in the treatment of multiple myeloma: a review about the future. *J Hematol Oncol*. 2016;9(1):52.

70. Varga C, Laubach J, Hideshima T, Chauhan D, Anderson KC, Richardson PG. Novel targeted agents in the treatment of multiple myeloma. *Hematol Oncol Clin North Am*. 2014;28(5):903-925.

71. Laubach J, Garderet L, Mahindra A, et al. Management of relapsed multiple myeloma: recommendations of the International Myeloma Working Group. *Leukemia*. 2016;30(5):1005-1017.

72. Hansen JD, Correa M, Nagy MA, et al. Discovery of CRBN E3 Ligase Modulator CC-92480 for the Treatment of Relapsed and Refractory Multiple Myeloma. *J Med Chem*. 2020;63(13):6648-6676.

73. Kumar SK, Harrison SJ, Cavo M, et al. Venetoclax or placebo in combination with bortezomib and dexamethasone in patients with relapsed or refractory multiple myeloma (BELLINI): a randomised, double-blind, multicentre, phase 3 trial. *Lancet Oncol*. 2020;21(12):1630-1642.

74. Caraccio C, Krishna S, Phillips DJ, Schürch CM. Bispecific Antibodies for Multiple Myeloma: A Review of Targets, Drugs, Clinical Trials, and Future Directions. *Front Immunol*. 2020;11:501.

75. Teoh PJ, Journal WJCBC. CAR T-cell therapy in multiple myeloma: More room for improvement. *naturecom*.

76. Dingli D, Ailawadhi S, Bergsagel PL, et al. Therapy for Relapsed Multiple Myeloma: Guidelines From the Mayo Stratification for Myeloma and Risk-Adapted Therapy. *Mayo Clin Proc*. 2017;92(4):578-598.

77. Chapman MA, Lawrence MS, Keats JJ, et al. Initial genome sequencing and analysis of multiple myeloma. *Nature*. 2011;471(7339):467-472.

78. Lohr JG, Stojanov P, Carter SL, et al. Widespread genetic heterogeneity in multiple myeloma: implications for targeted therapy. *Cancer Cell*. 2014;25(1):91-101.

79. Lohr JG, Kim S, Gould J, et al. Genetic interrogation of circulating multiple myeloma cells at single-cell resolution. *Sci Transl Med*. 2016;8(363):363ra147.

80. Glavey SV, Naba A, Manier S, et al. Proteomic characterization of human multiple myeloma bone marrow extracellular matrix. *Leukemia*. 2017;31(11):2426-2434.

81. Podar K, Chauhan D, Anderson KC. Bone marrow microenvironment and the identification of new targets for myeloma therapy. *Leukemia*. 2009;23(1):10-24.

82. Papadas A, Asimakopoulos F. Mechanisms of Resistance in Multiple Myeloma. *Handb Exp Pharmacol*. 2018;249:251-288.

83. Papadas A, Asimakopoulos F. Mechanisms of Resistance in Multiple Myeloma. *Handbook of experimental pharmacology*. 2018;249:251-288.

84. Glotzer M, Murray AW, Kirschner MW. Cyclin is degraded by the ubiquitin pathway. *Nature*. 1991;349(6305):132-138.

85. Dou QP, Levin AH, Zhao S, Pardee AB. Cyclin E and cyclin A as candidates for the restriction point protein. *Cancer Res*. 1993;53(7):1493-1497.

86. Wong AH, Shin EM, Tergaonkar V, Chng WJ. Targeting NF-κB Signaling for Multiple Myeloma. *Cancers (Basel)*. 2020;12(8).

87. Antonangeli F, Natalini A, Garassino MC, Sica A, Santoni A, Di Rosa F. Regulation of PD-L1 Expression by NF-κB in Cancer. *Front Immunol*. 2020;11:584626.

88. Jelinek T, Paiva B, Hajek R. Update on PD-1/PD-L1 Inhibitors in Multiple Myeloma. *Front Immunol*. 2018;9:2431.

89. Gawri R, Antoniou J, Ouellet J, et al. Best paper NASS 2013: link-N can stimulate proteoglycan synthesis in the degenerated human intervertebral discs. *Eur Cell Mater*. 2013;26:107-119; discussion 119.

90. Miyamoto S, Seufzer BJ, Shumway SD. Novel IkappaB alpha proteolytic pathway in WEHI231 immature B cells. *Mol Cell Biol*. 1998;18(1):19-29.

91. Subramanian A, Tamayo P, Mootha VK, et al. Gene set enrichment analysis: a knowledge-based approach for interpreting genome-wide expression profiles. *Proc Natl Acad Sci U S A*. 2005;102(43):15545-15550.

92. Kanehisa M, Furumichi M, Tanabe M, Sato Y, Morishima K. KEGG: new perspectives on genomes, pathways, diseases and drugs. *Nucleic Acids Res*. 2017;45(D1):D353-D361.

93. Lymphochip - NF-κB signature database.

94. Bartlett JB, Dredge K, Dalgleish AG. The evolution of thalidomide and its IMiD derivatives as anticancer agents. *Nature reviews Cancer*. 2004;4(4):314-322.

95. Kuruvilla J, Savona M, Baz R, et al. Selective inhibition of nuclear export with selinexor in patients with non-Hodgkin lymphoma. *Blood*. 2017;129(24):3175-3183.

96. Huang TT, Miyamoto S. Postrepression activation of NF-kappaB requires the amino-terminal nuclear export signal specific to IkappaBalpha. *Molecular and cellular biology*. 2001;21(14):4737-4747.

97. Huang TT, Kudo N, Yoshida M, Miyamoto S. A nuclear export signal in the N-terminal regulatory domain of IkappaBalpha controls cytoplasmic localization of inactive

NF-kappaB/IkappaBalpha complexes. *Proceedings of the National Academy of Sciences*. 2000;97(3):1014-1019.

98. O'Connor S, Shumway S, Miyamoto S. Inhibition of IkappaBalpha nuclear export as an approach to abrogate nuclear factor-kappaB-dependent cancer cell survival. *Mol Cancer Res*. 2005;3(1):42-49.

99. Grosicki S, Simonova M, Spicka I, et al. Once-per-week selinexor, bortezomib, and dexamethasone versus twice-per-week bortezomib and dexamethasone in patients with multiple myeloma (BOSTON): a randomised, open-label, phase 3 trial. *Lancet*. 2020;396(10262):1563-1573.

100. Hungria VTdM, Crusoé EdQ, Bittencourt RI, et al. New proteasome inhibitors in the treatment of multiple myeloma. *Hematology, transfusion and cell therapy*. 2019;41(1):76-83.

101. in SPEJF. Carfilzomib: A Promising Proteasome Inhibitor for the Treatment of Relapsed and Refractory Multiple Myeloma. *frontiersinorg*.

102. Dimopoulos MA, Goldschmidt H, Niesvizky R, et al. Carfilzomib or bortezomib in relapsed or refractory multiple myeloma (ENDEAVOR): an interim overall survival analysis of an open-label, randomised, phase 3 trial. *Lancet Oncol*. 2017;18(10):1327-1337.

103. Nikesitch N, Tao C, Lai K, et al. Predicting the response of multiple myeloma to the proteasome inhibitor Bortezomib by evaluation of the unfolded protein response. *Blood Cancer J*. 2016;6:e432.

104. Murray MY, Auger MJ, Bowles KM. Overcoming bortezomib resistance in multiple myeloma. *Biochem Soc Trans*. 2014;42(4):804-808.

105. Dong H, Chen L, Chen X, et al. Dysregulation of unfolded protein response partially underlies proapoptotic activity of bortezomib in multiple myeloma cells. *Leuk Lymphoma*. 2009;50(6):974-984.

106. Oerlemans R, Franke NE, Assaraf YG, et al. Molecular basis of bortezomib resistance: proteasome subunit beta5 (PSMB5) gene mutation and overexpression of PSMB5 protein. *Blood*. 2008;112(6):2489-2499.

107. Lü S, Wang J. The resistance mechanisms of proteasome inhibitor bortezomib. *Biomark Res*. 2013;1(1):13.

108. Xie H, Gu Y, Wang W, et al. Silencing of SENP2 in Multiple Myeloma Induces Bortezomib Resistance by Activating NF-κB Through the Modulation of IκBα Sumoylation. *Scientific reports*. 2020;10(1):766-710.

109. Barrio S, Stühmer T, Da-Viá M, et al. Spectrum and functional validation of PSMB5 mutations in multiple myeloma. *Leukemia*. 2019;33(2):447-456.

110. Siegel DS, Martin T, Wang M, et al. A phase 2 study of single-agent carfilzomib (PX-171-003-A1) in patients with relapsed and refractory multiple myeloma. *Blood*. 2012;120(14):2817-2825.

111. Besse A, Besse L, Kraus M, et al. Proteasome Inhibition in Multiple Myeloma: Head-to-Head Comparison of Currently Available Proteasome Inhibitors. *Cell chemical biology*. 2019;26(3):340-351.e343.

112. Besse A, Stolze SC, Rasche L, Weinhold N, Leukemia GJM. Carfilzomib resistance due to ABCB1/MDR1 overexpression is overcome by nelfinavir and lopinavir in multiple myeloma. *naturecom*.

113. Nair JS, Musi E, Schwartz GK. Selinexor (KPT-330) Induces Tumor Suppression through Nuclear Sequestration of IκB and Downregulation of Survivin. *Clin Cancer Res*. 2017;23(15):4301-4311.

114. Kashyap T, Argueta C, Aboukameel A, et al. Selinexor, a Selective Inhibitor of Nuclear Export (SINE) compound, acts through NF-κB deactivation and combines with proteasome inhibitors to synergistically induce tumor cell death. *Oncotarget*. 2016;7(48):78883-78895.

115. Crochiere M, Senapedis W, Kashyap T, et al. The Selective Inhibitor of Nuclear Export Compound, Selinexor, Inhibits NF-κB and Induces Anti-Non-Small Cell Lung Cancer Activity Regardless of p53 Status. *International Journal of Cancer Research and Molecular Mechanisms*. 2016.

116. Wu M, Gui H, Feng Z, et al. KPT-330, a potent and selective CRM1 inhibitor, exhibits anti-inflammation effects and protection against sepsis. *Biochem Biophys Res Commun*. 2018;503(3):1773-1779.

117. Kashyap T, Murray J, Walker CJ, et al. Selinexor, a novel selective inhibitor of nuclear export, reduces SARS-CoV-2 infection and protects the respiratory system in vivo. *Antiviral Res*. 2021;192:105115.

118. Subhash VV, Yeo MS, Wang L, et al. Anti-tumor efficacy of Selinexor (KPT-330) in gastric cancer is dependent on nuclear accumulation of p53 tumor suppressor. *Scientific reports*. 2018;8(1):12248.

119. Currier AW, Kolb EA, Gorlick RG, Roth ME, Gopalakrishnan V, Sampson VB. p27/Kip1 functions as a tumor suppressor and oncoprotein in osteosarcoma. *Scientific reports*. 2019;9(1):6161.

120. Nie D, Huang K, Yin S, et al. KPT-330 inhibition of chromosome region maintenance 1 is cytotoxic and sensitizes chronic myeloid leukemia to Imatinib. *Cell death discovery*. 2018;4:48.

121. Machlus KR, Wu SK, Vijey P, et al. Selinexor-induced thrombocytopenia results from inhibition of thrombopoietin signaling in early megakaryopoiesis. *Blood*. 2017;130(9):1132-1143.

122. Hope C, Foulcer S, Jagodinsky J, et al. Immunoregulatory roles of versican proteolysis in the myeloma microenvironment. *Blood*. 2016;128(5):680-685.

123. Asimakopoulos F, Hope C, Johnson MG, Pagenkopf A, Gromek K, Nagel B. Extracellular matrix and the myeloid-in-myeloma compartment: balancing tolerogenic and immunogenic inflammation in the myeloma niche. *Journal of leukocyte biology*. 2017;102(2):265-275.

124. Gajewski TF. The Next Hurdle in Cancer Immunotherapy: Overcoming the Non-T-Cell-Inflamed Tumor Microenvironment. *Semin Oncol*. 2015;42(4):663-671.

125. Zitvogel L, Galluzzi L, Kepp O, Smyth MJ, Kroemer G. Type I interferons in anticancer immunity. *Nat Rev Immunol*. 2015;15(7):405-414.

Figure 1

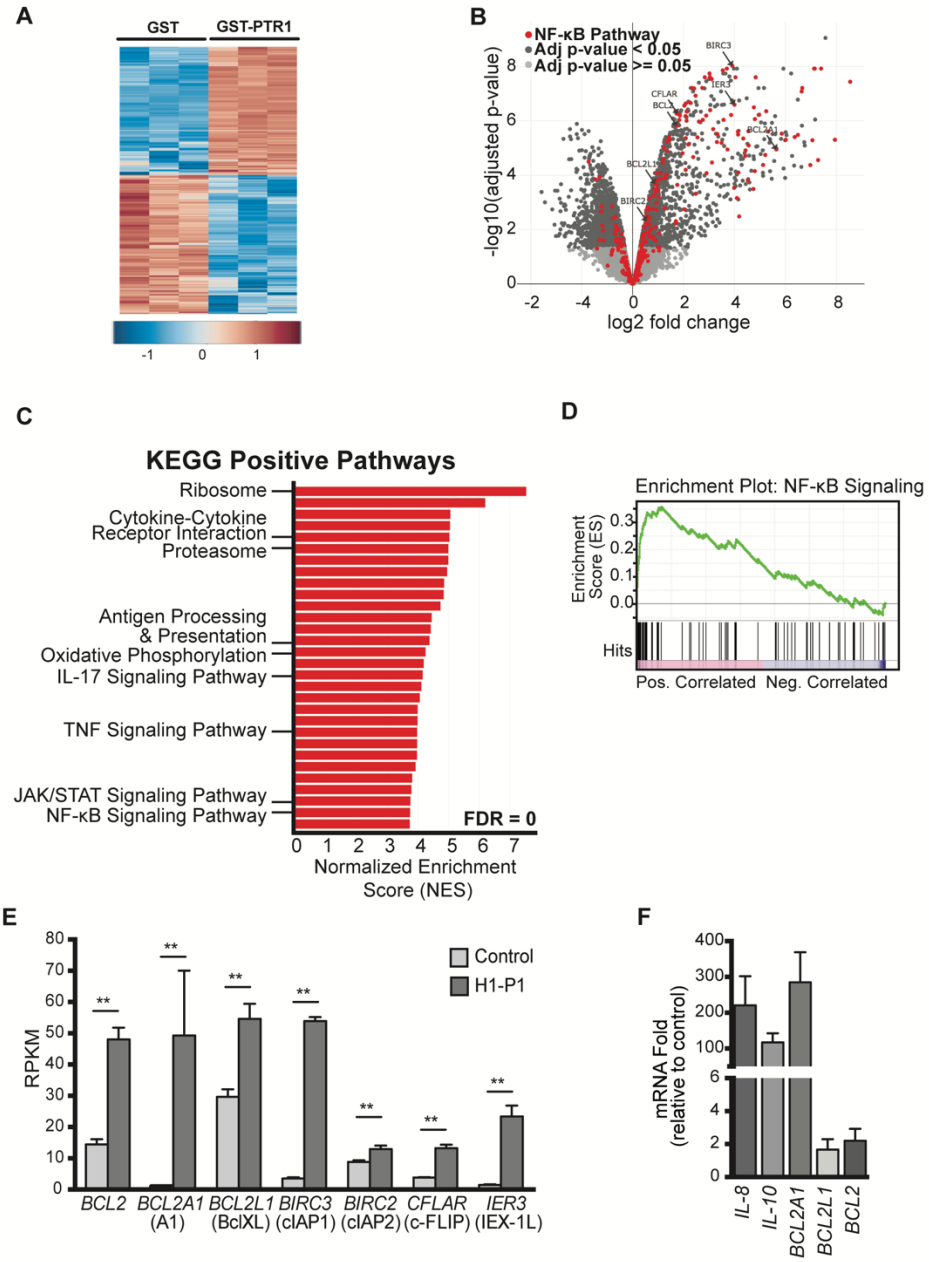
A
GST
GST-PTR1
-1
0
1
B
NF-κB Pathway
Adj p-value < 0.05
Adj p-value >= 0.05
-log10(adjusted p-value)
log2 fold change
BIRC3
IER3
CFLAR
BCL2
BCL2A1
BCL2L1
BIRC2
C
KEGG Positive Pathways
Ribosome
Cytokine-Cytokine Receptor Interaction
Proteasome
Antigen Processing & Presentation
Oxidative Phosphorylation
IL-17 Signaling Pathway
TNF Signaling Pathway
JAK/STAT Signaling Pathway
NF-κB Signaling Pathway
FDR = 0
Normalized Enrichment Score (NES)
D
Enrichment Plot: NF-κB Signaling
Enrichment Score (ES)
Hits
Pos. Correlated
Neg. Correlated
E
Control
H1-P1
RPKM
BCL2
BCL2A1 (A1)
BCL2L1 (BclXL)
BIRC3 (cIAP1)
BIRC2 (cIAP2)
CFLAR (c-FLIP)
IER3 (IEX-1L)
F
mRNA Fold (relative to control)
IL-8
IL-10
BCL2A1
BCL2L1
BCL2

Fig 1. HAPLN1-PTR1 induces transcriptional changes, including an NF-κB transcriptional program. (A) Heatmap summarized all the differentially expressed genes of two-fold. Each row is a gene, each column is a sample. (B) Volcano plot of RNA-Seq data illustrating significantly (dark gray) and non-significantly (light gray) changed genes in RPMI8226 cells treated with 100 nM GST-PTR1 for 6 hr, relative to control (100 nM GST). Genes depicted in red indicate known NF-κB regulated genes. The RNA-seq analysis was done in three biological replicates. (C) Gene set enrichment analysis (GSEA) for indicated KEGG pathways and the genes differentially regulated by HAPLN1-PTR1 versus control (GST). Shown are bars indicating normalized enrichment scores (NES) for top 30 positive pathways, all with an FDR = 0. The identities of some of the pathways are indicated. For more details, see S1 Table. (D) GSEA normalized enrichment score (NES) plots of the signature of the NF-κB pathway. (E) Reads per kilobase million (RPKM) values of select NF-κB target survival genes from the RNA-Seq results in A. (F) qRT-PCR analysis of select genes detected by RNA-Seq analysis in A. RNA levels of indicated genes in GST-PTR1-treated condition were normalized to GAPDH and fold change relative to control (100 nM GST) for each gene is plotted. Results represent the mean ± SD of three biological replicates. ** $p<0.01$

Figure 2

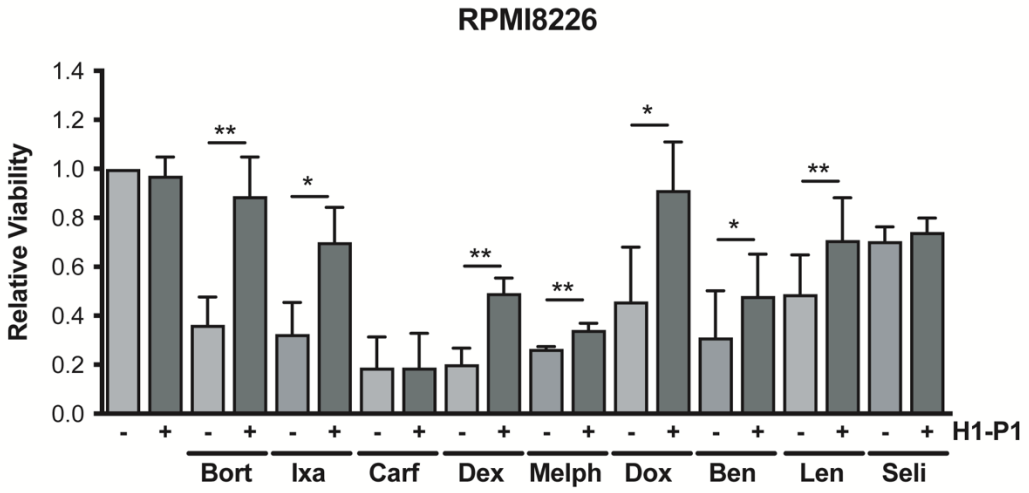
RPMI8226
Relative Viability
1.4
1.2
1.0
0.8
0.6
0.4
0.2
0.0
**
*
**
**
*
*
**
- + - + - + - + - + - + - + - + - + - +
H1-P1
Bort
Ixa
Carf
Dex
Melph
Dox
Ben
Len
Seli

Fig 2. HAPLN1-PTR1 causes RPMI8226 MM cell resistance to different classes of therapeutic agents. RPMI8226 cells were cultured with 100 nM GST-PTR1 (H1-P1) or GST (-) in the presence or absence of indicated drugs at 50-80% cytotoxicity and the cell viability was measured as described in Materials and Methods. Results represent the mean ± SD of three biological replicates, each performed in triplicate. * $p<0.05$, ** $p<0.01$.

Figure 3

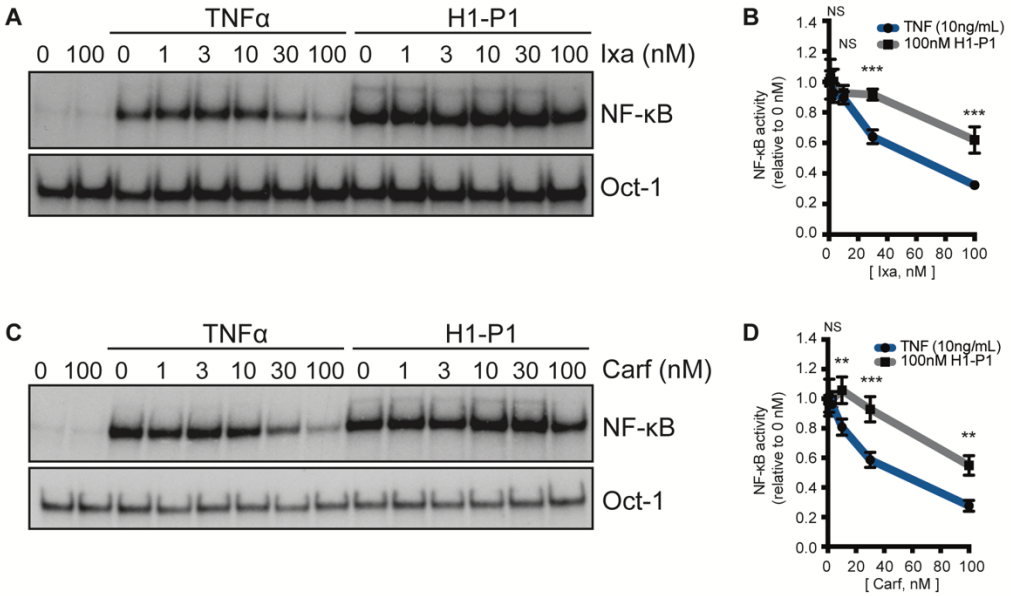
A
TNFα
H1-P1
0 100 0 1 3 10 30 100 0 1 3 10 30 100 Ixa (nM)
NF-κB
Oct-1
B
NS
NS
***
***
TNF (10ng/mL)
100nM H1-P1
NF-κB activity (relative to 0 nM)
0.0 0.2 0.4 0.6 0.8 1.0 1.2 1.4
0 20 40 60 80 100
[Ixa, nM]
C
TNFα
H1-P1
0 100 0 1 3 10 30 100 0 1 3 10 30 100 Carf (nM)
NF-κB
Oct-1
D
NS
**
***
**
TNF (10ng/mL)
100nM H1-P1
NF-κB activity (relative to 0 nM)
0.0 0.2 0.4 0.6 0.8 1.0 1.2 1.4
0 20 40 60 80 100
[Carf, nM]

Fig 3. HAPLN1-PTR1-induced NF-κB activation is resistant to clinical PI's. (A) Representative EMSA analysis of RPMI8226 cells incubated with 10 ng/mL TNFα or 100 nM GST-PTR1 (H1-P1) in the absence or presence of increasing concentrations (nM) of ixazomib (Ixa). (B) Graph depicts the mean ± SD of the quantification of three independent replicates of EMSA analysis as in A. (C) Representative EMSA analysis as in A with increasing concentrations (nM) of carfilzomib (Carf). (D) Graph depicts the mean ± SD of the quantification of three independent replicates of EMSA analysis as in C. ** $p<0.01$, *** $p<0.001$.

Figure 4

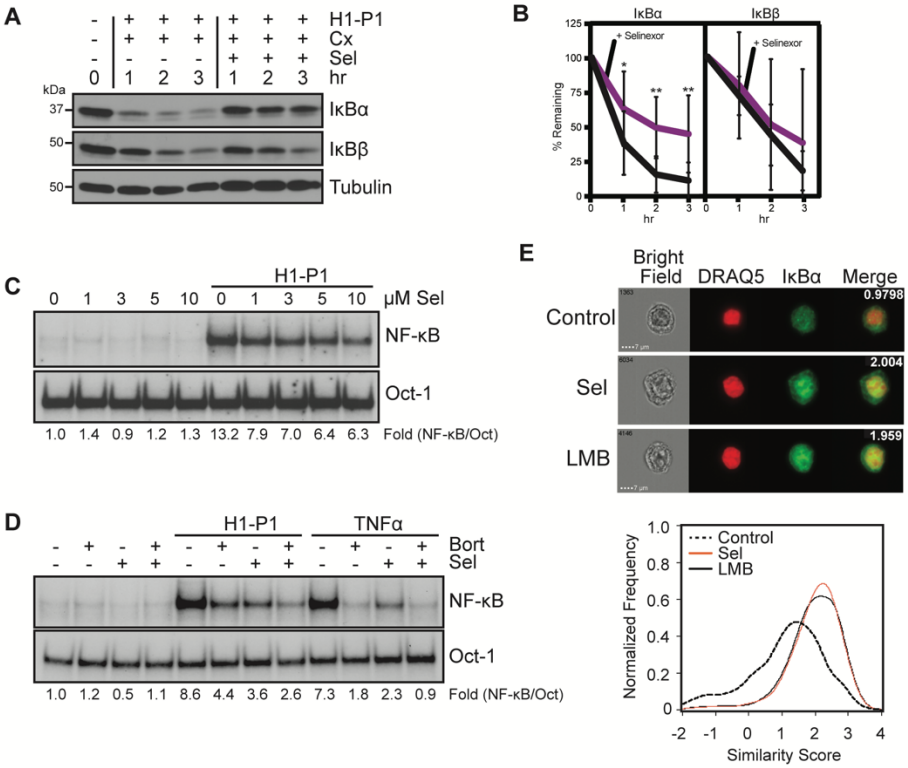
A
H1-P1
Cx
Sel
hr
kDa
IκBα
IκBβ
Tubulin
B
IκBα
IκBβ
+ Selinexor
% Remaining
hr
C
H1-P1
μM Sel
NF-κB
Oct-1
Fold (NF-κB/Oct)
D
H1-P1
TNFα
Bort
Sel
NF-κB
Oct-1
Fold (NF-κB/Oct)
E
Bright Field
DRAQ5
IκBα
Merge
Control
Sel
LMB
Normalized Frequency
Similarity Score

Fig 4. Selinexor inhibits HAPLN1-PTR1-induced IκBα degradation and NF-κB activation. (A) Representative immunoblot analysis of IκBα, IκBβ and tubulin in RPMI8226 cells pretreated for 30 min with 20 μg/mL cycloheximide (Cx) with 10 μM selinexor (Sel) and stimulated with GST-PTR1 (H1-P1) for indicated times. (B) Graph depicts the mean ± SD of the quantification of three independent replicates of western blot analysis as in A. (C) EMSA analysis of RPMI8226 cells pretreated for 30 min with increasing concentrations of selinexor (Sel) and stimulated with GST-PTR1 (H1-P1). (D) EMSA analysis of RPMI8226 cells pretreated for 30 min with 10 μM Sel or 100 nM Bort and stimulated with 100 nM GST-PTR1 (H1-P1) or 10 ng/mL TNFα. (E) Upper: Images of RPMI8226 cells control and treated with 10 μM Selinexor (Sel) or 20 μg/mL Leptomycin B (LMB) for 45 min. The similarity score for each set of representative images is included in merged image. Lower: A representative similarity histogram for control and treated cells showing the co-localization of IκBα and the nuclear dye, DRAQ5.

Figure 5

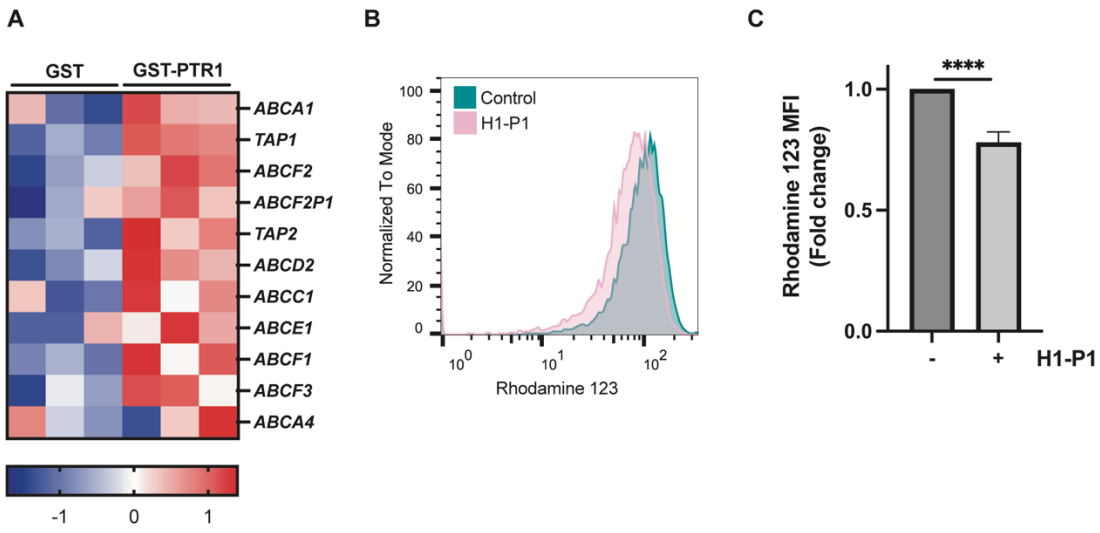
A
GST
GST-PTR1
ABCA1
TAP1
ABCF2
ABCF2P1
TAP2
ABCD2
ABCC1
ABCE1
ABCF1
ABCF3
ABCA4
-1
0
1
B
Control
H1-P1
Normalized To Mode
100
80
60
40
20
0
10^0
10^1
10^2
Rhodamine 123
C
****
Rhodamine 123 MFI
(Fold change)
1.0
0.5
0.0
-
+
H1-P1

Fig 5. HAPLN1-PTR1 increases expression of MDR genes and function. (A) Heatmap of upregulated MDR genes after GST-PTR1 treatment in RNA-seq analysis colored by Z-score. (B) Representative histogram of rhodamine 123 efflux assay. RPMI8226 cells were treated with 100 nM GST-PTR1 (H1-P1) or control GST for 24 h and subjected to the rhodamine 123 efflux assay. (C) Graph depicts the mean fluorescent intensity (MFI) ± SEM of three independent replicates of rhodamine 123 efflux assay as in B. **** $p<0.0001$.

Figure 6

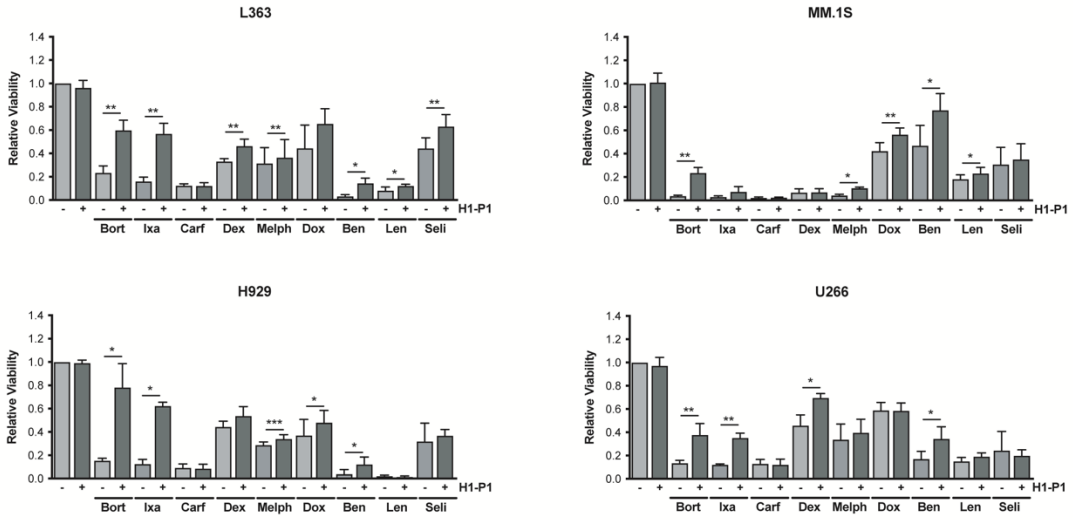
L363
MM.1S
H929
U266
Relative Viability
H1-P1
Bort
Ixa
Carf
Dex
Melph
Dox
Ben
Len
Seli

Fig 6. HAPLN1-PTR1 causes resistance of several MM cell lines to multiple clinical drugs. MM cell lines (L363, MM.1S, H929, U266) were cultured with 100 nM GST-PTR1 (H1-P1) or GST (-) in the presence or absence of indicated drugs and the cell viability was measured as described in Materials and Methods. Results represent the mean ± SD of three biological replicates, each performed in triplicate. * $p<0.05$, ** $p<0.01$, *** $p<0.001$.

Supporting information

Supplmental Figure 1

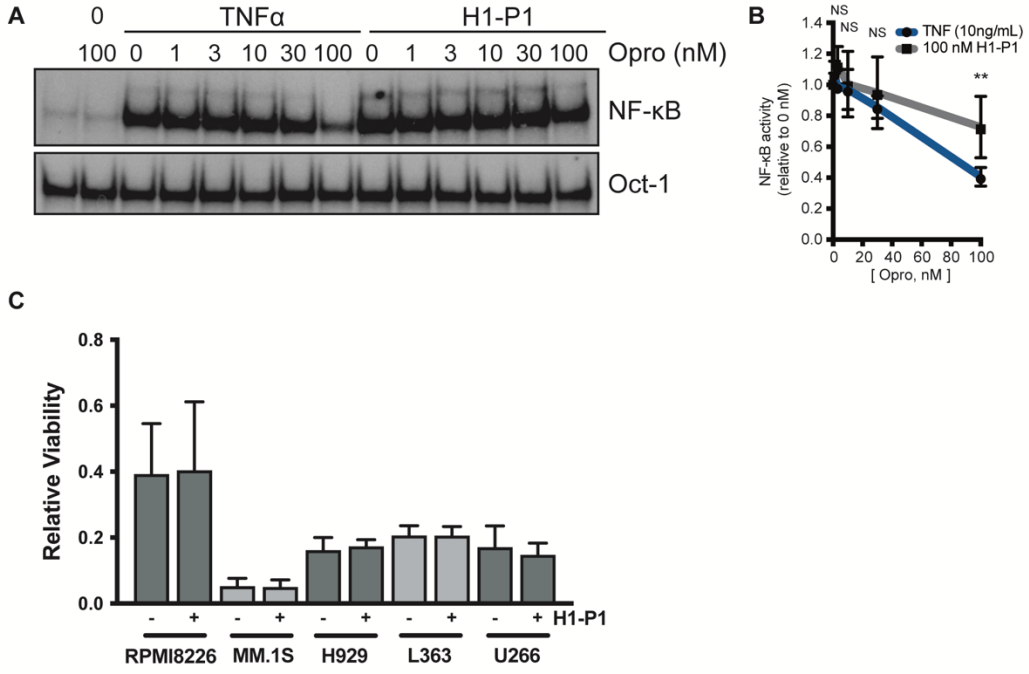

S1 Fig. HAPLN1-PTR1-induced NF-κB activation is resistant to oprozomib. (A) Representative EMSA analysis of RPMI8226 cells incubated with 10 ng/mL TNFα for 15 min or 100 nM GST-PTR1 (H1-P1) for 2 hr in the absence or presence of increasing concentrations (nM) of oprozomib (Opro). (B) Graph depicts the mean ± SD of the quantification of three independent replicates of EMSA analysis as in A. (C) MM cell lines (RPMI8226, L363, MM.1S, H929, U266) were cultured with 100 nM GST-PTR1 (H1-P1) or GST (-) in the presence of oprozomib (200 nM) and the cell viability was measured as described in Materials and Methods. Results represent the mean ± SD of three biological replicates, each performed in triplicate. ** $p<0.01$.

Supplmental Table 1

Rank	KEGG Positive Pathway	Size	ES	NES	NOM p-value	FDR q-value	FWER p-value
1	Ribosome	127	0.5892	7.5352	0	0	0
2	Spliceosome	126	0.4701	6.1981	0	0	0
3	Graft versus Host Disease	24	0.8500	5.0562	0	0	0
4	RNA Transport	154	0.3449	5.0429	0	0	0
5	Cytokine-Cytokine Receptor Interaction	135	0.3788	5.0268	0	0	0
6	Proteasome	39	0.6807	4.9904	0	0	0
7	Allograft Rejection	26	0.8180	4.9899	0	0	0
8	Herpes Simplex Infection	154	0.3439	4.9508	0	0	0
9	Ribosome Biogenesis in Eukaryotes	79	0.4574	4.8543	0	0	0
10	Autoimmune Thyroid Disease	24	0.8083	4.8390	0	0	0
11	Type I Diabetes Mellitus	28	0.7581	4.7355	0	0	0
12	Th17 Cell Differentiation	81	0.4180	4.4459	0	0	0
13	Inflammatory Bowel Disease	46	0.5612	4.4162	0	0	0
14	Antigen Processing and Presentation	54	0.4996	4.3764	0	0	0
15	Oxidative Phosphorylation	106	0.3568	4.2461	0	0	0
16	Parkinson's Disease	110	0.3406	4.1867	0	0	0
17	IL-17 Signaling Pathway	67	0.4271	4.1528	0	0	0
18	Measles	99	0.3549	4.1068	0	0	0
19	Staphylococcus Aureus Infection	31	0.6061	4.0565	0	0	0
20	Viral Myocarditis	46	0.4951	3.9875	0	0	0
21	Epstein Barr Virus Infection	184	0.2557	3.9859	0	0	0
22	TNF Signaling Pathway	94	0.3523	3.9714	0	0	0
23	Huntington's Disease	158	0.2727	3.9690	0	0	0
24	Intestinal Immune Network for IgA Production	33	0.5680	3.9652	0	0	0
25	Leishmaniasis	60	0.4300	3.9217	0	0	0
26	Th1 and Th2 Cell Differentiation	69	0.3873	3.8100	0	0	0
27	Influenza A	140	0.2771	3.7823	0	0	0
28	JAK/STAT Signaling Pathway	99	0.3096	3.7474	0	0	0
29	NF-κB Signaling Pathway	77	0.3564	3.7417	0	0	0
30	Toxoplasmosis	96	0.3261	3.7297	0	0	0

S1 Table. Gene set enrichment analysis (GSEA) using KEGG pathways of the ranked genes differentially regulated by GST-PTR1 versus GST control. Top 30 significant (FDR<0.05) pathways are shown. KEGG, Kyoto Encyclopedia of Genes and Genomes; ES, enrichment score; NES, normalized enrichment score; NOM, nominal; FDR, false discovery rate; FWER, family-wise error rate.